
A model of volcanic explosions at Popocatépetl volcano (Mexico): Integrating fragmentation experiments and ballistic analysis

Miguel Angel Alatorre Ibarra



München 2011

A model of volcanic explosions at Popocatépetl volcano (Mexico): Integrating fragmentation experiments and ballistic analysis

Miguel Angel Alatorre Ibarquengoitia

Dissertation zur Erlangung des Doktorgrades
an der Fakultät für Geowissenschaften
der Ludwig-Maximilians-Universität
München

vorgelegt von
Miguel Angel Alatorre Ibarquengoitia
aus Mexiko Stadt

München, den 2. März 2011

Erstgutachter: Prof. Dr. Donald Bruce Dingwell
Zweitgutachter: Prof. Dr. Stuart Gilder
Tag der mündlichen Prüfung: 27 Juni 2011

Contents

List of figures	III
List of tables	V
Acknowledgments	IX
Summary	XI
Zusammenfassung	XIII
1. Introduction	1
1.1 Background	1
1.2 Popocatepetl Volcano	3
1.3 Vulcanian eruptions and shock-tube theory	4
1.4 Fragmentation experiments	6
1.5 General objective and thesis structure	8
2. Energy consumption by magmatic fragmentation and pyroclast ejection during Vulcanian eruptions	11
Abstract	11
2.1 Introduction	12
2.2 Caprock model	13
2.3 Experimental method	15
2.4 Results	19
2.5 Fragmentation energy	23
2.6 Discussion	26
2.7 Summary	30
Acknowledgments Chapter 2	30
Appendix 2A. Derivation of Eqs. 2.3 and 2.4.	31
Appendix 2B. Determination of P_{ext} in the fragmentation apparatus	33
3. Influence of the fragmentation process on the dynamics of Vulcanian eruptions: an experimental approach	37
Abstract	37
3.1. Introduction	37
3.2. Model	39
3.3. Experimental method	40

3.4. Results	42
3.4.1 <i>Two-phase flow characteristics</i>	42
3.4.2 <i>Fragmentation speed and ejection velocities.</i>	44
3.5. Interpretation	46
3.6. Discussion	49
3.7. Summary	53
Acknowledgments Chapter 3	54
Appendix 3A. Derivation of equations (3.1) and (3.2)	54
Appendix 3B. Determination of P_{fi} in the fragmentation apparatus and volcanic conduits	56
4. Hazard Map for Volcanic Ballistic Impacts at Popocatépetl Volcano (Mexico) .	59
Abstract	59
4.1 Introduction	60
4.2 Eruptive activity of Popocatépetl Volcano	61
4.3 Ballistic projectiles from Popocatépetl Volcano	64
4.4 Models	65
4.4.1 <i>Ballistic models</i>	65
4.4.2 <i>Caprock model.</i>	67
4.4.3 <i>Coupling of caprock and ballistic models</i>	69
4.4.4 <i>Comparison with videos of Vulcanian eruptions from Popocatépetl Volcano.</i>	71
4.5 Explosive scenarios definition	72
4.6 Maximum range calculation	75
4.7 Volcanic ballistic projectile-hazard map construction for Popocatépetl Volcano . .	76
4.8 Summary	80
Acknowledgments Chapter 4	81
5. Conclusions and Outlook	83
5.1 Conclusions.	83
5.2 Outlook	85
References	87
Curriculum vitae	97

List of figures

Chapter 1

Figure 1.1. Fatal volcanic eruptions per century, cumulative documented fatalities caused by volcanic eruptions and cause of fatalities in volcanic eruptions	2
Figure 1.2. Schematic illustration of the shock-tube problem	5
Figures 1.3. Sketch of the glass transition field	7

Chapter 2

Figure 2.1. Experimental setup of the fragmentation apparatus	16
Figure 2.2. Pictures of the types of samples used in the experiments.	17
Figure 2.3. Thin section photographs of Popocatépetl samples	18
Figure 2.4. Fragmentation threshold of volcanic samples at 850 °C	19
Figure 2.5. Ejection velocities of a plate set on top of volcanic samples	21
Figure 2.6. Example of ejection velocities of particles measured through image analysis of high-speed camera footage.	23
Figure 2.7. Energy consumed by fragmentation in a unit volume of sample	25
Figure 2.8. Ejection velocity as a function of pressure in Vulcanian eruptions of Popocatépetl volcano and Colima volcano	28
Figure 2.B1. Sketch illustrating the sample, the plate and the regions with the different pressure above it	35

Chapter 3

Figure 3.1. Setup for fragmentation speed experiments	41
Figure 3.2. Sequence of still-frames showing the front of the gas-particle mixture after fragmentation	43
Figure 3.3. Fragmentation speed and ejection velocity in fragmentation experiments	45
Figure 3.4. Ejection velocity at the front of the gas-particle mixture in fragmentation experiments	48
Figure 3.5. Final pressure, ejection velocity, density and mass discharge rate per unit area at the front of the gas-particle mixture as a function of pressure in transient eruptions . .	51
Figure 3.6. Ejection velocity and mass discharge rate per unit area at the front of the gas-particle mixture as a function of the initial pressure considering different values of f . .	52

Chapter 4

Figure 4.1. Geographic location of Popocatépetl volcano	61
Figure 4.2. Ejection velocity and maximum range of the VBP as a function of the initial gas pressure for different magma porosities	70
Figure 4.3. Schematic illustration of Vulcanian eruptions and video stills of different Vulcanian events at Popocatépetl volcano	72
Figure 4.4. Ballistic range as a function of ballistic diameter for different launching kinetic energies	76
Figure 4.5. Volcanic ballistic projectile hazards map for Popocatépetl volcano	77
Figure 4.6. Aerial hazard zones for ballistic projectile impact from Popocatépetl volcano shown with topographic profiles South-North and West-East	79

List of tables

Chapter 2

Table 2.1. Values of the parameters used for the simulations corresponding to the experiments (Fig. 2.5) and the application to natural cases (Fig. 2.8)	20
Table 2.2. Maximum ejection velocities for monodisperse particles during decompression experiments at $P_o = 10$ MPa	22

Chapter 3

Table 3.1. Values of the parameters used for the simulations corresponding to the experiments (Figs. 3.3 and 3.4) and the application to natural cases (Figs. 3.5 and 3.6) . .	50
--------------------------------------------------------------------------------------------------------------------------------------------------------------------------------	----

Chapter 4

Table 4.1. Characteristics of the investigated ballistics ejected during different eruptive events of Popocatépetl volcano	65
Table 4.2. Comparison between the mean observed values and theoretical calculations for different parameters corresponding to three phases for four Vulcanian events	72
Table 4.3. Kinetic energies associated with ballistic projectiles, corresponding maximum ranges and altitudes for the three explosive scenarios defined for Popocatépetl volcano and probability that at least one eruption occurs in any 20-year interval	74

A mi amada esposa, **Julietta**, por tu amor y tu apoyo cercano, comprensivo y cariñoso siempre. Esta tesis es solamente uno de los frutos de esta experiencia que hemos vivido juntos. Recuerdo bien el día en que con lágrimas aceptaste que viviéramos esta aventura que ahora valoramos y recordamos con alegría. Hoy tenemos la satisfacción de que regresaremos con los títulos esperados, de los cuales el doctorado es el segundo más importante.

A mi hija **Andrea** que está por nacer. Este trabajo va con mucho amor para ti. Con el deseo de que esta tesis sea para siempre el recuerdo y testigo de un proceso muy hermoso en el que te hemos visto llegar a la vida. Quizá a tus biógrafos les interese algún día saber por qué naciste en Alemania y entonces puedas citar este trabajo.

A mis papás, **Lupita** y **Miguel Ángel**, con mucho cariño y mucho agradecimiento por su amor y por todo el apoyo que nos dieron desde el primer minuto que iniciamos esta aventura. **Mamá**, estuviste conmigo cuando lloraba por entrar en la primaria porque no quería ser grande, después fue encontrarte en los pasillos de la Facultad de Ciencias y decirte “hola má” y ahora fue encontrarnos por Skype para mandarnos besos. Siempre has estado conmigo y me has impulsado a crecer. Con mucho amor y agradecimiento te dedico esta tesis. **Papá**, alguna vez deseaste hacer un doctorado en Alemania. Seguramente no imaginabas que el doctorado de Miguel Alatorre en Deutschland te llevaría a ser abuelo. Esta tesis va por ti.

A mis queridos suegros **Rodolfo** y **Conchita** por habernos acompañado de forma tan cercana a pesar de la distancia, por todo su apoyo y por haber contribuido tanto para que nuestra experiencia en un país tan lejano haya transcurrido de forma mucho más fácil de lo que hubiera podido ser. Gracias por su apoyo, sin ustedes este trabajo no hubiera sido posible.

A mis hermanos **Paulina** y **Jerónimo**.

A mis cuñados y concuños: **Guille** y **Ernesto**, **Conchita** y **Gonzalo**, **Claudia** y **Beny**, **Chío** y **Omar**.

A mis sobrinos: **Melissa**, **Ernesto**, **Mary Fer**, **Juan Pablo**, **Sofía**, **Arturo**, **Regina**, **Omar**, **María** y **Pablo**.

A mi **Abuelita**, mis tíos y mis primos.

A todos mis amigos que desde la distancia me han acompañado tanto, en especial a mi gran compañero de batalla, **Jorge el Oso**, ahora en distintos lugares, pero compartiendo la lucha y **Andrea**.

A los que esta tesis les podrá servir y a los que no han tenido las mismas oportunidades que yo.

Acknowledgments

I would like to express my gratitude to all those who have made this thesis possible. First of all to my supervisor Prof. Donald Bruce Dingwell for offering me the opportunity to come to Munich and gave me the freedom and resources to work in a topic that have always interested me.

Special thanks to Bettina Scheu, Ulrich Küppers and Oliver Spieler who guided me through the work in the lab and were always there for discussions, solving technical problems and ordering new toys for the lab. I also thank Dominique Richard, Sandra Karl, Teresa Scolamacchia, Rosie Smith, Warna Downey, Oryaëlle Chevrel, Jackie Kendrick, Yan Lavalee, Jonathan Hanson, Axel Gerik, Benoit Cordonnier, Corrado Cimarelli, Alex Rocholl, Daniele Morgavi, Kai Hess, Werner Ertel-Ingrisch, Guilhem Douillet, Michael Heap, Fabian Goldstein, Stefan Gottschaller and some more unmentioned but not forgotten. I thank you all for nice discussions, help with a number of problems, support, sharing a “cafecito” or two, and especially for make me feel accepted and appreciated during my experience in Munich.

I am indebted to Helen Pfuhl for her invaluable help in getting started in Munich and constant administrative and financial support. I also want to thank all the faculty of THESIS for accepting me as part of the team and granted me to work under the best conditions.

Special thanks to my coauthors who contributed in the papers presented in this thesis: Donald Dingwell, Betty Scheu, Hugo Delgado-Granados and Jacopo Taddeucci. I also thank all the people with whom I have worked in different projects not presented herein that have been presented in several meetings and will be published soon, in particular Alejandra Arciniega.

Many thanks to Prof. Stuart Gilder for agreeing to act as a second reviewer and Prof. Matthias Hort who kindly accepted to be the external member of my committee. I also thank all the members of my committee for their time.

I would like to express my gratitude to my “sherpas” who helped me bringing several hundreds of kilograms of volcanic rocks from Popocatepetl Volcano to Munich just to be destroyed (in alphabetic order): Jerónimo Alatorre, Miguel Alatorre-Mendieta, Corrado

Cimarelli, Isaac Farraz-Montes, Carlos Fernández, Patricia Jácome-Paz, Patricia Julio-Miranda, Ulrich Kueppers, Yan Lavallée and Eric Téllez. Many thanks to Federico Tarrats and Miguel Alatorre-Mendieta for help in the measurements of the bulk density of some of these rocks.

I also thank Roberto Quaas for allowing us the access to the video collection of CENAPRED and Lucio Cárdenas (CENAPRED) for the observation and careful selection of explosive events at Popocatepetl Volcano.

Thanks to Yvonne Nessler, Margot Lieske, Sandra Großkopf, Renata Döring and Isabel Heggmaier for help with administrative issues and Markus Sieber, Wolfgang Poppe and Martin Kiening for technical help.

Last but not least, I thank the financial support provided by the International Graduate School IDK 31 THESIS (Complex Processes in the Earth: Theory, Experiments, Simulations) funded by the Elite Network of Bavaria (ENB) and the EVOKES project of the European Research Council. This study was partially funded by the FONCICYT program (Mexican Government-European Union), grant 93645 (FIEL-VOLCAN) and was also benefited by the Research Professorship (LMUexcellent) of the Bundesexzellenzinitiative granted to Prof. Donald Dingwell. Fieldwork in Mexico was partially funded by the PROALMEX program (CONACYT-DAAD).

Summary

The dynamics of magma fragmentation is a controlling factor in the behavior of explosive volcanic eruptions. Fragmentation changes the eruption dynamics from a system of bubbly flow to one of gas-particle flow. To date, the influence of the fragmentation process itself on the eruption dynamics has been largely neglected in eruption models. This is understandable, as the explosive expansion of mixtures of pressurized gases and pyroclasts in volcanic eruptions is a complex process that cannot be studied directly. The dynamics of the gas-particle mixture resulting after magma fragmentation in volcanic eruptions was experimentally investigated in a shock-tube apparatus. We performed fragmentation experiments with natural volcanic samples with diverse porosities (10 – 67 vol. %), different applied pressures (4-20 MPa) and distinct temperatures (room temperature and 850°C). Two different types of experiments were performed. In the first type, we measured the ejection velocity of a plate placed loosely on top of a volcanic sample in order to account for the ejection of the caprock in Vulcanian eruptions. In the second type we simultaneously measured the fragmentation speed and the ejection velocity of the gas-particle mixture in the absence of a plate. In both cases the results are in good agreement with a general model for Vulcanian eruptions based on 1-D shock-tube theory, including magma fragmentation, and considering the specific conditions of each experiment.

Our results show that the fragmentation process plays an important role in the dynamics of the gas-particle mixture. The reasons include the following: 1) the energy consumed by fragmentation reduces the energy available to accelerate the gas-particle mixture; 2) the fragmentation speed controls the pressure available for the ejection of the gas-particle mixture which in turn determines the velocity, density and mass discharge rate; 3) the grain-size distribution produced during fragmentation controls the mechanical and thermal coupling between the gas phase and the particles; 4) the fragmentation process may produce heterogeneities in the concentration of particles. In volcanic eruptions all these factors can affect the eruption dynamics significantly.

The model presented herein is consistent with the experimental results and is capable of describing the dynamics of brittle fragmentation in Vulcanian eruptions and yielding more realistic initial pressures at the onset of fragmentation than previous models. We applied this model to recent Vulcanian eruptions of Popocatépetl and Colima volcanoes (Mexico) and

estimated the initial gas pressure required to disrupt the caprock, fragment the underlying magma and eject ballistic projectiles to the observed distances. Further, the model is used in concert with a ballistic model to relate initial pressure and gas content with ballistic range. This coupled model was calibrated and validated with field and video observations of ballistics ejected during different Vulcanian eruptions at Popocatepetl Volcano. The model relates the zones which could be affected by the impact of ballistic projectiles to the initial pressure that can be estimated from seismic and geophysical monitoring, providing valuable information for more refined short-term hazard assessment at active explosive volcanoes.

Finally, a general methodology to delimit the zones that can be affected by ballistic projectiles is presented and applied to Popocatepetl Volcano. Three explosive scenarios with different intensities have been defined according to the past activity of the volcano and parameterized considering the maximum kinetic energy associated with ballistic projectiles ejected during previous eruptions. For each explosive scenario, the ballistic model is used to calculate the maximum range of the projectiles considering the optimum launch conditions. Our results are presented in a ballistic hazard map with topographic profiles that depict the likely maximum ranges of ballistic projectiles (horizontally and vertically) under the three explosive scenarios defined specifically for Popocatepetl Volcano. The multi-level hazard zones shown on the map are intended to allow the responsible authorities to plan the definition, development and mitigation of restricted areas during volcanic crises.

Zusammenfassung

Die Dynamik der Magmenfragmentierung hat großen Einfluss auf den Ablauf von explosiven Vulkanausbrüchen, da sich der physikalische Zustand des Magmas grundlegend ändert. Vor der Fragmentation steigt im Vulkan eine Flüssigkeit (mit darin enthaltenen Gasblasen und Kristallen) auf, danach ein Gas (mit darin enthaltenen Pyroklasten). Bis heute ist dieser Sachverhalt in Eruptionsmodellen weitgehend vernachlässigt worden. Dies ist verständlich, denn die explosive Expansion von unter Druck stehenden Gasen und Pyroklasten ist ein komplexer Prozess, der nicht direkt untersucht werden kann. In dieser Arbeit wurde das Verhalten einer durch Magmafragmentierung erzeugten Gas-Partikel-Mischung mit Hilfe eines auf dem Stoßrohr-Prinzip basierenden Fragmentationsapparates experimentell untersucht. Wir führten Fragmentationsexperimente mit natürlichen vulkanischen Proben (Porositätsbereich 10 - 67 %) bei angelegten Druckunterschieden von 4 bis 20 MPa und bei Temperaturen zwischen 25 und 850°C durch. Zwei unterschiedliche Typen von Experimenten wurden durchgeführt: Im ersten Typ maßen wir die Auswurfgeschwindigkeit einer Platte, die lose auf eine vulkanische Probe gelegt worden war. Damit wurde der Auswurf von Bruchstücken eines erkalteten Magmapfropfens über dem heißen Magma bei vulkanischen Explosionen simuliert. Im zweiten Typ maßen wir gleichzeitig die Fragmentationsgeschwindigkeit einer vulkanischen Probe sowie die Auswurfgeschwindigkeit der erzeugten Gas-Partikel-Mischung. Unter Berücksichtigung der spezifischen Bedingungen der jeweiligen Experimente sind die Ergebnisse in beiden Fällen in guter Übereinstimmung mit einem allgemeinen Modell für vulkanische Eruptionen, welches auf der eindimensionalen Stoßrohr-Theorie unter Einbeziehung der Magmafragmentierung beruht.

Unsere Ergebnisse zeigen, dass der Fragmentationsprozess aus den folgenden Gründen eine wichtige Rolle in der Dynamik der Gas-Partikel-Mischung spielt: 1) Die durch den Fragmentationsprozess verbrauchte Energie reduziert die verbliebene Energie, um die Gas-Partikel-Mischung zu beschleunigen; 2) Die Fragmentationsgeschwindigkeit kontrolliert den Druck für die Ejektion der Gas-Partikel-Mischung; dies wiederum bestimmt Auswurfgeschwindigkeit, Dichte der Gas-Partikel-Mischung und Massendurchsatz; 3) Die während der Fragmentation erzeugte Korngrößenverteilung kontrolliert die mechanische und thermische Kopplung zwischen Gasphase und Partikeln; 4) Der Fragmentationsprozess kann

Heterogenitäten in der Konzentration von Partikeln erzeugen. Alle diese Faktoren können die Ausbruchsdynamik wesentlich beeinflussen.

Das hier vorgestellte Modell beruht auf experimentellen Ergebnissen und kann die Dynamik des Sprödbruchs während vulkanianischer Eruptionen beschreiben. Dadurch ergeben sich im Vergleich zu früheren Modellen realistischere Werte für den zu Beginn eines Ausbruchs herrschenden Überdruck. Wir haben dieses Modell auf die jüngsten vulkanianischen Eruptionen der Vulkane Popocatépetl und Colima (Mexiko) angewendet und abgeschätzt, welcher anfängliche Gasdruck erforderlich war, um einen erkalteten Magmapfropfen zu zerbrechen, das darunter liegende heiße Magma zu fragmentieren und ballistische Geschosse über Distanzen auszuwerfen, die bei den jüngsten Ausbrüchen beobachtet worden waren. Das vorliegende Modell setzt die Zonen, die durch ballistische Geschossen betroffen waren, mit dem zum Beginn des Vulkanausbruchs herrschenden Überdruck in Zusammenhang. Dieser Druck kann aus seismischen und geophysikalischen Überwachungssignalen abgeschätzt werden. Dadurch kann das Gefährdungspotential an aktiven explosiven Vulkanen schnell und zuverlässig abgeschätzt werden.

Abschließend wird eine allgemeine Methode präsentiert, mit der diejenigen Zonen abgegrenzt werden können, die mit einer bestimmten Wahrscheinlichkeit durch ballistische Geschosse getroffen werden können. Im Falle des Vulkans Popocatépetl wurden auf Grundlage von Ausbrüchen in der jüngeren Vergangenheit und unter Einbeziehung der zum Auswurf beobachteter ballistischer Objekte nötigen maximalen kinetischen Energie drei Ausbruchsszenarien unterschiedlicher Intensität definiert. Für jedes Szenario wurde das ballistische Modell verwendet, um die maximal zu erwartende Auswurfentfernung der Geschosse unter optimalen „Abschuss“-Bedingungen zu berechnen. Unsere Ergebnisse sind in einer Gefährdungskarte präsentiert. Mit Hilfe von topographischen Profilen wird an Hand der drei Ausbruchsszenarien des Vulkans Popocatépetl der wahrscheinlich maximale Bereich von ballistischen Geschossen (horizontal und vertikal) dargestellt. Die abgebildeten Zonen unterschiedlichen Gefährdungspotentials erlauben den zuständigen Behörden, Sperrgebiete im Umfeld des Vulkans während vulkanischer Krisen zu planen und gegebenenfalls anzupassen.

Chapter 1

Introduction

1.1 Background

Volcanic eruptions are one of the most spectacular and powerful of natural phenomena. They also represent a significant threat that, depending on the eruptive style, may have local, regional or global impact. Even though volcanic eruptions are not the most deadly manifestation of nature's force (like earthquakes and tropical storms), volcanic disasters since 1600 have claimed an estimated toll of more than 270,000 lives (Sigurdsson, 2000; Simkin et al., 2001). Since 1800, at least 480 volcanoes have produced ca. 8,000 eruptions and more than 400 of these are believed to have produced fatalities (Small and Naumann, 2001). The number of fatal volcanic eruptions has been increasingly systematically during the last centuries (Fig. 1.1). This is linked to global population increase and not to eruption frequency worldwide, which has been roughly constant through the recent centuries (Simkin et al., 2001).

Nowadays, it has been estimated that almost 9 % (~ 500 million people) of the world's total population live within 100 km of a historically active volcano and 12 % within 100 km of a volcano believed to have been active during the last 10,000 years. In tropical areas, the elevation and fertile soils associated with volcanic regions and the availability of cheap land can provide sufficient incentive for people to settle close to potentially active volcanoes. Many of these areas are currently experiencing dramatic increases in population growth, urbanization and economic development, which increase the potential impact of volcanic activity (Small and Naumann, 2001).

There are a remarkable number of potentially lethal hazards associated with volcanic eruptions. Perhaps most notably, in terms of human impact, are pyroclastic density currents, tephra fall and other large scale phenomena (Fig. 1.1). Pyroclastic flows and surges have proven to be the deadliest. Post-eruption famine and volcanogenic tsunamis have also produced a significant number of fatalities, but most of them are associated to only two eruptions in Indonesia: Tambora (1815) and Krakatau (1883). On the other hand, tephra, which includes all fragmental material thrown from volcanoes, is the hazard most commonly resulting in fatalities, generally through the collapse of ash covered roofs and ballistic projectile impacts. Of those, ballistic impacts are the most frequent (Simkin et al., 2001).

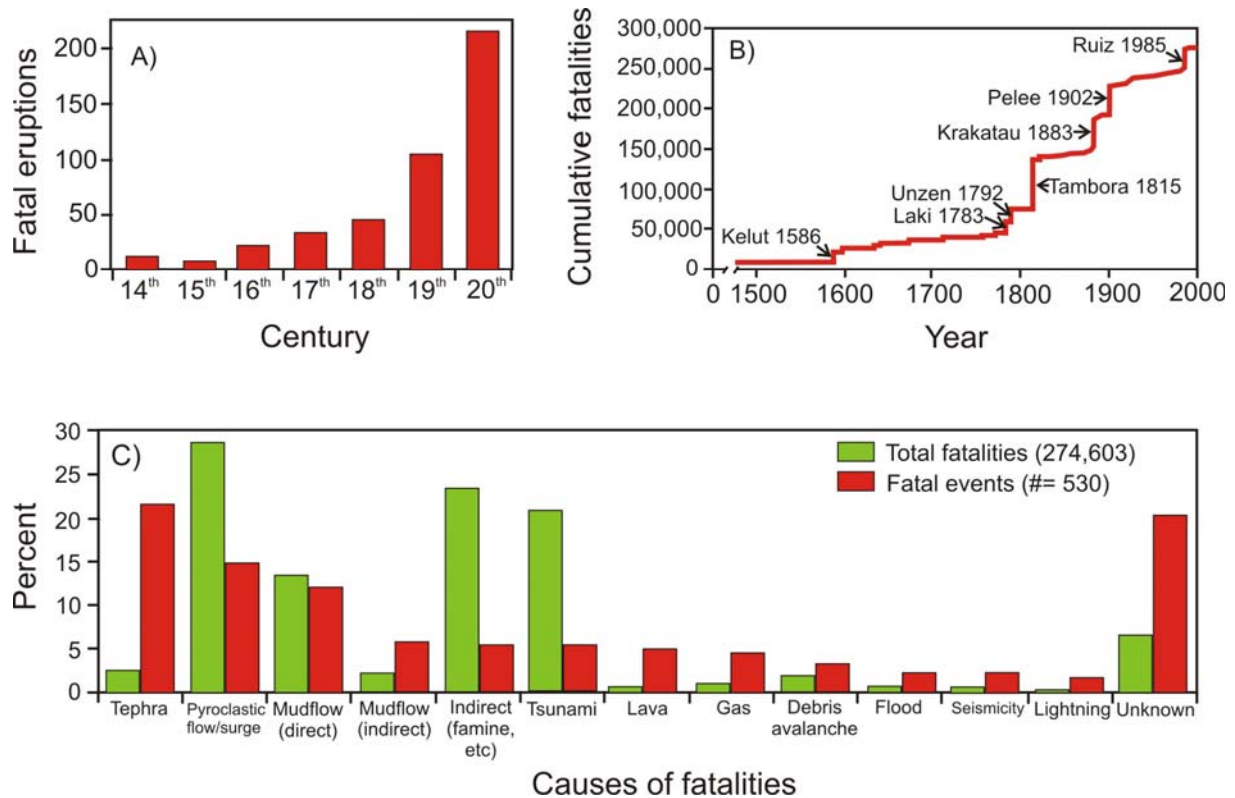


Figure 1.1. A) Fatal volcanic eruptions per century. Even when the historical records might be incomplete or have inaccuracies, it is believed that the tendency indicated in this figure is real, revealing an increase in the global population living in the vicinity of active volcanoes. B) Cumulative documented fatalities caused by volcanic eruptions. The seven named eruptions claimed more than 10,000 victims. C) Cause of fatalities in volcanic eruptions. In some eruptions, fatalities result from more than one cause (modified after Simkin et al., 2001).

Potentially destructive phenomena such as volcanic eruptions occur independently of any human action. Disasters may occur when a social group fails to respond to a threatening situation resulting from volcanic activity or any other natural phenomenon. Nowadays, one of the main goals of society is the reduction of risk to life and property, and it expects scientists to provide knowledge and technologies aimed at increasing protection from natural hazards (De la Cruz-Reyna et al., 2000). The effective management of a volcanic crisis usually involves several components which can be aggregated into three elements (De la Cruz-Reyna and Tilling, 2008):

1. Identification of the areas threatened by a given volcano, together with the definition of the probabilities that specific hazardous volcanic phenomena may occur in a given interval of time. The ultimate product of these studies is a hazard map depicting the areas that could be affected by the different phenomena.
2. Geophysical, geochemical and remote-sensing monitoring of a restless volcano (in real time where possible) to document its changes in state. The data from volcano monitoring

provide the only scientific basis for making a dynamic estimate of the probability of occurrence of specific scenarios in the short term. Therefore, an adequate interpretation of these data is crucial to assess the level of potential hazards.

3. Development and implementation of a hazards-warning system and response scheme that allows the civil authorities and vulnerable population to adopt mitigation measures according to pre-established levels of risk.

A comprehensive understanding of pre- and syn-eruptive processes is required in order to interpret and evaluate adequately the data from volcanic monitoring. However, the scientific investigation of volcanic phenomena cannot rely solely on field data, as direct observations of eruptive processes in the field are very limited in terms of accessibility and safety. For this reason, detailed observations are restricted to a limited range of superficial processes. Laboratory experiments and theoretical models are complementary elements essential for our understanding of volcanic processes. In particular, laboratory experiments are becoming increasingly important in volcanic research and are used for the following primary purposes: 1) to explore novel or inaccessible phenomena; 2) to provide systematic observation of volcanic processes; 3) to determine the values of key parameters; and 4) to test hypothesis and validate theoretical and numerical models (Mader et al., 2004). For a better understanding of volcanic eruptions and their forecasting, field observations and experimental studies should be combined and eruptive models consistent with the available information developed.

1.2 Popocatépetl Volcano

In this study we investigated the explosive eruptive activity of Popocatépetl Volcano (19.02° N, 98.62° W, with an altitude of 5452 m), located in central Mexico, just 70 km from downtown Mexico City (see Fig. 4.1). Popocatépetl is situated within the central part of the Trans-Mexican Volcanic Belt, which most authors relate to the subduction of the Cocos plate beneath the North American plate. This belt is an approximate east-west aligned zone that extends for more than 1,000 km from the Pacific coast to the Gulf of Mexico and consists of a large number of late Tertiary and Quaternary cinder cones, maars, domes, and stratovolcanoes, the chemical and mineralogical composition of which is largely calcalkaline (Siebe and Macías, 2004). Popocatépetl is one of the most dangerous volcanoes in Mexico due to the highly explosive eruptions that have occurred in the past (Siebe et al., 1996), and that it is one of the 10 most populated active volcanoes in the world (Small and Naumann, 2001). Presently

~ 500,000 people live within 10–30 km from the crater and nearly 1.3 million within 40 km (De la Cruz-Reyna and Tilling, 2008). Moreover, within 40-80 km from the vent, more than 20 million inhabitants may be exposed to the effects of a large-magnitude explosive eruption.

The volcano's geologic past clearly indicates that it is capable of producing catastrophic eruptions. In the last ~23,000 years (corresponding to the formation of the present cone), Popocatépetl has had at least seven Plinian eruptions that produced extensive deposits, including three within the last 5000 years that destroyed several human settlements (Macías and Siebe, 2005). Fortunately, the current eruptive episode, which started in December 1994, has been characterized by the repeated formation of small domes inside the summit crater and Vulcanian eruptions generating 1-10-km-high ash plumes associated with the destruction of these domes. This kind of activity has characterized Popocatépetl's activity in the last 600 years as indicated in the historical records (Siebe and Macías, 2004). One of the most common hazards associated with these Vulcanian eruptions is the ejection of large rock and magma fragments (>10-15 cm), which follow nearly parabolic trajectories. Such fragments are called volcanic ballistic projectiles and represent an important hazard to life, property, vegetation and air navigation (Alatorre-Ibargüengoitia et al., 2006). In fact, ballistic projectiles caused the only casualties that have been directly related to Popocatépetl current eruptive activity, the deaths of five climbers which had neglected official warnings.

1.3 Vulcanian eruptions and shock-tube theory

Vulcanian eruptions, such as those occurring at Popocatépetl Volcano, are small to moderate-sized volcanic explosions that last on the order of seconds to minutes. Such eruptions are characterized by violent discrete events which produce atmospheric shock waves, eject ballistic blocks and bombs and generate eruptive columns < 20 km in height (Morrisey and Mastin, 2000). Typically on the order of $10^5 - 10^9$ kg of material is erupted from the vent and often a significant fraction of this material is non-juvenile (Self et al., 1979). The juvenile components range in composition from andesitic basalt to dacitic. Two main mechanisms have been recognized for Vulcanian events: 1) Brittle failure of a dense, impermeable caprock beneath which magmatic gas has accumulated; and 2) interaction of rising magma with external water producing hydromagmatic eruptions (Morrisey and Mastin, 2000). In this study we will concentrate on the first mechanism.

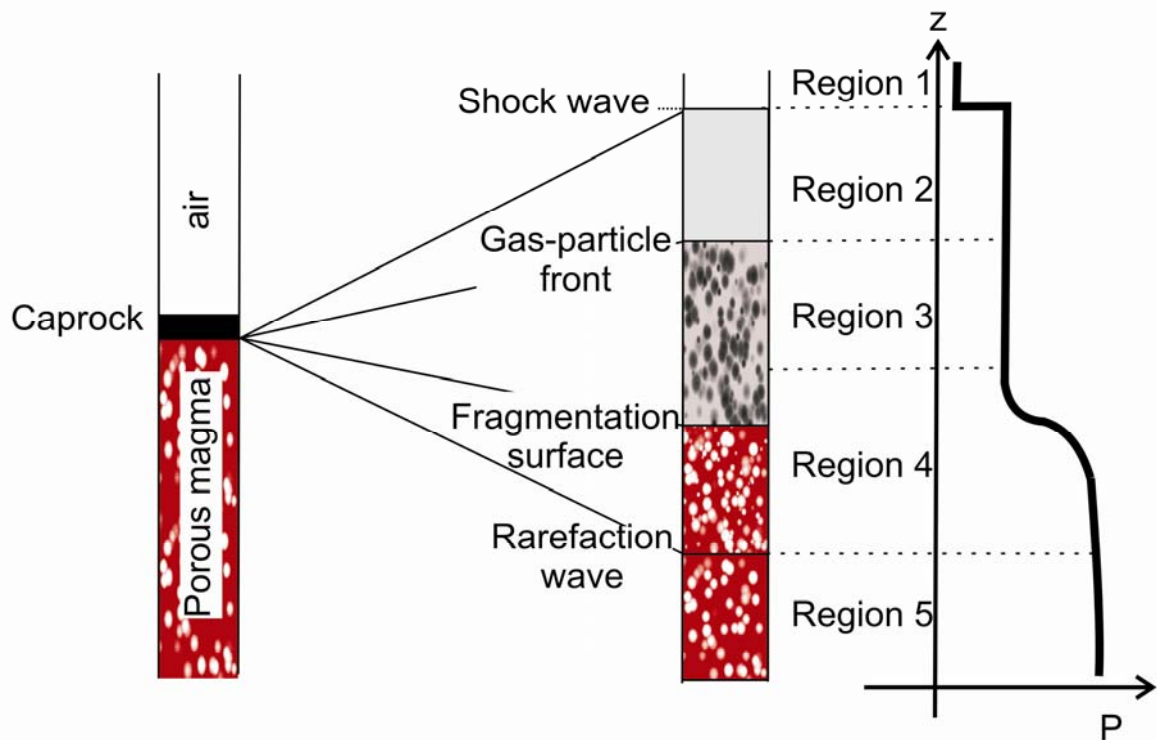


Figure 1.2. Schematic illustration of the shock-tube problem. After the caprock is disrupted, a shock wave propagates into the air and a rarefaction wave propagates into the porous magma. As a consequence, five regions can be defined in the air and the magma, which are described in the text. A typical pressure profile is also schematically shown (modified after Koyaguchi and Mitani, 2005).

A standard approach to the modeling of Vulcanian eruptions is to consider a one-dimensional, time-dependent expanding flow traveling in a cylindrical conduit according to the shock-tube theory (Turcotte et al., 1990; Ramos, 1995; Woods, 1995; Cagnoli et al., 2002; Koyaguchi and Mitani, 2005; Chojnicki et al., 2006). The considered system is illustrated in Figure 1.2. In the initial state, the pressurized porous magma (typically 10^1 - 10^2 MPa) is separated from the air at atmospheric conditions (10^1 MPa) by the caprock. After the caprock is disrupted, a shock wave propagates into the air and a rarefaction wave propagates into the porous magma. As the rarefaction wave propagates into the magma, a zone with a steep pressure gradient develops within the magma, which may lead to fragmentation, i.e. the process through which magma is transformed into a gas-particle dispersion. The flow of the air and the porous magma is divided into five regions (Koyaguchi and Mitani, 2005): Regions 1 and 5 are the stationary regions of the air and the magma under the initial condition, respectively. Region 2 is a uniform region where the air is compressed after the propagation of the shock wave. Region 3 is another uniform region where the gas-particle mixture is decompressed. In Region 4 a pressure gradient is developed within the magma and it is in this region that the porous magma is fragmented due to rapid decompression. The boundary

between porous magma and gas-particle dispersion is defined as the fragmentation front and the velocity at which this front propagates downwards into the magma is the fragmentation speed (e.g. Scheu et al., 2006).

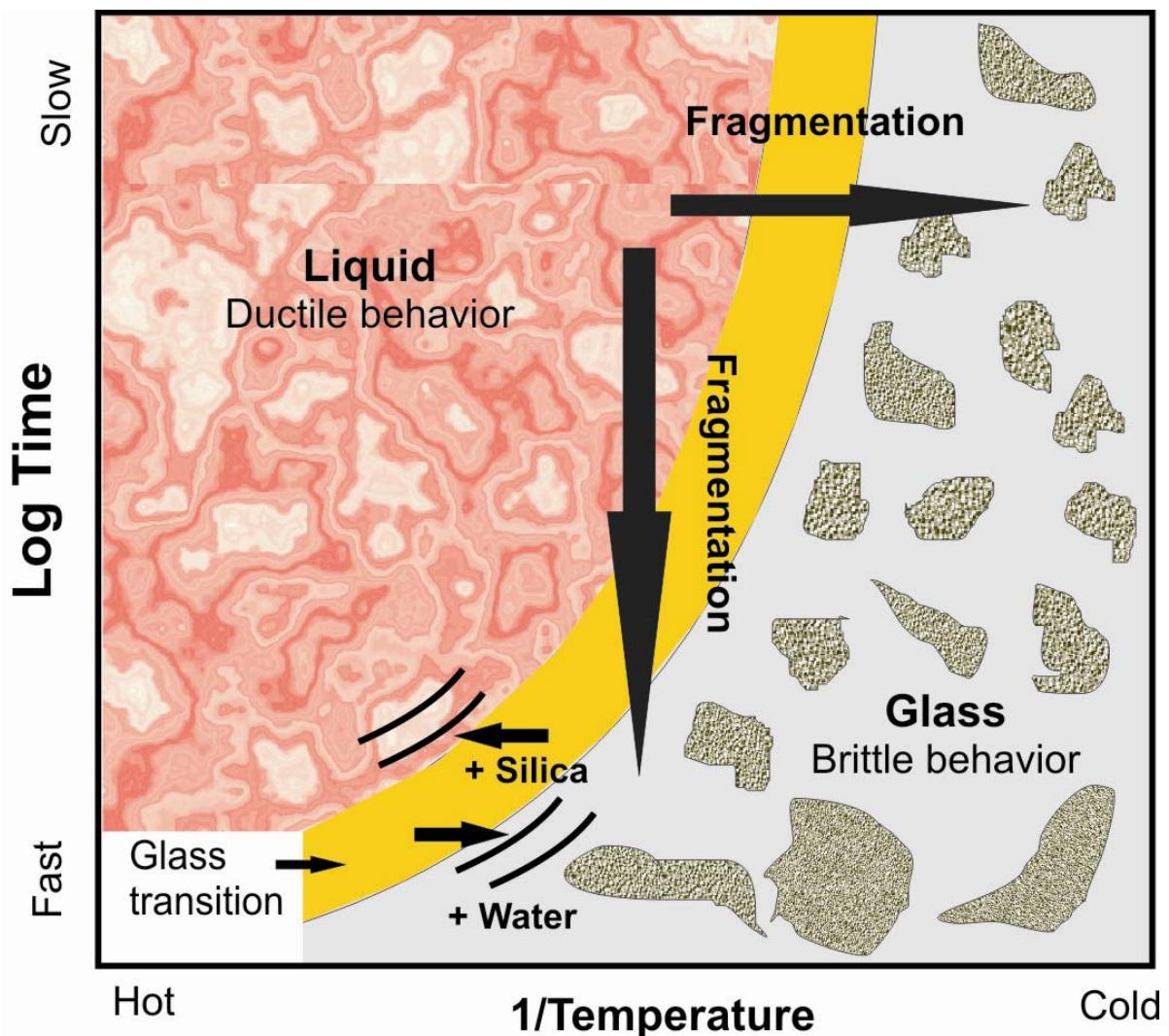
To date, the influence of the fragmentation process itself on the dynamics of the gas-particle flow has not been considered, mainly due to the lack of experimental data. In particular, the energy consumed during fragmentation has been neglected in current models of conduit flow in volcanic eruptions (e.g. Sahagian 2005 and references cited therein). This lack of consideration leads to either an overestimation of the pyroclasts ejection velocity calculated considering a certain initial pressure, or an underestimation of the initial gas pressure considering the pyroclasts ejection velocity. Furthermore, the fragmentation process might have a controlling influence on key parameters which can significantly affect eruption dynamics.

1.4 Fragmentation experiments

Magmatic fragmentation (i.e., in the case where magma does not interact with external water) may be the result of high ascent rates of magma, as in Plinian eruptions, or via rapid decompression of the magma (by e.g. dome collapse or caprock disruption) resulting mostly in Vulcanian eruptions (Cashman et al., 2000). In most cases, high-viscosity magma will disrupt in a brittle manner. The glass transition is temperature dependent and marks the change from ductile to brittle response of magma to strain (Fig. 1.3). It can be crossed either by cooling due to magma ascent or emplacement, or an increase in the strain rate (Dingwell, 1996). As magma fragmentation is a relatively rapid physical process, subjecting vesicular magma to high deformation rates, the fracture process is frequently brittle in nature.

The “fragmentation bomb”, a shock-tube apparatus designed by Alidibirov and Dingwell (1996 a, b) allows the investigation of magmatic fragmentation of natural samples upon rapid decompression under controlled conditions. Several studies have been developed in modified versions of this apparatus (Spieler et al., 2004a, b; Mueller et al., 2005, 2008; Kennedy et al., 2005; Kueppers et al., 2006 a, b; Scheu et al., 2006, 2008; Kremers et al., 2010) which have advanced the current understanding of magma fragmentation and the associated physical processes.

The fragmentation bomb mimics Vulcanian eruptions and provides a unique opportunity to investigate the influence of the fragmentation process on the dynamics of the gas-particle mixture and validate theoretical models. Moreover, the equations describing the ejection of the gas-particle mixture in a shock-tube system can be considered self-similar, which means that the solutions do not depend on the scale. For this reason, the results obtained in the laboratory can be applied to Vulcanian eruptions, provided that adequate values of the parameters and other constraints (geometry and dynamics of the gas above the sample) are considered.



Figures 1.3. Sketch of the glass transition in a plot of the deformation time against the reciprocal temperature. Above the glass transition, magma behaves as a viscous fluid and responds in a ductile manner to deformation. Below the glass transition, magma behaves as a solid resulting in brittle deformation and fragmentation. The glass transition curve can be crossed, from ductile to brittle behavior, either by cooling or by a fast deformation process. An enhancement in silica content increases the melt viscosity and thus widens the brittle field towards higher temperature. An increase of volatiles (water) shifts the glass transition to lower temperatures (modified after Dingwell, 1996).

1.5 General objective and thesis structure

Vulcanian eruptions are the more frequent type of explosive activity of Popocatepetl Volcano and ballistic projectiles are one of the most common hazards associated with this kind of eruptions. Accordingly, the main objective of this study is to establish a model for Vulcanian eruptions that relates the zones that could be affected by ballistic projectiles with the initial gas pressure and gas content. Since these parameters can be estimated by continuous monitoring techniques, this model will provide valuable information for more refined short-term hazard assessment. The model will be tested via fragmentation experiments with natural samples and then calibrated and validated with field and video observations of ballistics ejected during different Vulcanian eruptions at Popocatepetl Volcano. The maximum ranges expected for the ballistics in three different explosive scenarios defined for Popocatepetl Volcano will be presented in a ballistic hazard map. This map allows the exposed population and concerned authorities to plan the definition, development and mitigation of restricted areas during volcanic crises.

Chapter 2 is dedicated to the estimation of the energy that is consumed during fragmentation and a model of Vulcanian eruptions considering the ejection of the caprock propelled by the expansion of the gas-particle mixture after fragmentation. The model is applied to Vulcanian eruptions of Popocatepetl and Colima volcanoes. In Chapter 3 the influence of the fragmentation process itself on the eruption dynamics is investigated by exploring the relationship between fragmentation speed and ejection velocity, which were measured simultaneously in fragmentation experiments. It is shown that the fragmentation process controls the eruptive parameters and can significantly affect the eruption dynamics.

A general methodology to delimit the hazards zones by ballistic projectiles during volcanic eruptions is presented and applied to Popocatepetl Volcano in Chapter 4. A ballistic model is used to calculate the maximum expected range of the ballistics according to three different explosive scenarios. In the case of the Vulcanian eruptions, this model was used in concert with the caprock model presented in Chapter 2 to correlate ballistic range with the initial gas pressure and gas content. The coupled model is then calibrated and validated with field and video observations of ballistics ejected during different Vulcanian eruptions at Popocatepetl. Finally, chapter 5 presents the conclusions and outlook.

Chapters 2 to 4 of this thesis correspond to papers published in or submitted to peer-review journals. These articles appear with only small modifications in this thesis. While this causes some redundancies, it improves readability. These three chapters can be read independently. The relevant papers are (in order of their appearance):

Alatorre-Ibargüengoitia, M.A., Scheu, B., Dingwell, D.B., Delgado-Granados, H., and Taddeucci, J., 2010. Energy consumption by magmatic fragmentation and pyroclast ejection during Vulcanian eruptions. *Earth Planet. Sci. Lett.* 291, 60-69.

doi:10.1016/j.epsl.2009.12.051

Alatorre-Ibargüengoitia, M.A., Scheu, B., Dingwell, D.B., 2011. Influence of the fragmentation process on the dynamics of Vulcanian eruptions: An experimental approach, *Earth Planet. Sci. Lett.*, 302, 51-59. doi:10.1016/j.epsl.2010.11.045

Alatorre-Ibargüengoitia, M.A., Delgado-Granados, H., Dingwell, D.B. Hazard Map for Volcanic Ballistic Impacts at Popocatepetl Volcano (Mexico). Submitted to *Bulletin of Volcanology*. February 2011.

In addition, the application of the model to Vulcanian eruptions of Colima Volcano (Mexico) is part of the following paper:

Lavallée, Y., Varley, N. Alatorre-Ibargüengoitia, M. A., Hess, K.U., Kueppers, U. Mueller, S., Richard, D., Scheu, B., Spieler, O. and Dingwell, D.B. Magmatic architecture of dome-building eruptions at Volcán de Colima, Mexico. *Bulletin of Volcanology*, doi:10.1007/s00445-011-0518-4.

Chapter 2

Energy consumption by magmatic fragmentation and pyroclast ejection during Vulcanian eruptions¹

Abstract

Magmatic fragmentation during explosive eruptions consumes a significant amount of energy by the creation of new surface via fracturing. This process reduces the energy that can be imparted to the resulting pyroclasts in the form of kinetic energy. To date, models of Vulcanian eruptions have neglected the energy balance consumed by magmatic fragmentation. We present a 1-D model of Vulcanian eruption that considers the energy balance in rapid decompression of a pressurized magma below a caprock, followed by fragmentation and acceleration of particles. We then tested the model via decompression experiments at different temperatures (room vs 850 °C) and initial pressure (<20 MPa) with a fragmentation apparatus. Different series of experiments involving either fragmentation of an intact volcanic rock followed by ejection of the particles, or simply the ejection of loose particles were performed to quantify the energy consumed by fragmentation and the kinetic energy available to eject the particles. The ejection velocities observed in the fragmentation experiments of intact rocks are systematically lower than the ones with loose particles due to the energy consumed by fragmentation. This energy depends on the fragmentation threshold (i.e. the minimum pressure required to completely fragment the sample) and is inversely proportional to the fraction of pressurized pores. We propose that the effective pressure propelling the gas-particle mixtures after fragmentation corresponds to the pressure initially stored in the pore fraction minus the fragmentation threshold. We applied our caprock model to Vulcanian eruptions of Popocatepetl Volcano (February 2003) and Colima volcano (10 February 1999) and obtained gas pressures at the onset of fragmentation of 11-13 MPa and 19-22 MPa, respectively. These pressures might correspond to the gas pressures required to disrupt the caprock, fragment the underlying porous magma and eject the ballistics at the observed distances. The model presented herein may help describe the dynamics of Vulcanian eruptions, and improve hazard assessment.

¹ This chapter has been published as: Alatorre-Ibargüengoitia, M.A., Scheu, B., Dingwell, D.B., Delgado-Granados, H., and Taddeucci, J., 2010. Energy consumption by magmatic fragmentation and pyroclast ejection during Vulcanian eruptions. *Earth Planet. Sci. Lett.* 291, 60-69. doi:10.1016/j.epsl.2009.12.051

2.1 Introduction

Vulcanian eruptions are cannon-like explosions that occur when a caprock plugging the vent is disrupted (Morrisey and Mastin, 2000). In response to rapid decompression, magma may fragment explosively and erupt as a gas-particle dispersion. Magmatic fragmentation (i.e., in the case where magma does not interact with external water) is considered to occur when 1) gas pressure in the pores overcomes the dynamic tensile strength of the enclosing magma (Mc Birney and Murase, 1970; Alidibirov, 1994; Zhang, 1999; Alidibirov and Dingwell, 1996a, 2000; Spieler et al., 2004a); or 2) the strain rate of the melt exceeds its structural relaxation rate (Dingwell and Webb, 1989; Papale, 1999).

The minimum pressure differential that leads to complete fragmentation of the pressurized porous magma is called the fragmentation threshold and is inversely related to the porosity (Spieler et al., 2004a). Porosity is the key parameter as it holds the gas available for expansion during decompression and determines the bubble walls thickness, whereas chemical composition and crystallinity of magma appear to play minor roles on fragmentation processes (Spieler et al., 2004a). Koyaguchi et al. (2008) proposed a theoretical fragmentation criterion to explain the relationship between the fragmentation threshold and the porosity of the magma. They assumed that total fragmentation occurs when the tensile stress at the midpoint between pores exceeds the effective tensile strength of the magma. This effective strength is determined by Griffith theory considering a stress concentration at the crack tip. Their criterion can be expressed as follow:

$$P_{th} = \frac{2S_3(1-\phi)}{3\phi\sqrt{\phi^{-1/3}-1}} \quad (2.1)$$

where P_{th} is the fragmentation threshold, ϕ the porosity and S_3 is the effective strength. Mueller et al. (2008) presented an empirical equation to evaluate the influence of the permeability on P_{th} . They showed that the fragmentation behavior is influenced by permeability only if this is above a critical value ($\sim 10^{-12} \text{ m}^2$).

During magmatic fragmentation, most of the energy of the pressurized gas inside the pores is used to fracture the magma and accelerate the resulting gas-particle mixture. Fragmentation itself is expected to consume a considerable amount of energy in the formation of new

surfaces, thus significantly decreasing the energy available to accelerate the gas-particle mixture. Current models of conduit flow in volcanic eruptions (e.g. Sahagian 2005 and references cited therein) neglect the energy consumed by fragmentation. This lack of an estimate leads either to an overestimation of the pyroclast ejection velocity calculated considering a certain initial pressure, or to an underestimation of the initial gas pressure considering the pyroclasts ejection velocity (e.g. Fagents and Wilson, 1993; Nakada et al., 1999; Cagnoli et al., 2002; Taddeucci et al., 2004). Here, we stress that the fragmentation energy should be taken into account in models of Vulcanian eruptions.

Some models of Vulcanian eruptions have considered the acceleration of the caprock propelled by the expansion of an underlying pocket of gas (Self et al., 1979; Wilson, 1980; Fagents and Wilson, 1993). More recent models have considered the time history of the expansion of a gas-particle mixture according to the 1-D shock-tube theory (Turcotte et al., 1990; Ramos, 1995; Woods, 1995; Cagnoli et al., 2002). Although these latest models are more accurate, they neglect the ejection of the caprock which represents a significant proportion of the ballistics.

Here we present a 1-D model of the energy balance involved in fragmentation and ejection of pyroclasts caused by the destabilization of a caprock. We have tested this model via a series of controlled decompression experiments on natural volcanic rocks. Our setup allows for the quantification of ejection velocities of the caprock and the fragmented particles, and in turn enables the quantification of energy consumed by fragmentation. We demonstrate that the 1-D caprock model describes the observed ejection velocities and therefore can be used in concert with ballistic models (e.g. Alatorre-Ibargüengoitia and Delgado-Granados, 2006) to estimate the areas that could be affected by ballistics in Vulcanian eruptions.

2.2 Caprock model

The following theoretical model merges the criteria for fragmentation with the energy available to eject fragmented particles. As a first step, we simply propose that the effective pressure (P_{ef}) available for particle ejection is given by:

$$P_{ef} = P_o - P_{th} \quad (2.2)$$

where P_o is the initial sample pressure and P_{th} is the fragmentation threshold of the magma. The ejection velocity of the particles thus needs to rely on the surplus kinetic energy available after fragmentation.

The model proposed herein is an adaptation of the 1-D inviscid shock-tube theory (Turcotte et al., 1990; Ramos, 1995; Woods, 1995) which till now, had not taken into consideration the energy consumed by fragmentation. We consider the ejection of a caprock propelled by the expansion of an underlying gas-particle mixture assuming that: (1) the mixture behaves as a ‘pseudo-gas’ (e.g. Woods, 1995; Formenti et al., 2003; Koyaguchi and Mitani, 2005); (2) viscosity, heat conduction, wall friction and weight of the mixture can be neglected (Turcotte et al., 1990; Woods, 1995); and (3) only pyroclasts smaller than a certain size (depending on the expansion time) remain in thermal equilibrium with the gas (Woods, 1995). Under these conditions the movement equation of the caprock propelled by the expansion of the gas-particle mixture is (see appendix 2A for derivation):

$$\frac{dV}{dt} = \frac{A_c}{m} \left\{ P_{ef} \left[1 - \frac{1}{2}(\gamma - 1) \frac{V}{\sqrt{n\gamma RT_o}} \right]^{\frac{2\gamma}{\gamma-1}} - P_{ext} \right\} - g \quad (2.3)$$

where V represents the caprock velocity and also corresponds to the velocity at the top of the underlying gas-particle mixture, m and A_c are mass and cross-sectional area of the caprock, respectively, t is time, γ is the specific heat capacity ratio of the mixture considering only the fraction of particles in thermal equilibrium with gas (see appendix 2A), n is the mass fraction of gas, R is the gas constant, T_o is the initial temperature, P_{ext} is the pressure above the caprock (see appendix 2B) and g is gravitational deceleration. Eq. 2.3 can be solved numerically to obtain the caprock velocity as a function of time as long as the flow remains one-dimensional.

The caprock reduces the velocity of the gas-particle mixture because part of the energy is used to accelerate it, but also reduces the amount of gas that can escape and thus maintains the coupling between gas and particles. When maintaining the same conditions and assumptions as mentioned before but without considering the presence of a caprock, the ejection velocity at the top of the gas-particle mixture (v) would be given by (see appendix 2A for derivation):

$$v = \frac{2\sqrt{n\gamma RT_o}}{\gamma - 1} \left[1 - \left(\frac{P_{ext}}{P_{ef}} \right)^{\frac{\gamma-1}{2\gamma}} \right] \quad (2.4)$$

This equation corresponds to the model proposed originally by Woods (1995). If most of the particles remain in thermal equilibrium with the gas phase, $\gamma \sim 1$ and Eq. 2.4 can be approximated by the isothermal expression proposed by Turcotte et al. (1990):

$$v = \sqrt{nRT_o} \ln\left(\frac{P_{ext}}{P_{ef}}\right) \quad (2.5)$$

2.3 Experimental method

Several studies have been developed in the fragmentation apparatus used here (Alidibirov and Dingwell, 1996 a, b; Spieler et al., 2004a; Mueller et al., 2005; Kennedy et al., 2005; Kueppers et al., 2006 a, b; Scheu et al., 2006), which is a shock-tube apparatus consisting of a high-pressure steel autoclave (corresponding to a volcanic conduit) overlain by a voluminous tank at atmospheric conditions (Fig. 2.1). Pressurization of the autoclave and subsequent depressurization is regulated by a system of three scored diaphragms that open at a reproducible pressure differential. This setup mimics Vulcanian eruptions.

Cylindrical samples drilled from volcanic rocks are loaded in the autoclave, pressurized with Argon gas to the desired experimental pressure and heated with an external furnace to 850° C. Decompression of the autoclave is triggered by opening a valve which induces the failure of the uppermost diaphragm, followed by the immediate failure of the other two diaphragms. The rapid decompression of the high-pressure autoclave induces a rarefaction wave that travels through the sample. If the resulting pressure differential is sufficient, the sample fragments brittlely layer-by-layer (Alidibirov and Dingwell, 2000; Fowler et al., 2010) and the fragments are ejected into the voluminous tank. After every experiment, we used desalinated water to rinse the voluminous tank and thus recover more than 99% of the initial sample mass.

The ejection velocities of fragmented particles are measured via a set of four charged copper wires obstructing the ejecta trajectory in the voluminous tank (Fig. 2.1). The wires are held in a plastic tube placed above the diaphragms and when the ejecta break a wire, the electric signal drops and the corresponding time is recorded. Particle ejection velocity is calculated using the signal-drop times and distance between wires. Complementary experiments performed at room temperature were filmed using a high-speed camera (NAC

HotShot 512 SC) at 10,000 frames per second to measure the ejection velocity of particles throughout the experiment (in contrast with the wire setup which allowed for the monitoring of the plate solely) and validate the velocities obtained with the wires during high-temperature experiments.

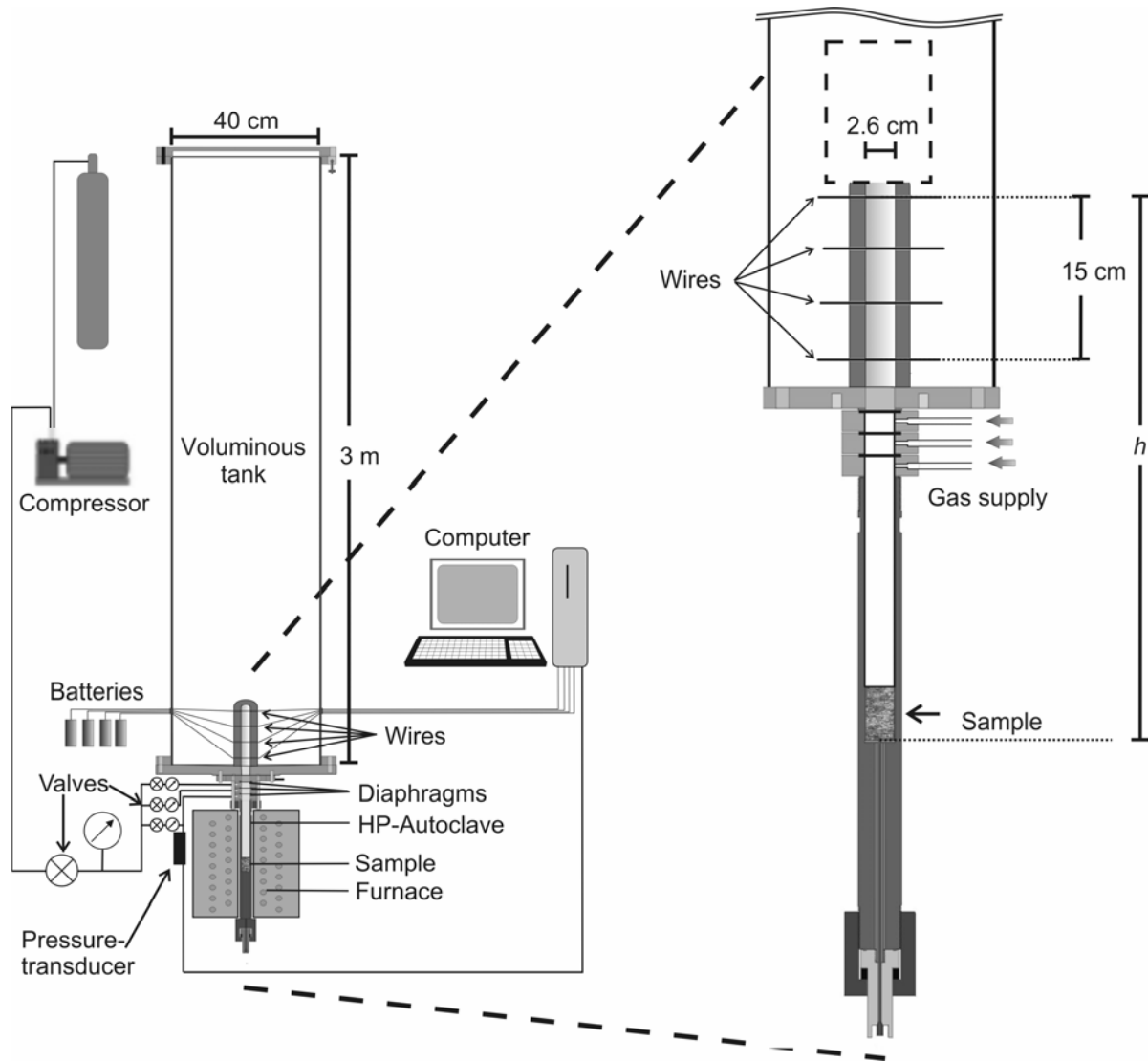


Figure 2.1. Experimental setup of the fragmentation apparatus. The sample ($l = 6$ cm, $d = 2.5$ cm) is placed in the high pressure (HP-) autoclave and heated with an external furnace. A set of diaphragms allows reproducible pressurization of the sample using Argon gas. After disruption of the diaphragms, the particles are ejected into the voluminous tank at atmospheric conditions. Four charged-wires are placed inside a plastic tube, and their disruption by the ejected caprock is used to measure the ejection velocity. The dashed box indicates the area observed with the high-speed camera (ca. 12 cm high). Modified from Kueppers et al. (2006a).

In order to simulate the ejection of a caprock during Vulcanian eruptions, we placed a cylindrical plate of either dense rock or steel² loosely on top of the samples. Moreover, this plate efficiently disrupts the charged wires and as such ensures the reproducibility of the measured velocities.

To investigate the influence of the fragmentation energy and the grain-size distribution of the particles on the dynamics of the gas-particle mixture, we performed sets of experiments with three different kinds of samples (Fig. 2.2): cylindrical samples drilled from volcanic rocks (type I), loose particles with a complex grain-size distribution, produced by fragmentation in a type I experiment (type IIa) and monodisperse particles (type IIb). For experiments on loose particles (type IIa), the volume occupied by the gas-particle mixture was extended because it was impossible to place all the particles in the volume of the original cylinder. In this case, the initial mixture porosity was calculated from the mixture volume and the density and mass of the particles.

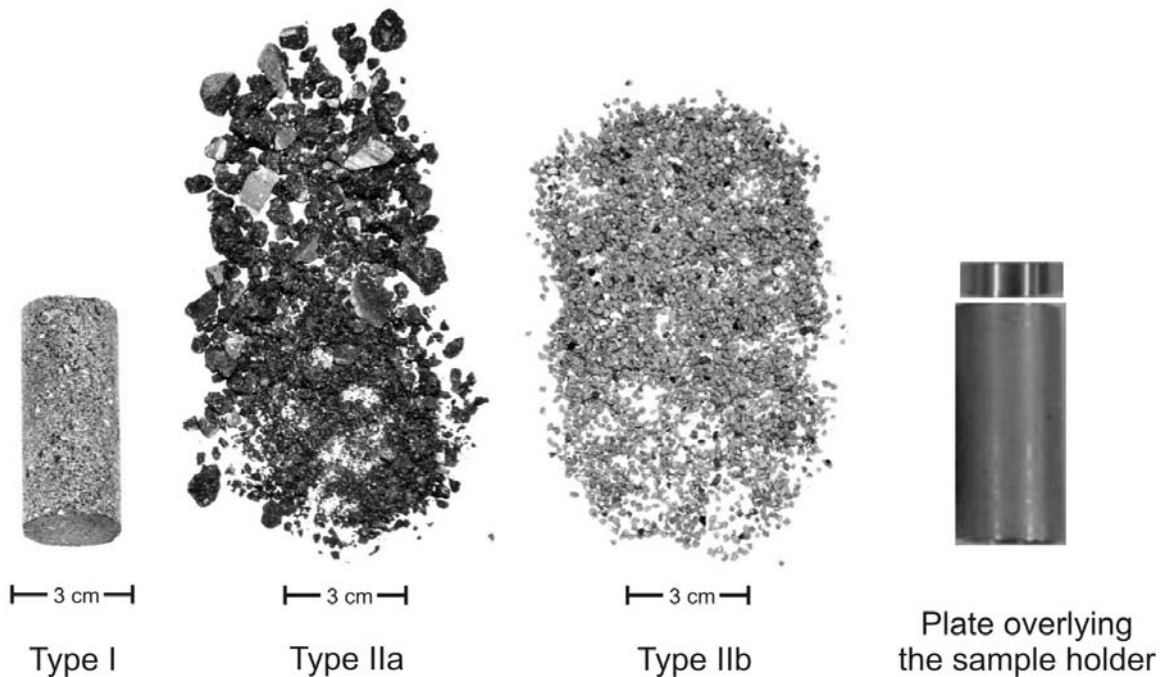


Figure 2.2. Pictures of the types of samples used in the experiments: cylindrical core drilled from a natural volcanic rock (type I), pre-fragmented particles with the original grain-size distribution produced by fragmentation during decompression (type IIa) and monodisperse rock particles (type IIb). All the samples were placed inside a sample holder (6 cm high, 2.5 cm internal diameter). In experiments mimicking the presence of a caprock in Vulcanian eruptions, a plate was loosely set atop the sample.

² The first experiments were performed with dense rock plates but later steel plates were used to standardize the caprock mass and avoid fragmentation of the plates in experiments performed at higher pressures. We observed no difference in the experiments related to the material of the plates.

Samples from explosive eruptions of Popocatepetl Volcano were used in this study. We selected pumice fragments from the pyroclastic flow deposit produced on January 22, 2001 (Smithsonian Institution, 2000) and dense ballistic blocks from a crater dome which were ejected during the explosive events of February 2003 (Smithsonian Institution, 2003a). The pores inside these samples are in general non-spherical (Fig. 2.3). We measured the density and porosity of all the samples by Helium pycnometry (Accupyc 1330, Micrometrics, USA). The ballistic blocks have open (interconnected) porosities of 3-21% and closed (isolated) porosities of 1-1.5%. The pumice fragments have open porosities of 56-73% and closed porosities of 1-3%. Closed pores are few and during an experiment they do not get pressurized by Argon; as such, their contribution in the energy from gas expansion is negligible.

The chemical composition of both kinds of samples, the 2001 pumice and 2003 ballistic blocks, ranges from andesite to dacite (SiO_2 of 61-65%), similar with the compositions reported for other explosive events of Popocatepetl Volcano (Martín del Pozzo et al., 2003; Witter et al., 2005). Phenocrysts are up to 4 mm long (although the majority are <1 mm) and their abundance ranges from 25 to 45 vol.% (vesicle-free basis) in the block samples, and from 30 to 50 vol.% (vesicle-free basis) in the pumice samples. The main phenocrysts are plagioclase (75-80%), pyroxene (10-15%), amphibole (<5%), Fe-Ti oxides (<5%) and olivine only in the andesite samples (5-10%).

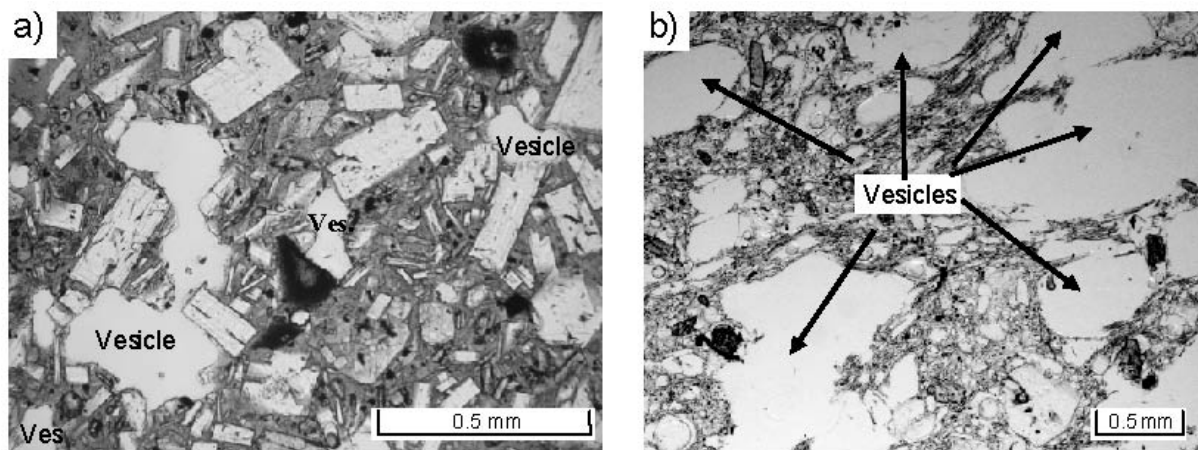


Figure 2.3. Thin section photographs of Popocatepetl samples. (a) Image of a block sample with 15% open porosity. Phenocrysts (mostly plagioclase) are often in contact with the vesicles. (b) Image of a pumice sample with 58% open porosity.

2.4 Results

The first set of experiments involved the fragmentation of the type I samples at 850°C to assess the fragmentation threshold. Results for samples with different porosity are in agreement with the fragmentation threshold obtained in previous studies (Fig. 2.4; e.g., Spieler et al., 2004a). Our threshold data is found to be inversely proportional to the open porosity and can be approximated with the theoretical fragmentation criterion of Koyaguchi et al. (2008). We find that an effective tensile strength of 2 MPa (S_3 in Eq. 2.1) reproduces best the data presented in Figure 2.4. The high porous samples of Popocatépetl Volcano deviate from this criterion because of their high permeability which significantly reduces the pressure differential in and below a fragmentation layer (Mueller et al., 2008). In the decompression experiments using a plate as caprock analogue, the obtained fragmentation threshold is equivalent to that obtained for experiments not topped by a plate, which suggest a negligible effect of the plate on the fragmentation threshold.

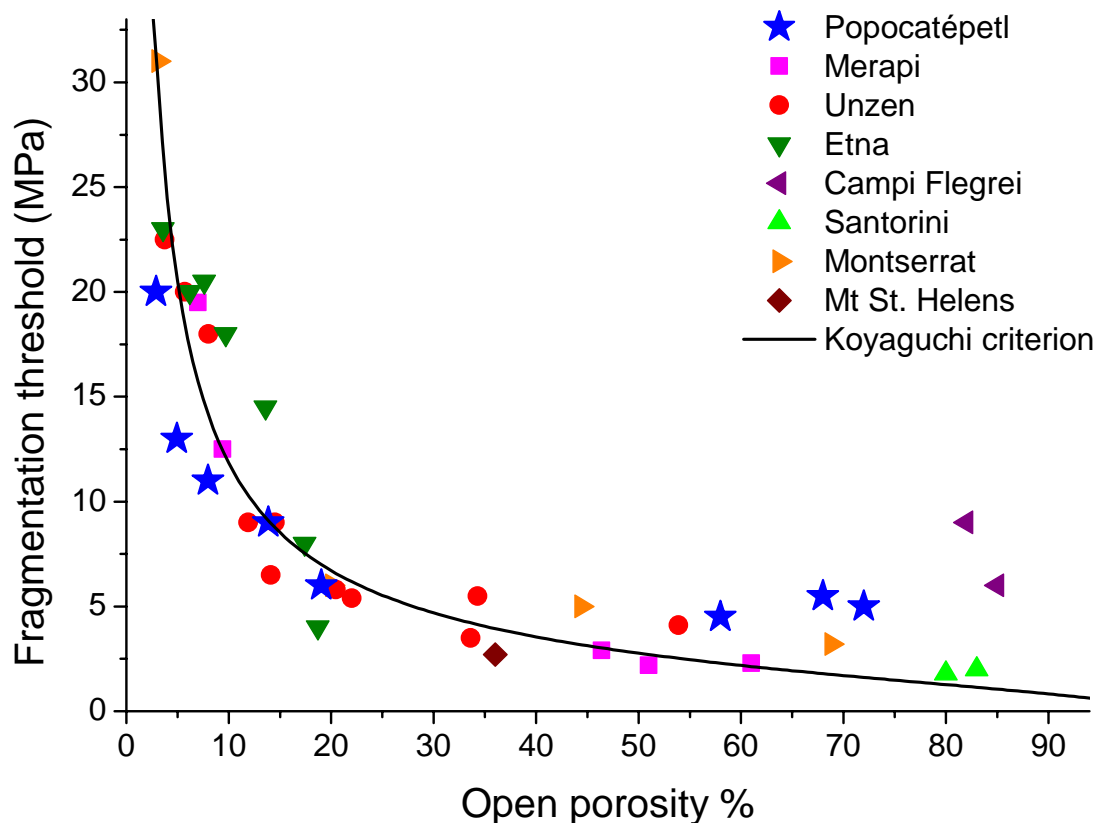


Figure 2.4. Fragmentation threshold of volcanic material at 850 °C during rapid decompression (modified from Spieler et al., 2004a). Experimental data obtained in this study using Popocatépetl sample are also compiled (stars). The line corresponds to the fragmentation criterion (Eq. 2.1) proposed by Koyaguchi et al. (2008), assuming that the effective tensile strength of the material is 2 MPa.

Below the fragmentation threshold ($<P_{th}$), the sample does not fragment or it does only partially. In the absence of fragmentation, no particles were ejected. Partial fragmentation occurs if the initial pressure is within ~ 1.5 MPa below P_{th} . Since in this case the experiment does not fully achieve our fragmentation criteria, we consider the velocity to be 0 m/s. Above the fragmentation threshold, all fragments as well as the plate were ejected out of the autoclave. Ejection of the plate disrupted the charged wires at a constant rate (i.e., without showing any acceleration). Figure 2.5a shows that a pressure threshold needs to be exceeded to instigate fragmentation and that only the remaining pressure is used to accelerate the fragments. Moreover, we observed that the ejection velocity of the plate increases non-linearly with applied pressure. The parameters used in the calculations are given in Table 2.1.

In order to calibrate the model in the absence of fragmentation and thus highlight the effect of kinetic energy used to eject the fragments, experiments using loose particles (type IIa) topped by a plate were performed at room temperature (Fig. 2.5b). In this case, we observed ejection of fragments even at low pressures (i.e., at initial pressures below that of P_{th} for an intact sample with an equivalent porosity). Likewise, the ejection velocity of the plate increased non-linearly with an increase in initial pressure. Grain-size analysis of the loose particles before and after the experiments reveals that during a second decompression test, only minor re-fragmentation of particles takes place (i.e., the mean diameter is only reduced by an additional 20%).

Parameter	Experiments	Popocatépetl	Colima
Caprock specific area m/A_c (kg/m ²)	21	65000	37500
Specific gas constant R (J kg ⁻¹ K ⁻¹)	207.8 (Ar)	461.7 (H ₂ O)	461.7 (H ₂ O)
Gas specific heat capacity C_v (J kg ⁻¹ K ⁻¹)	312 (Ar)	2000 (H ₂ O)	2000 (H ₂ O)
Magma specific heat capacity C_s (J kg ⁻¹ K ⁻¹)	1400	1400	1400
Fraction of particles in thermal equilibrium with the gas f (%)	0-0.1	10	10
Temperature T (K)	1123	1123	1123
Magma mean porosity ϕ (%)	10-67	65	26 ^{a)}
Fragmentation threshold P_{th} (MPa)	Fig. 4	5.5	6 ^{a)}

Table 2.1. Values of the parameters used for the simulations corresponding to the experiments (Fig. 2.5) and the application to natural cases (Fig. 2.8). The caprock specific area in Vulcanian eruptions was calculated from $m/A_c = \rho_c \cdot T_c$ where ρ_c and T_c are the density and thickness of the caprock, respectively. It is worth noting that the main differences between the values used for the experiments and the Vulcanian eruptions are that in the second case the caprock specific area is much higher, we consider water vapor instead of Argon gas and the time of the eruptions (few seconds instead of 5-10 ms in our experiments) allows a larger fraction of particles to remain in thermal equilibrium with gas during decompression. In the case of the experiments, the value of the parameter f was estimated from the fraction of particles smaller than the 0.063 mm sieve. The magma specific heat capacity was calculated with CONFLOW software (Mastin and Ghirso, (2000) and references cited therein). ^{a)} Data from Lavallée et al. (submitted for publication).

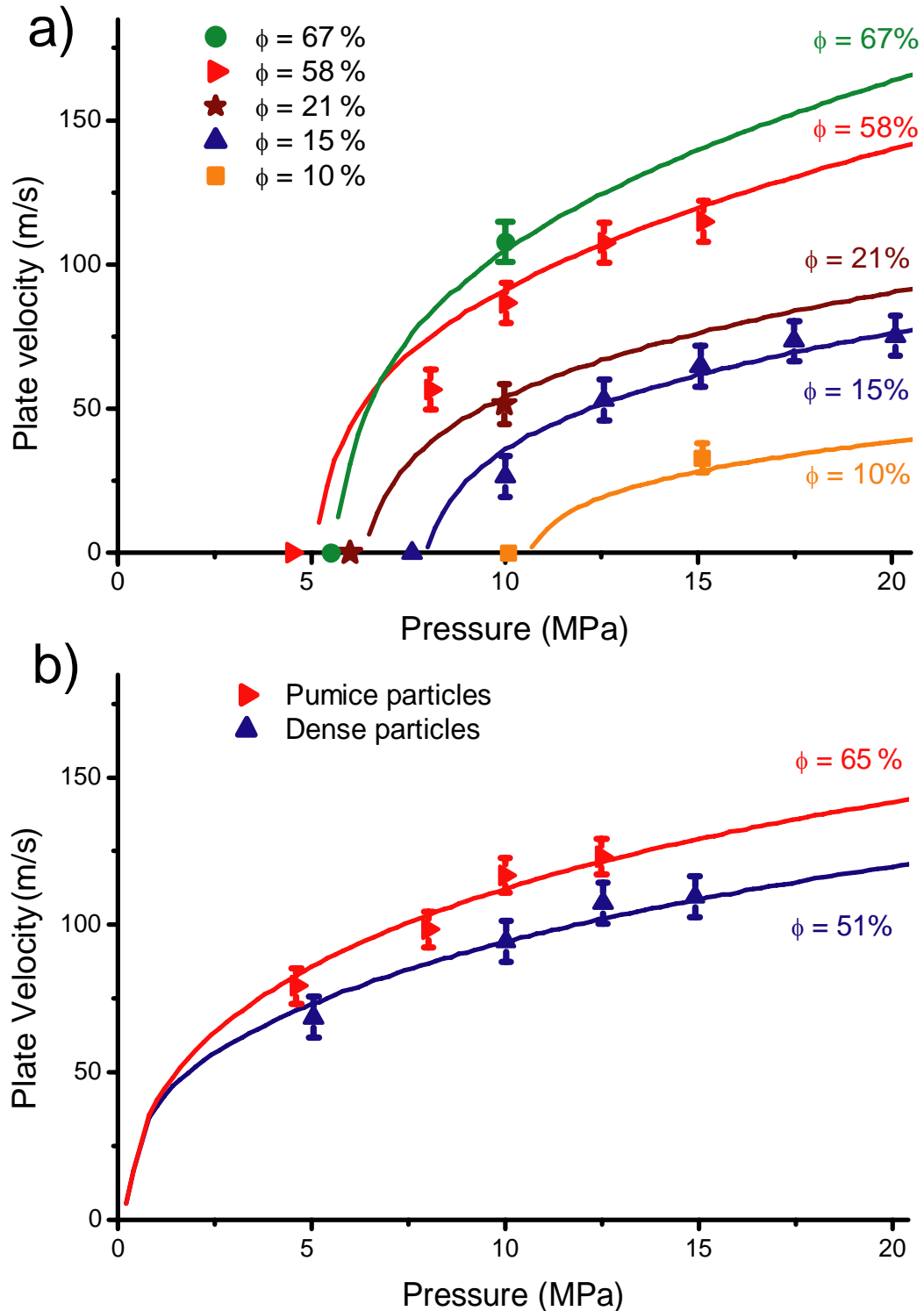


Figure 2.5. Ejection velocities of a plate set on top of a) type I samples, and b) type IIa samples. With type I samples, a threshold had to be exceeded for fragmentation and ejection of the plate to take place; hence, the velocity at the fragmentation threshold are set to 0 m/s. With type IIa samples, the sample did not require fragmentation to be ejected and therefore particles are accelerated even at low applied pressures. The lines are obtained from theoretical calculation using Eq. 2.3 with $P_{ef}=P_0-P_{th}$ and $T=850^\circ\text{C}$ (in type I experiments), and $P_{ef}=P_0$ and $T=22^\circ\text{C}$ (in type IIa experiment). The other parameters used in these simulations are given in Table 2.1.

The effect of fragment size on the ejection velocity was investigated through experiments on monodisperse particles (type IIb) ranging between 0.5 and 8 mm (Table 2.2). The comparison of the velocities measured in experiments with a plate with our theoretical calculation using Eq. 2.3 revealed an agreement within an experimental uncertainty of 8% (Table 2.2, Fig. 2.5). In contrast, experiments without a plate did not yield reproducible velocities calculated via Eq. 2.4 (Table 2). These observations suggest that the presence of a plate prevents gas from significantly escaping and, in turn, support the assumption that the plate is propelled by the expansion of an underlying gas-particle mixture which is approximately in mechanical equilibrium. Nevertheless, this assumption is not valid for decompression experiments that are not capped by a plate, and adequate interphase drag terms would need to be considered during high-acceleration stages (Chojnicki, et al., 2006).

Particles size (mm)	Particles mass (g)	Plate mass (g)	Temperature (°C)	V_{measured} (m/s)	V_{theory} (m/s)	Difference (%)
8	22.8	16.1	22	83.6	93.3	10.4
1.4	27.6	8.0	22	89.9	96.0	6.3
0.5	29.3	17.2	22	82.1	84.4	2.7
1.4	27.5	7.0	850	115.6	115.1	- 0.5
2.8	27.8	0	22	82.8	112.9	26.7
2.8	28.1	0	22	78.7	112.0	29.8

Table 2.2. Maximum ejection velocities for monodisperse particles (type IIb samples) during decompression experiments at $P_o = 10$ MPa. The experimental uncertainty in the determination of the ejection velocities with the charged-wires was estimated to be around $\pm 8\%$. The calculated velocities of experiments with and without a plate were obtained with Eqs. 2.3 and 2.4, respectively. The maximum velocities of the particles in the experiments without a plate were measured with the high-speed camera. The difference between measured and calculated velocities is defined as $(V_{\text{theory}} - V_{\text{measured}}) * 100 / V_{\text{theory}}$.

In complementary experiments performed at room temperature the ejection velocities of particles throughout the experiment were monitored using a high-speed video camera. Videos of experiments performed with loose particles with and without a plate can be found in the supplementary material. The measured velocities of the plate were found to be within the uncertainty of the measurements with the wire setup ($\sim 8\%$). In all the experiments, with and without a plate and with the three kinds of samples, we observed a non-linear decay of the velocity of particles as a function of time irrespective of their size (ranging between 0.5 and 8 mm; Fig. 2.6). We suggest that most of the kinetic energy is released at the initial stage of the flow. This might be due to the fact that the pressure gradient is higher at the beginning and that there is more gas coming from below. As decompression continues and the upper layer of fragments gets ejected, less gas is available beneath to accelerate the following layers. We

empirically fitted the velocity of the particles (v_p) as a function of time (t) and distance from the bottom of the sample (h ; see Fig. 2.1):

$$v_p = \frac{v_{\max}}{1 + \frac{v_{\max}}{h} t} \quad (2.6)$$

where $t=0$ corresponds to the time in which the first particle is observed and v_{\max} is the maximum measured velocity.

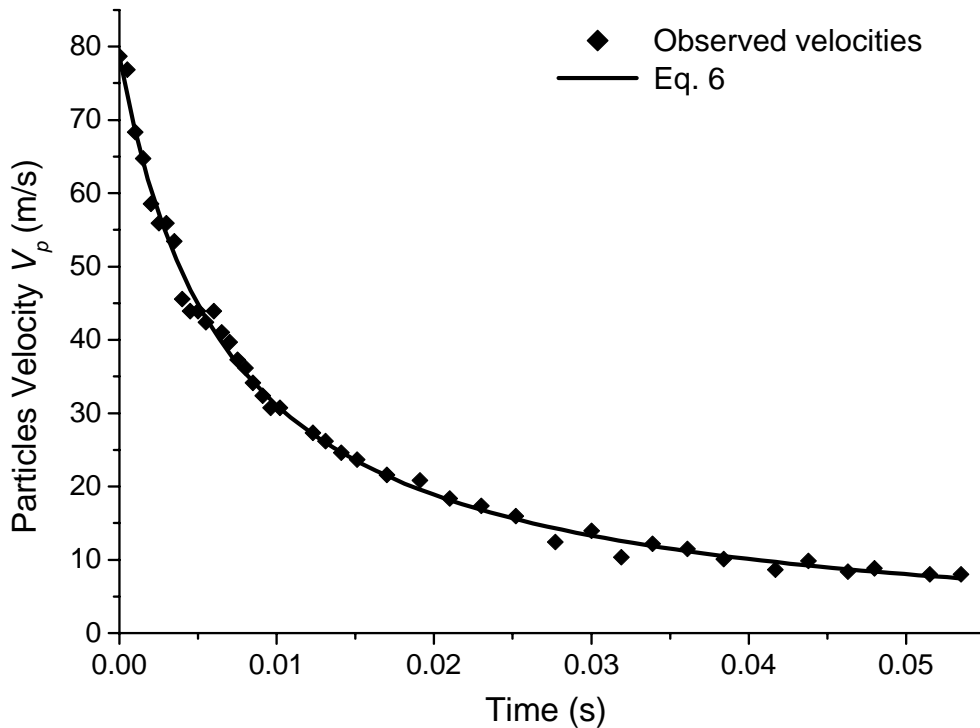


Figure 2.6. Example of ejection velocities of particles measured through image analysis of high-speed camera footage. This decompression experiment (type IIb not topped by a plate) was performed at room temperature and $P_o = 10$ MPa. The temporal decrease of velocities was similar for experiments with type I, IIa, and IIb samples, with and without a plate. The velocity of the particles decays with time according to the empirical equation (2.6).

2.5 Fragmentation energy

The energy of the compressed gas stored in the pores in a unit volume of the sample (ρ_{E-g}) corresponds to the adiabatic work that is done by the gas when the initial pressure P_o decreases to the ambient pressure P_a , and is given by (Alidibirov, 1994):

$$\rho_{E-g} = \frac{P_o \phi}{\gamma - 1} \left[1 - \left(\frac{P_a}{P_o} \right)^{\frac{\gamma-1}{\gamma}} \right] \quad (2.7)$$

As Eq. 2.2 reveals, the fragmentation process reduces the gas pressure from P_o to P_{ef} . Accordingly, the energy consumed by fragmentation in a unit volume (ρ_{E_f}) can be estimated by replacing P_a in Eq. 2.7 with $P_{ef} = P_o - P_{th}$:

$$\rho_{E_f} = \frac{P_o \phi}{\gamma - 1} \left[1 - \left(\frac{P_o - P_{th}}{P_o} \right)^{\frac{\gamma-1}{\gamma}} \right] \quad (2.8)$$

Equation 2.8 shows that ρ_{E_f} is not a constant, but depends on P_o , γ , ϕ and P_{th} (which also depends on ϕ , Fig. 2.4). The ratio ρ_{E_f}/ρ_{E_g} represents the fraction of the initial energy that is consumed by fragmentation. This ratio is close to one if $P_o \sim P_{th}$ and decreases as P_o increases (for instance, $\rho_{E_f}/\rho_{E_g} \sim 0.2$ if $P_o = P_{th} + 10$ MPa). Figure 2.7a shows the ρ_{E_f} values estimated for our experiments performed at $P_o = 10$ MPa and $P_o = 15$ MPa. This figure shows that the ρ_{E_f} values computed considering the experimental P_{th} for pumice samples ($\phi = 58\%$ and $\phi = 67\%$) are much above the ρ_{E_f} values computed considering P_{th} obtained with Eq. 2.1. This may be due to their high permeability, in which case, the value of ρ_{E_f} estimated with Eq. 2.8 corresponds not only to the energy required to fracture the sample, but also to the energy lost by gas filtration during fragmentation.

The energy consumed by fragmentation in Vulcanian eruptions can be estimated using Eq. 2.8 considering the appropriate value of γ instead of $\gamma = 1.67$ corresponding to Argon gas used in the experiments. Figure 2.7b shows that the amount of energy consumed by fragmentation increases as γ decreases. However, the energy stored in the compressed gas also increases as γ decreases, and therefore the ratio ρ_{E_f}/ρ_{E_g} in Vulcanian eruptions is expected to be similar to the experiments with the same P_o .

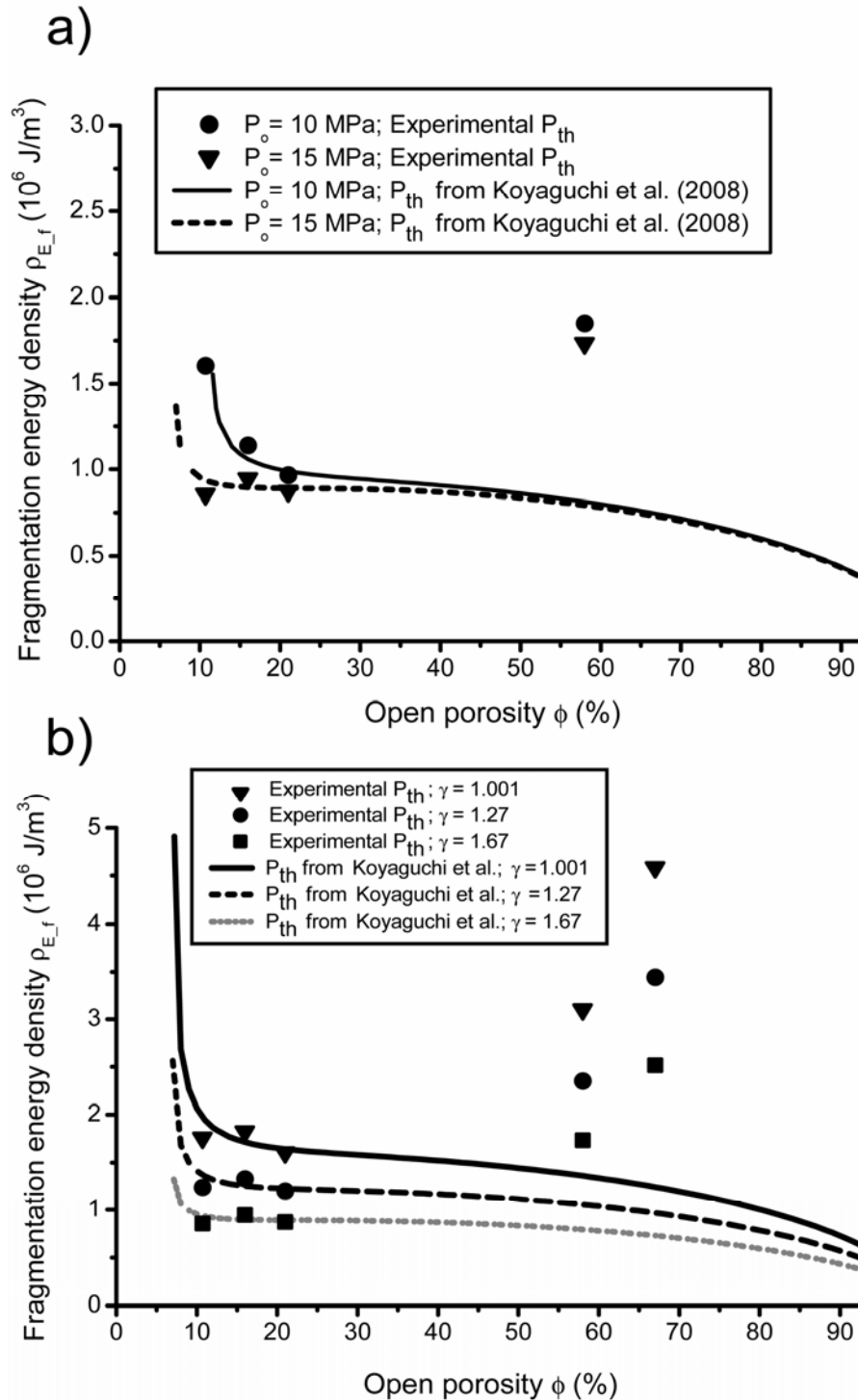


Figure 2.7. Energy consumed by fragmentation in a unit volume of sample (ρ_{E_f}) estimated with Eq. 2.8. The symbols indicate the values computed with the P_{th} measured experimentally for the samples of Popocatepetl Volcano used in this study, whereas the lines indicate the estimations considering P_{th} from the fragmentation criterion of Koyaguchi et al. (2008) (Eq. 2.1). a) ρ_{E_f} computed for the experiments performed at $P_o=10$ MPa and $P_o=15$ MPa ($\gamma = 1.67$). b) ρ_{E_f} computed using $P_o=15$ MPa and different specific heat capacity ratios: $\gamma=1.67$ (Argon gas), $\gamma=1.27$ (water vapor at 850° C) and $\gamma\sim 1$ (isothermal expansion where the gas and particles are in thermal equilibrium). Both graphs show that for the porous samples there is a significant difference between the values estimated considering the experimental P_{th} with respect to the values estimated with P_{th} given by the criterion of Koyaguchi et al. This difference may be due to the high permeability of these samples (see text section 2.5).

2.6 Discussion

Vulcanian eruptions are violent processes that restrict direct observation; especially, magma ascent and fragmentation remain unclear. During our experiments, the fragmentation threshold that leads to complete failure of magma is inversely proportional to the fraction of pressurized pores and is on the order of 5 to 20 MPa. Experimental conditions may differ from those in nature and as such can only approximate the overpressure at which ascending magma will fragment during the course of a Vulcanian eruption. Consequently, experimental data should be combined with field observations.

The initial gas pressure in volcanic eruptions is commonly estimated from the ejection velocities of ballistics (e.g. Fagents and Wilson, 1993; Nakada et al., 1999; Cagnoli et al., 2002; Formenti et al., 2003; Taddeucci et al., 2004). Here, we reiterate that these models have overlooked the energy consumed by fragmentation, which may represent a significant portion of the energy initially stored in the magma. The energy balance considered in the caprock model allows us to estimate the gas pressure at the onset of fragmentation during Vulcanian eruptions based on the ejection velocity of ballistics.

We applied the caprock model to the February 2003 eruptions of Popocatépetl Volcano, which expelled incandescent ballistic fragments to a maximum distance of 2.7 km from the crater. The conduit at Popocatépetl was plugged by a lava dome (i.e., caprock) with an average thickness of ~25 m, and we assume a porosity of the underlying magma of ~65% (which is the most common value observed in the pyroclastic flow deposit). Using the ballistic model of Alatorre-Ibargüengoitia and Delgado-Granados (2006), we estimate the initial velocities of the ballistics to range between 130 and 160 m/s. Figure 2.8a shows the initial gas pressures corresponding to these velocities calculated with the caprock model with and without the energy consumed by fragmentation and with the models of Woods (1995) and Turcotte et al. (1990) which neglect the ejection of the caprock. The values of the parameters used for the simulations are shown in Table 2.1.

Using the caprock model and considering the fragmentation energy we estimate initial pressures of 11-13 MPa, whereas pressures of 7-9 MPa are obtained if this energy is not taken into account. The latter pressures are around 50% lower with respect to the former, which

shows that, in this case, significant amount of energy was used to fragment the magma. On the other hand, using the models of Woods (1995) and Turcotte et al. (1990) we obtain initial pressures of 2-3 MPa (Fig. 2.8a). These pressures are much lower because these models do not consider the energy consumed by magmatic fragmentation and the energy required to accelerate the caprock. The calculated pressures of 11-13 MPa might correspond to the gas pressures required to disrupt the caprock, fragment the underlying porous magma and eject the ballistics at the observed distances.

We also applied the caprock model to the Vulcanian eruption of Colima volcano on 10 February 1999 which ejected ballistic blocks of up to 80-90 cm as far as ~4 km from the vent (Smithsonian Institution, 1999). Using the ballistic model of Alatorre-Ibargüengoitia and Delgado-Granados (2006), we estimate the initial velocities of these blocks to range between 180 and 200 m/s. The porosity of the juvenile magma at Colima is in average 26%, and the fragmentation threshold corresponding to this magma is ~6 MPa (Lavallée et al., submitted). Assuming a 15-m thick caprock (Smithsonian Institution, 1999), we estimate the initial pressure for this eruption at 19-22 MPa (Fig. 2.8b). For comparison, using the caprock model without considering the energy consumed by fragmentation we obtain pressures of 16-19 MPa, whereas using the models of Woods (1995) and Turcotte et al. (1990) we find pressures of 9-11 MPa (Fig. 2.8b). In this case, the pressure calculated with the caprock model without considering the fragmentation energy is only ~20% less with respect with the pressure calculated taking this energy into account because the calculated pressures are significantly higher than the fragmentation threshold of the magma. In the case of Colima, 19-22 MPa might represent the pressures required to disrupt the caprock, fragment the underlying porous magma and eject the ballistics at the observed distances.

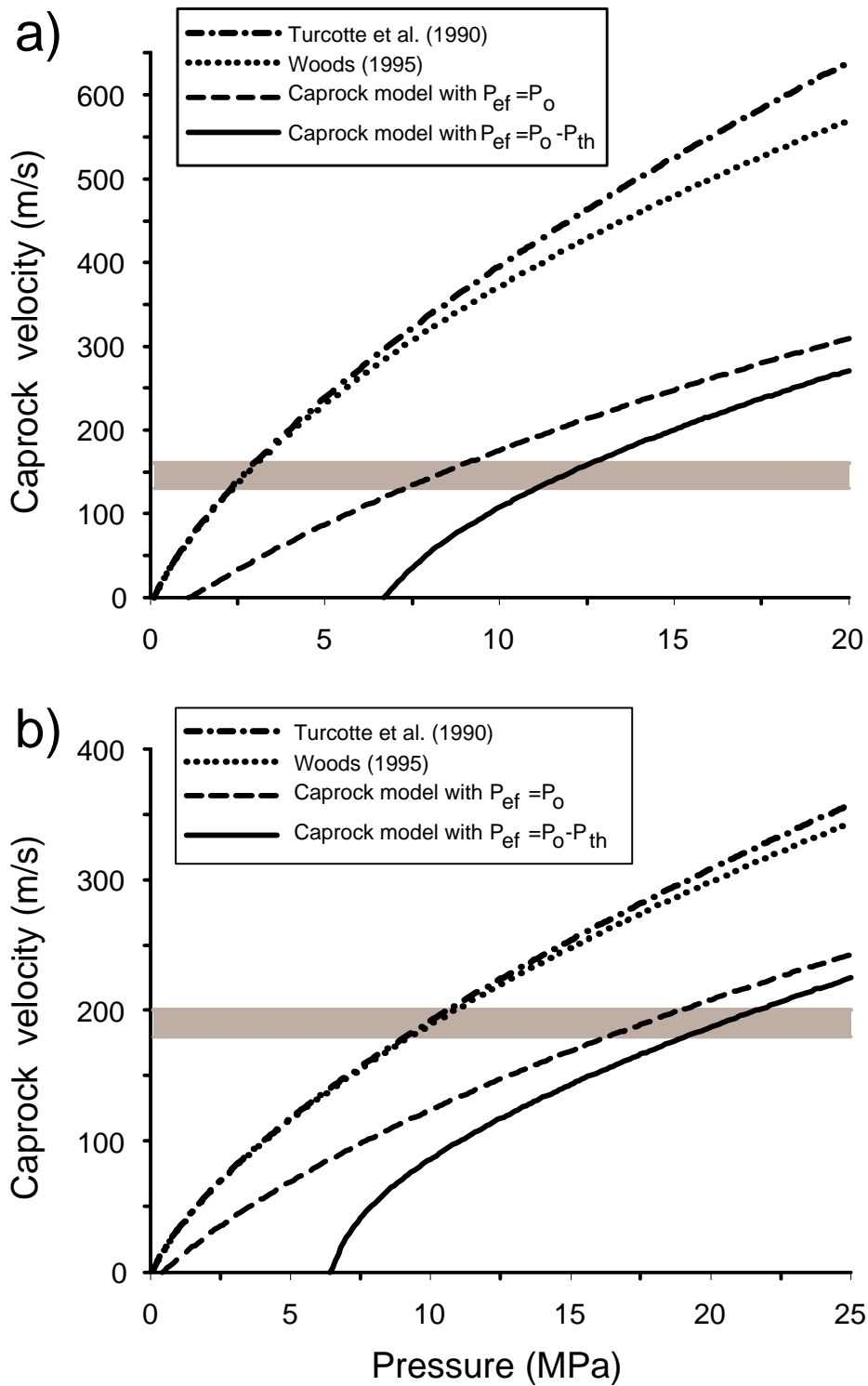


Figure 2.8. Application of different models to the Vulcanian eruptions of Popocatepetl Volcano (a) and Colima volcano (b): Caprock model taking into account the energy consumed by fragmentation (Eq. 2.3 with $P_{ef} = P_o - P_{th}$), caprock model without considering this energy (Eq. 2.3 with $P_{ef} = P_o$), the model of Woods (1995) (Eq. 2.4) and the model of Turcotte et al. (1990) (Eq. 2.5). The gray boxes indicate the range of the ejection velocities of the ballistics expelled by each volcano. The parameters used in these simulations are given in Table 2.1.

The pressures estimated above should be considered as lower limits for the following reasons:

- 1) The caprock model can only be applied for the first few seconds of expansion because gas-particle flows in the atmosphere is too complex to be approximated as one-dimensional;
- 2) In Vulcanian eruptions, fragmentation promote permeable gas loss, thereby reducing the coupling of the gas-particle mixture and the energy available for ejection;
- 3) In general, the external pressure P_{ext} in Eq. 2.3 corresponds to the pressure after the shock wave, which should be calculated using standard equations for shock waves (e.g. Landau and Lifshitz, 1987). However, if the decompression is caused by the collapse of a caprock resting on the top of a conduit, the shock wave will be nearly spherical and its intensity will drop quickly; in this case, the external pressure could be approximated to atmospheric pressure (Cagnoli et al., 2002).

Another important limitation of our model is that Eqs. 2.2 and 2.8 correspond solely to the static component of the fragmentation energy and do not account for the dynamics of fragmentation, which is a complex process that requires a more comprehensive parameterization.

Despite the limitations, the caprock model retrieves consistent estimates of fragmentation threshold and ejection velocities, and yields plausible eruptive scenarios. This model can be combined with a ballistic model to calculate the maximum range of projectiles under different explosive scenarios and define ballistic-related-hazard zones to improve hazard assessment (e.g. Alatorre-Ibargüengoitia et al., 2006). Calculating more realistic gas pressures at the onset of fragmentation is important to adequately interpret the data obtained by monitoring techniques such as ground deformation and gas emissions. Future applications would benefit from an increase coupling of geophysical data (seismic and ground deformation) with Doppler radar measurements during monitoring of Vulcanian eruptions.

Moreover, the parameter h in the empirical Eq. 2.6 holds the premise that the evolution of velocities of particles measured by Doppler radar during Vulcanian eruptions may be used to infer the maximal depth reached by fragmentation. Nevertheless, this equation can only be applied when the amount of exsolved gas does not change during the course of the eruption and the magma volume involved is small enough so that the pressure is approximately constant. If a pressure gradient exists, the density of the gas will change with depth and Eq. 2.6 might break down.

2.7 Summary

We presented a 1-D model considering the energy balance involved in fragmentation and ejection of pyroclasts induced by the destabilization of a caprock. We assumed that in Vulcanian eruptions the caprock is propelled by the expansion of a gas-particle mixture which is approximately in mechanical equilibrium, and validated our model through a series of decompression experiments on volcanic rocks and on loose volcanic particles. The ejection velocities observed in the fragmentation experiments of intact rocks are systematically lower than the ones with loose particles. We propose that the effective pressure available to eject the particles after fragmentation corresponds to the difference between the pressure from the gas initially stored in the pores and the fragmentation threshold. We estimated the energy consumed by fragmentation and found that it represents a significant amount of the initial energy and therefore should be considered in models of explosive eruptions.

We applied our caprock model to Vulcanian eruptions of Popocatepetl Volcano (February 2003) and Colima volcano (10 February 1999) and obtained gas pressures at the onset of fragmentation of 11-13 MPa and 19-22 MPa, respectively. These pressures might correspond to the gas pressures required to disrupt the caprock, fragment the underlying porous magma and eject the ballistics at the observed distances. We believe that the model presented herein yield more realistic gas pressures at the onset of fragmentation in Vulcanian eruptions than previous models. Moreover, when combined with ballistic models and data from continuous monitoring of active volcanoes, the caprock model may serve to improve hazard assessment.

Acknowledgments

The authors wish to express their gratitude to Oliver Spieler for help with the design of the setup for velocity measurements and to Carlos Linares-López from the Laboratorio Universitario de Petrología (UNAM) for help with the characterization of the samples. We also thank Dominique Richard, Yan Lavallée and Ulrich Kueppers for helpful comments and Patricia Julio-Miranda, Miguel Alatorre-Mendieta, Jerónimo Alatorre, Isaac Farraz-Montes, Carlos Fernández, Ulrich Kueppers and Yan Lavallée for field assistance while collecting the samples. Financial support to the first author and for the visit of Jacopo Taddeucci to Munich was provided by the THESIS program of the Bavarian Elite Network. Donald B. Dingwell

acknowledges the support of a research Professorship (LMUexcellent) of the Bundes exzellenzinitiativ. The visit of Hugo Delgado-Granados to Munich and fieldwork at Popocatepetl Volcano were partially funded by the PROALMEX program (CONACYT-DAAD). We are grateful to Larry Mastin and Alain Burgisser for their careful review and useful and constructive comments.

Appendix 2A. Derivation of Eqs. 2.3 and 2.4

The model proposed herein is based on the 1-D inviscid shock-tube theory (Turcotte et al., 1990; Ramos, 1995; Woods, 1995). We assume that after fragmentation, the gas-particle mixture behaves as a ‘pseudo-gas’ with an average density ρ given by (e.g., Woods, 1995; Koyaguchi and Mitani, 2005):

$$\frac{1}{\rho} = \frac{nRT}{P} + \frac{1-n}{\rho_p} \quad (2A.1)$$

where n is the mass fraction of gas in the mixture, $R=8.31 \text{ Jmol}^{-1}\text{K}^{-1}$ /(molecular mass) is the specific gas constant, T is temperature (in K), P is the gas pressure and ρ_p is the particles density. During the experiments n remains constant and therefore is convenient to rewrite Eq. 2A.1 by inverting the density to porosity (ϕ), and thus we obtain:

$$n = \frac{1}{1 + \frac{RT\rho_p(1-\phi)}{P\phi}} \quad (2A.2)$$

The time for thermal equilibrium between particles and gas scales as $\pi d^2/k_d$ where d is the diameter of the particles and k_d is the thermal diffusion coefficient, with typical value $10^{-6} \text{ m}^2/\text{s}$ for magma (Woods, 1995). The expansion in the shock-tube occurs over 5-10 ms and therefore only particles in the order of $\sim 0.05 \text{ mm}$ can remain in thermal equilibrium with the gas. In contrast, during Vulcanian eruptions which last on the order of few seconds, particles $\sim 1 \text{ mm}$ may remain in thermal equilibrium. Following Woods (1995), we assumed that a fixed fraction f of the particles remain in thermal equilibrium with the gas during the expansion phase; i.e., it is the fraction of particles that provides additional thermal energy to the expanding gas. When the gas-particle mixture decompresses adiabatically (neglecting heat transfer to the walls), the temperature of the gas decreases according to:

$$T = T_o \left(\frac{P}{P_o} \right)^{\frac{(\gamma-1)}{\gamma}} \quad (2A.3)$$

where T_o and P_o are the initial temperature and pressure of the sample, and γ is the heat capacity ratio given by (Woods, 1995):

$$\gamma = 1 + \frac{nR}{C_v n + C_s (1-n) f} \quad (2A.4)$$

where C_v is the specific heat capacity of the gas at constant volume and C_s is the magma specific heat capacity. We can simplify Eq. 2A.3 by substituting for T and T_o using Eq. 2A.1, and we obtain:

$$P \left(\frac{1}{\rho} - \frac{1-n}{\rho_p} \right)^\gamma = P_o \left(\frac{1}{\rho_o} - \frac{1-n}{\rho_p} \right)^\gamma \quad (2A.5)$$

Neglecting the effects of viscosity, heat conduction, wall friction and weight of the mixture (Turcotte et al., 1990; Woods, 1995), the mass and momentum equations are:

$$\frac{\partial \rho}{\partial t} + v \frac{\partial \rho}{\partial z} = -\rho \frac{\partial v}{\partial z} \quad (2A.6)$$

$$\frac{\partial u}{\partial t} + v \frac{\partial v}{\partial z} = -\frac{1}{\rho} \frac{\partial P}{\partial z} \quad (2A.7)$$

The general solution to these equations for the sound speed c and flow velocity v is given by (Landau and Lifshitz, 1987):

$$c = \left(\frac{\partial P}{\partial \rho} \right)^{1/2} \quad (2A.8)$$

$$v = -\int \frac{dP}{c\rho} \quad (2A.9)$$

Through substitution of Eqs. 2A.1, 2A.3 and 2A.5 into Eqs. 2A.8 and 2A.9, we find the solution for the gas-particle mixture:

$$c = \sqrt{\frac{\gamma}{nRT_o} \left(\frac{P}{P_o} \right)^{\frac{1-\gamma}{2\gamma}} \frac{P}{\rho}} \quad (2A.10)$$

$$v = \frac{2\sqrt{n\gamma RT_o}}{\gamma - 1} \left[1 - \left(\frac{P}{P_o} \right)^{\frac{\gamma-1}{2\gamma}} \right] \quad (2A.11)$$

Eq. 2A.11 corresponds to the maximum velocity of ejected particles not capped by a plate (Eq. 2.4 in the text).

The equation of movement of the plate (caprock in Vulcanian eruptions) propelled by the gas-particle mixture is based on Newton's second law:

$$\frac{dV}{dt} = \frac{A_c}{m} (P - P_{ext}) - g \quad (2A.12)$$

where V represents the velocity of the plate and also corresponds to the velocity at the top of the underlying gas-particle mixture, m and A_c are the mass and cross-sectional area of the plate, respectively, P_{ext} is the pressure above the plate (see Appendix B) and g is gravitational deceleration. Substituting Eq. 2A.11 into Eq. 2A.12 we obtain:

$$\frac{dV}{dt} = \frac{A_c}{m} \left\{ P_o \left[1 - \frac{1}{2}(\gamma - 1) \frac{V}{\sqrt{n\gamma RT_o}} \right]^{\frac{2\gamma}{\gamma-1}} - P_{ext} \right\} - g \quad (2A.13)$$

This equation can be solved numerically using a fourth order Runge-Kutta method to obtain the plate velocity as a function of time (or position) until it reaches the voluminous tank, where the flow is not longer one-dimensional. Eq. 2A.13 is used in our study to model the plate velocity during rapid decompression of volcanic material (Eq. 2.3 in the text).

Appendix 2B. Determination of P_{ext} in the fragmentation apparatus

In our experimental apparatus there is a volume of compressed gas between the diaphragms and the sample (Fig. 2.1). To determine the pressure above the plate (P_{ext}), it is necessary to calculate the dynamics of the gas after decompression using the technique for Riemann rarefaction waves in perfect gases (Landau and Lifshitz, 1987). After the disruption of the diaphragm, a compression wave propagates into the voluminous tank and a rarefaction wave moves downwards through the gas towards the sample. Between these waves, there is an expanding region of constant pressure P_3 with a value between the initial gas pressure P_o and

the atmospheric pressure $P_a=0.1$ MPa (Landau and Lifshitz, 1987). Assuming that the thickness of the rarefaction wave is small (Cagnoli et al., 2002), P_3 can be calculated before the rarefaction wave enters the sample from:

$$\frac{1}{\gamma_1 - 1} \frac{c_1}{c_2} \left[1 - \left(\frac{P_3}{P_o} \right)^{\frac{\gamma_1 - 1}{2\gamma_1}} \right] = \frac{\left(\frac{P_3}{P_a} - 1 \right)}{\sqrt{2\gamma_2 \left[(\gamma_2 - 1) + (\gamma_2 + 1) \frac{P_3}{P_a} \right]}} \quad (2B.1)$$

where $\gamma_1=1.67$ and $\gamma_2= 1.4$ are the heat capacity ratio of Argon and air, respectively, $c_1 = \sqrt{347T}$ is the sound speed in Argon at temperature T and $c_2 = \sqrt{402T_2}$ m/s is the sound

speed of air at temperature T_2 . If the pressure P_3 is such that $P_3 > P_o \left[\frac{2}{\gamma_1 + 1} \right]^{\frac{2\gamma_1}{\gamma_1 - 1}} = 0.237P_o$, the

gas pressure at the top of the gas region above the sample after decompression is $P_g=P_3$, otherwise the gas reaches the chock condition and $P_g=0.237P_o$, whereas the remaining pressure drop occurs in the voluminous tank. The velocity of the expanding gas V_g is given by:

$$V_g = \frac{2c_1}{\gamma_1 - 1} \left[1 - \left(\frac{P_g}{P_o} \right)^{\frac{\gamma_1 - 1}{2\gamma_1}} \right] \quad (2B.2)$$

This velocity is higher than the velocity V of the plate propelled by the gas-particle mixture. Therefore, a region of relative low pressure P_{ext} develops between the expanding gas and the plate, which can be estimated from (Landau and Lifshitz, 1987):

$$V_g - V = \frac{2c_1}{\gamma_1 - 1} \left[1 - \left(\frac{P_{ext}}{P_g} \right)^{\frac{\gamma_1 - 1}{2\gamma_1}} \right] + \frac{2c_o}{\gamma - 1} \left[1 - \left(\frac{P_{ext}}{P} \right)^{\frac{\gamma - 1}{2\gamma}} \right] \quad (2B.3)$$

where $c_o = \sqrt{\frac{\gamma}{nRT_o} \frac{P_o}{\rho_o}}$ is the initial sound speed of the mixture. Since V and P change with

time, the pressure above the plate P_{ext} is calculated numerically for each step until the plate reaches the voluminous tank. A schematic cartoon illustrating the sample, the plate and the regions with different pressure above it can be found in figure 2.B1.

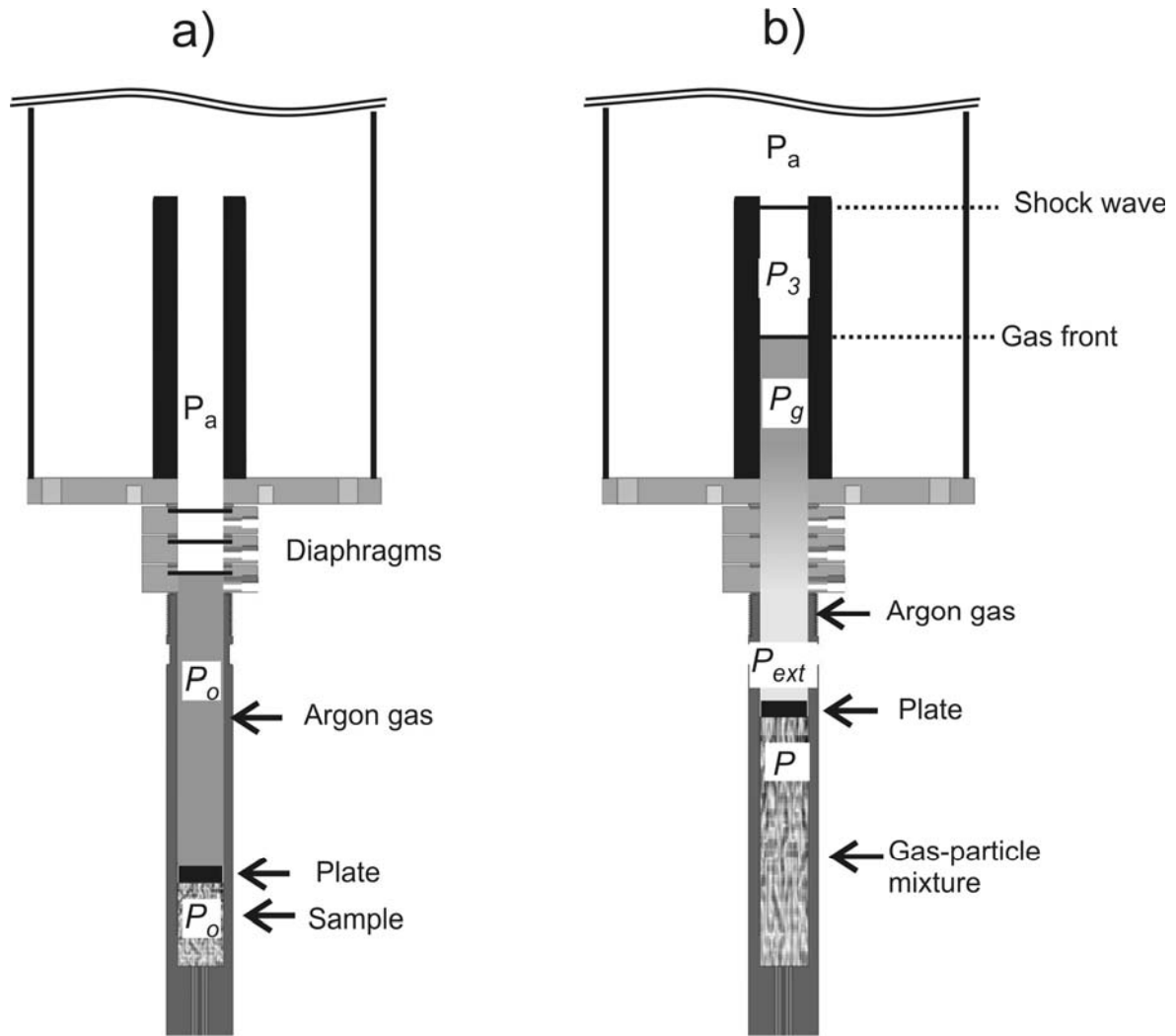


Figure 2.B1. Schematic cartoon illustrating the sample, the plate and the regions with different pressure above it. a) Initially, the sample and the Argon gas between the plate and the lowest diaphragm have an initial pressure P_o and the voluminous tank is at $P_a=0.1$ MPa. b) After the disruption of the diaphragms, a shock wave propagates into the voluminous-tank and a rarefaction wave moves downwards through the gas towards the sample. Between these waves, there is an expanding region of constant pressure P_3 between the initial gas pressure P_o and the atmospheric pressure P_a . The value of P_3 can be calculated using Eq. 2B.1. If $P_3 > 0.237P_o$ the pressure at the top of the gas region is $P_g = P_3$, otherwise the gas reaches the chock condition and $P_g = 0.237 P_o$. Since the velocity of the expanding gas is higher than the velocity of the plate propelled by the gas-particle mixture, a region of relative low pressure P_{ext} develops between the expanding gas and the plate, which can be estimated from Eq. 2B.3. The pressure P of the gas-particle mixture decreases from P_o to P_{ext} as it expands propelling the plate in the autoclave and the plastic tube above it, whereas the remaining pressure drop occurs in the voluminous tank where the flow is not longer one-dimensional.

Chapter 3

Influence of the fragmentation process on the dynamics of Vulcanian eruptions: an experimental approach³

Abstract

The dynamics of magma fragmentation is a controlling factor in the behavior of explosive volcanic eruptions. If porous magma is sufficiently decompressed, a fragmentation front develops and travels through the magma at a certain speed (fragmentation speed) while the resulting particles are being ejected. To investigate the influence of the fragmentation process on eruption dynamics, we have performed fragmentation experiments in a shock-tube apparatus using natural volcanic samples with diverse porosities and different applied pressures (4-20 MPa). For each experiment, we simultaneously measured the fragmentation speed and ejection velocities. The results are consistent with a theoretical model based on a 1-D shock-tube theory considering the conservation laws across the fragmentation front. Our results show that a certain pressure threshold has to be exceeded for fragmentation and ejection of the particles to take place and that the fragmentation speed determines the initial conditions of the expansion of the gas-particle mixture. The fragmentation process has a controlling influence on the velocity, density and mass discharge rate per unit area of the gas-particle mixture, all factors which can affect eruption dynamics significantly. The model presented herein may help describe the dynamics of Vulcanian eruptions and improve hazard assessment.

3.1. Introduction

The dynamics of magma fragmentation exert a strong influence on the explosive behavior of volcanic eruptions (Dingwell, 1996). Fragmentation changes the eruption dynamics from a system of bubbly flow to one of gas-particle flow. In theoretical models it is commonly assumed that this change occurs when a certain fragmentation criterion is reached (e.g. Sahagian (2005) and references cited therein). Magmatic fragmentation (i.e. fragmentation generated solely by the volatile phase originally dissolved in the magma) is considered to

³ This chapter has been published as: Alatorre-Ibargüengoitia, M.A., Scheu, B., Dingwell, D.B., 2011. Influence of the fragmentation process on the dynamics of Vulcanian eruptions: An experimental approach, *Earth Planet. Sci. Lett.*, 302, 51-59. doi:10.1016/j.epsl.2010.11.045.

occur when: 1) gas pressure in the pore space overcomes the tensile strength of the enclosing magma (McBirney and Murase, 1970; Alidibirov, 1994; Zhang, 1999; Alidibirov and Dingwell, 2000; Spieler et al., 2004a, Koyaguchi et al., 2008); or 2) the strain rate of the melt exceeds its structural relaxation rate (Dingwell and Webb, 1989; Papale, 1999). As has been suggested recently by Dellino et al. (2010), a quantitative knowledge of magma fragmentation, i.e. particle size (Kueppers et al., 2006 a, b), fragmentation energy (Alatorre-Ibargüengoitia et al., 2010a) and fragmentation speed (Scheu et al., 2006), is critical for determining the eruptive regime.

To date, the influence of the fragmentation process itself on the dynamics of the gas-particle flow has been largely neglected. In particular, experimental and theoretical investigations of Vulcanian eruptions have dealt with the expansion of a gas-particle mixture according to the 1-D shock-tube theory without considering the effects of the fragmentation process (Turcotte et al., 1990; Ramos, 1995; Woods, 1995; Cagnoli et al., 2002; Chojnicki et al., 2006). Alatorre-Ibargüengoitia et al. (2010) showed experimentally that magmatic fragmentation itself consumes a significant amount of energy, reducing the kinetic energy imparted to the resulting pyroclasts. They proposed that the effective pressure propelling the gas-particle mixtures after fragmentation corresponds to the pressure initially stored in the pore fraction minus the fragmentation threshold (i.e. the minimum pressure required to completely fragment a volcanic sample). Although this assumption is supported by their experimental results, it corresponds solely to the static component of the fragmentation energy and does not account for the dynamics of fragmentation, a complex topic that requires more comprehensive parameterization.

In this paper, we present a model based on the 1-D shock-tube theory that describes the relationship between the fragmentation speed and the ejection velocity of the gas-particle mixture considering the conservation laws across the fragmentation surface. We tested this model via a series of controlled fragmentation experiments on natural volcanic rocks in which we simultaneously measured the fragmentation speed and the ejection velocities of the resulting particles. We show that the fragmentation process plays an important role in the dynamics of the gas-particle mixture and can have important implications for the eruption dynamics.

3.2. Model

The shock-tube system consists of a pressurized bubbly magma at P_o separated from the air at P_a by a diaphragm. When the diaphragm is disrupted, a shock wave propagates into the air and a rarefaction wave propagates into the bubbly magma. As the rarefaction wave propagates into the magma, a zone with a steep pressure gradient develops within the magma. If the gas overpressure is large enough for the tangential stress around the bubbles to exceed the strength of the magma, this can lead to magma fragmentation (Spieler et al., 2004a; Koyaguchi et al., 2008). The boundary between bubbly magma and gas-particle dispersion is defined as the fragmentation front and the velocity at which this front propagates downwards into the magma is the fragmentation speed (e.g. Scheu et al., 2006).

The relationship between the fragmentation speed U and the ejection velocity v of the gas-particle mixture can be determined if the following assumptions are made (Koyaguchi and Mitani, 2005; Koyaguchi et al., 2008): (1) mass, momentum and energy are conserved across the fragmentation front; (2) the fragmentation front propagates at a constant speed; (3) the dynamics of the gas-particle mixture is described by the shock-tube theory for inviscid flow; (4) the gas-particle mixture behaves as a “pseudo-gas”; and (5) only particles smaller than a certain size (depending on the expansion time) remain in thermal equilibrium with the gas (Woods, 1995). From these constraints we obtain the following relationships (see Appendix A for derivation):

$$P_- = P_o \left(\frac{U}{a_o} \right)^{\frac{2\gamma}{\gamma+1}} \quad (3.1)$$

$$v = a_- - U + \frac{2\sqrt{n\gamma RT_o}}{\gamma-1} \left(\frac{P_-}{P_o} \right)^{\frac{\gamma-1}{2\gamma}} \left[1 - \left(\frac{P_{fi}}{P_-} \right)^{\frac{\gamma-1}{2\gamma}} \right] \quad (3.2)$$

where the subscripts “o” and “-” refer to parameters at the initial conditions and at the gas-particle mixture region just after fragmentation, respectively, a is the sound speed of the mixture (see Appendix A), T is temperature, n is the mass fraction of gas, R is the specific gas constant, γ is the specific heat capacity ratio of the mixture considering only the fraction of particles in thermal equilibrium with gas (see Appendix A) and P_{fi} is the final pressure. In the case of our experiments, P_{fi} is controlled by the dynamics of the expanding gas that is above

the sample (see Appendix B). Maintaining the assumptions (3) to (5) as mentioned above, but without considering fragmentation, v would be given by (Alatorre-Ibargüengoitia et al., 2010a):

$$v = \frac{2\sqrt{n\gamma RT_o}}{\gamma - 1} \left[1 - \left(\frac{P_{fi}}{P_o} \right)^{\frac{\gamma-1}{2\gamma}} \right] \quad (3.3)$$

Degrees of thermal disequilibrium between particles and gas during the experiments are related to the effective values of γ , which can be evaluated considering the fraction f of particles in thermal equilibrium with the gas (see Appendix A). The time for thermal equilibrium between the solid particles and the gas scales as $\pi d^2/4\kappa$, where d is the diameter of the particle and κ is the thermal diffusion coefficient with a typical value $10^{-6} \text{ m}^2/\text{s}$ for magma (Woods, 1995). If most of the particles remain in thermal equilibrium with the gas phase, then $\gamma \sim 1$ and Eq. (3.3) can be approximated by the isothermal expression proposed by Turcotte et al. (1990).

In order to obtain Eqs. (3.1) and (3.2) we assumed that the pressure at the fragmentation front remains at the initial pressure. This is not true if the gas is able to escape via permeable flow or if the bubbles can expand during decompression. Mueller et al. (2008) showed that permeability influences the fragmentation behavior only if it is above a critical value ($\sim 10^{-12} \text{ m}^2$). Additionally, bubble expansion in volcanic eruptions is prevented when the viscosity of the magma is $>10^7 \text{ Pa}\cdot\text{s}$ (Koyaguchi and Mitani, 2005).

3.3. Experimental method

We performed fragmentation experiments in a shock-tube apparatus (Alidibirov and Dingwell, 1996 a, b; Spieler et al., 2004a; Mueller et al., 2005; Kennedy et al., 2005; Kueppers et al., 2006 a, b; Scheu et al., 2006, 2008; Alatorre-Ibargüengoitia et al., 2010a; Kremers et al., 2010). It consists of a high-pressure autoclave overlain by a voluminous tank at atmospheric conditions (Fig. 3.1). Pressurization of the autoclave and subsequent depressurization are regulated by a system of three diaphragms that open at a defined pressure differential. Cylindrical samples drilled from volcanic rocks are loaded in the autoclave and pressurized with Argon gas to the desired experimental pressure. Decompression of the autoclave is triggered by controlled failure of the diaphragms, producing a rarefaction wave that travels

through the sample. If the resulting pressure differential is sufficient, the sample fragments brittlely layer-by-layer (Alidibirov and Dingwell, 2000; Fowler et al., 2010) and the particles are ejected into the voluminous tank.

Two dynamic pressure transducers, (601H, Kistler Instrumente AG, Switzerland) located directly above and below the sample, are used to quantify the speed of the fragmentation front traveling into the sample by recording the pressure drop during fragmentation. A high-speed camera (Phantom V710 and Photron SA-5) at 14,000 frames per second is used to measure the ejection velocities of the gas-particle mixture.

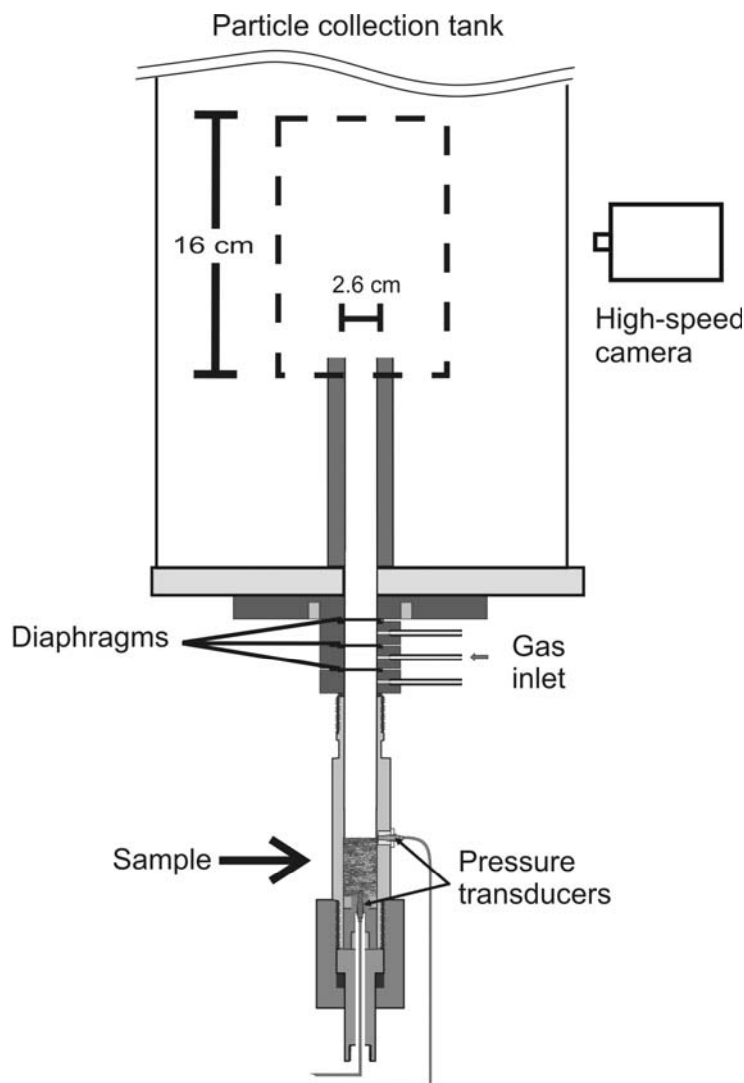


Figure 3.1. The experimental setup of the fragmentation apparatus. The sample ($l=6$ cm, $d=2.5$ cm) is placed in the high pressure autoclave. A set of diaphragms allows reproducible pressurization of the sample using Argon gas. Two dynamic pressure transducers located directly above and below the sample record the pressure drop during fragmentation. The dashed box indicates the area observed with the high-speed camera. Modified from Scheu et al. (2006).

We used samples from Popocatépetl Volcano (Mexico) consisting of andesitic pink pumice fragments corresponding to the Plinian eruption ca. 1200 yr. B.P. and dense andesitic samples from the Nealticán lava flow from a fissure eruption ca. 2100 yr. B.P. (Siebe and Macías, 2004). The density and porosity of all the samples were measured by Helium pycnometry (Accupyc 1330, Micrometrics, USA). The pumice samples have an open (interconnected) porosity of $\phi = 61\%$, total porosity of 64% and their matrix density is 2450 kg/m^3 . The dense lava samples have an open porosity of $\phi = 17\%$, total porosity of 18% and their matrix density is 2700 kg/m^3 . Phenocrysts in both kinds of samples have a maximum length of 3 mm and consist of plagioclase, pyroxene and olivine whereas Fe-Ti oxides are observed only in the pumice samples.

3.4. Results

The ejection of the gas-particle mixture was monitored during the course of all the experiments with the high-speed camera. The full ejection of the gas-particle mixture lasts 300-400 ms at the position observed with the high-speed camera. After the opening of the diaphragms, the gas above the sample escapes. Since the gas velocity is higher than the ejection velocity of the gas-particle mixture, a region of relative low pressure develops, which is followed by the front of the gas-particle mixture. The velocity of the gas-particle mixture reaches its maximum at this front. The initial stage of the flow is the more energetic stage, it lasts 15-30 ms and is characterized by a higher concentration of particles and a strong decrease in the velocity of the material ejected at different times. This stage is followed by a less energetic stage where the velocities and particle concentrations are much lower and particles decouple from the gas until they do not have enough energy to be ejected completely out of the autoclave. In this study we focus only on the initial stage of the two-phase flow.

3.4.1 Two-phase flow characteristics

Figure 3.2 presents a sequence of images showing the front of the gas-particle mixture after fragmentation in experiments with a pumice sample and a dense sample. Heterogeneities in particle concentration within the mixture can be observed, especially the presence of gaps with a low particle concentration as shown in Figure 3.2b. These gaps were observed in all the experiments but were more evident in the experiments with dense samples. We did not observe a systematic change in the particle size with time, with a diverse range of particle

sizes having been observed simultaneously throughout the initial stage of one experiment. We also observed that the number of large particles (> 8 mm) is reduced in experiments performed at higher initial pressures.

We did not observe any measurable acceleration of the gas-particle mixture at the place (0.40-0.55 m above the original position of the sample) and time (5-20 ms) recorded with the high-speed camera. Detailed analyses of the videos at the initial stage reveal that there is no systematic difference in the ejection velocities of particles with different sizes (ranging between 0.5 and 8 mm). It is very common to observe relatively large particles moving at approximately the same velocity as smaller particles.

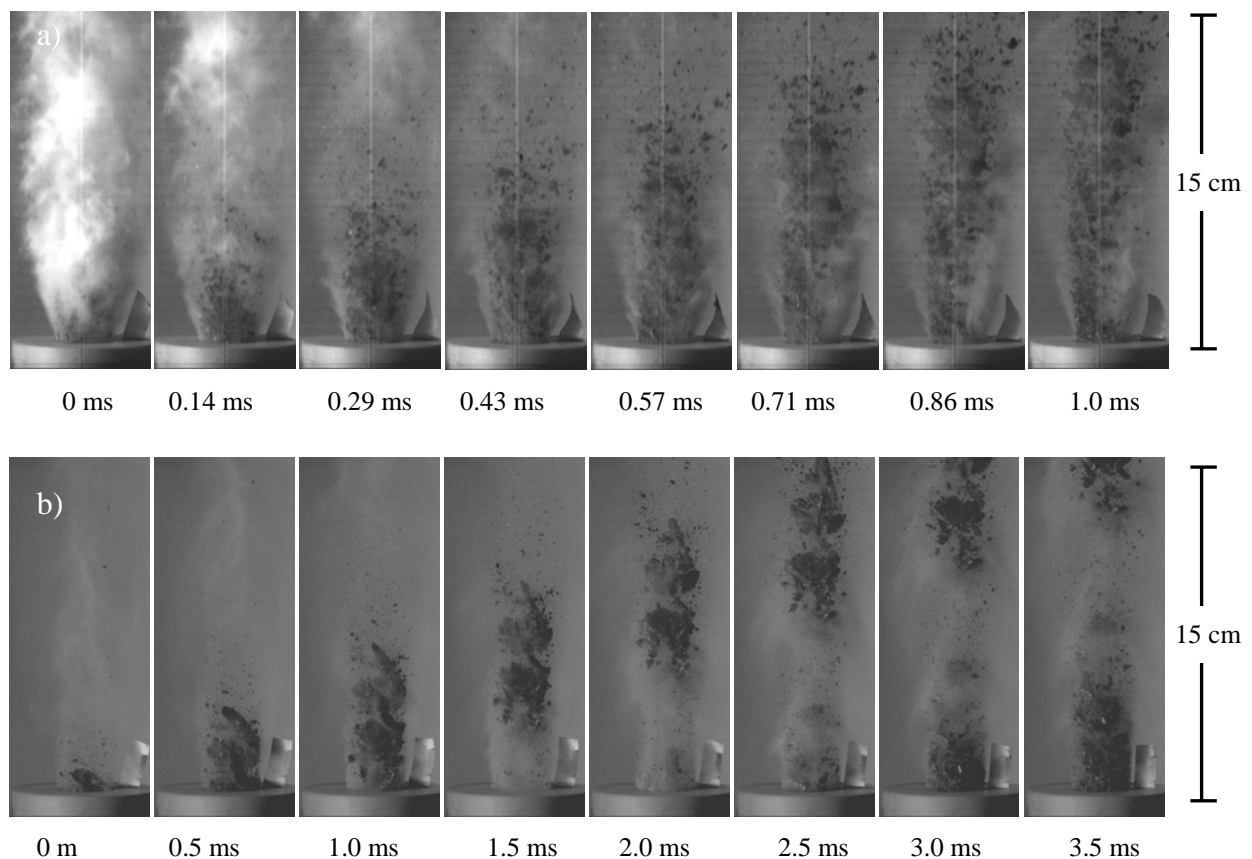


Figure 3.2. Sequence of still-frames from movies taken by a high-speed camera showing the front of the gas-particle mixture after fragmentation. a) Experiment with a pumice sample at 20 MPa. The outflow of the gas that was above the sample is observed at the beginning followed by the irregular front of the gas-particle mixture. b) Experiment with a dense sample at 17.6 MPa. A gap with low concentration of particles is observed after the first layer of particles, which could be associated to the different layers in which the fragmentation process occurs (Alidibirov and Dingwell, 2000; Fowler et al., 2010). Note the time difference between the two experiments due to the higher ejection velocity of the pumice sample.

3.4.2 Fragmentation speed and ejection velocities

The fragmentation speed was calculated from the distance between the dynamic pressure transducers and the time delay between the pressure drops of the signals (Scheu et al., 2006). The results for the pumice and dense samples are presented in Figure 3.3, relative to the initial pressure. The relationship between the fragmentation speed and the applied pressure can be fitted empirically using a logarithmic expression (Scheu et al., 2006) that can be defined as follows:

$$U = k_p \ln(P_o / P_{th}) \quad (3.4)$$

where k_p is a constant with velocity units that depends on the porosity of the sample and P_{th} is the fragmentation threshold, which is defined as the minimum pressure differential that leads to complete fragmentation of the pressurized rock sample (Spieler et al., 2004a). Below the fragmentation threshold ($P_o < P_{th}$), full fragmentation does not occur. If the initial pressure is within ~ 1.0 MPa below P_{th} , partial fragmentation of the sample occurs and only a fraction of the particles are ejected. More precisely, $U = 0$ m/s corresponds to the fragmentation initiation (FI) of the samples. Because of minor potential differences between individual sample cylinders and following Scheu et al. (2006), we decided to merge the values FI and P_{th} and define an average P_{th} value which has to be interpreted as a pressure range. We found experimentally that for the pumice samples $P_{th} = 4.0 \pm 0.5$ MPa and for the dense samples $P_{th} = 8.5 \pm 1.0$ MPa.

For each experiment above P_{th} , the velocity of the front of the gas-particle mixture was measured via high-speed videography. Because of the irregularity of the front of the gas-particle mixture (Fig. 3.2), we considered the average of the velocities of several particles traveling at this front. The results for both sets of samples are presented in Figure 3.3. We observed that the ejection velocity of the gas-particle mixture increases non-linearly with applied pressure and it is higher than the fragmentation speed.

The theoretical velocity of the front of the gas-particle mixture can be calculated using Eqs. (3.1) and (3.2) together with the empirical Eq. (3.4), which expresses U as a continuous function of P_o . The theoretical calculations for both sets of samples are shown in Figure 3.3. This figure reveals that the model presented in section 3.2 is in good agreement with the

experimental data. We note here that the theoretical model without considering the fragmentation process (Eq. 3.3) significantly overpredicts the observed ejection velocities of the mixture.

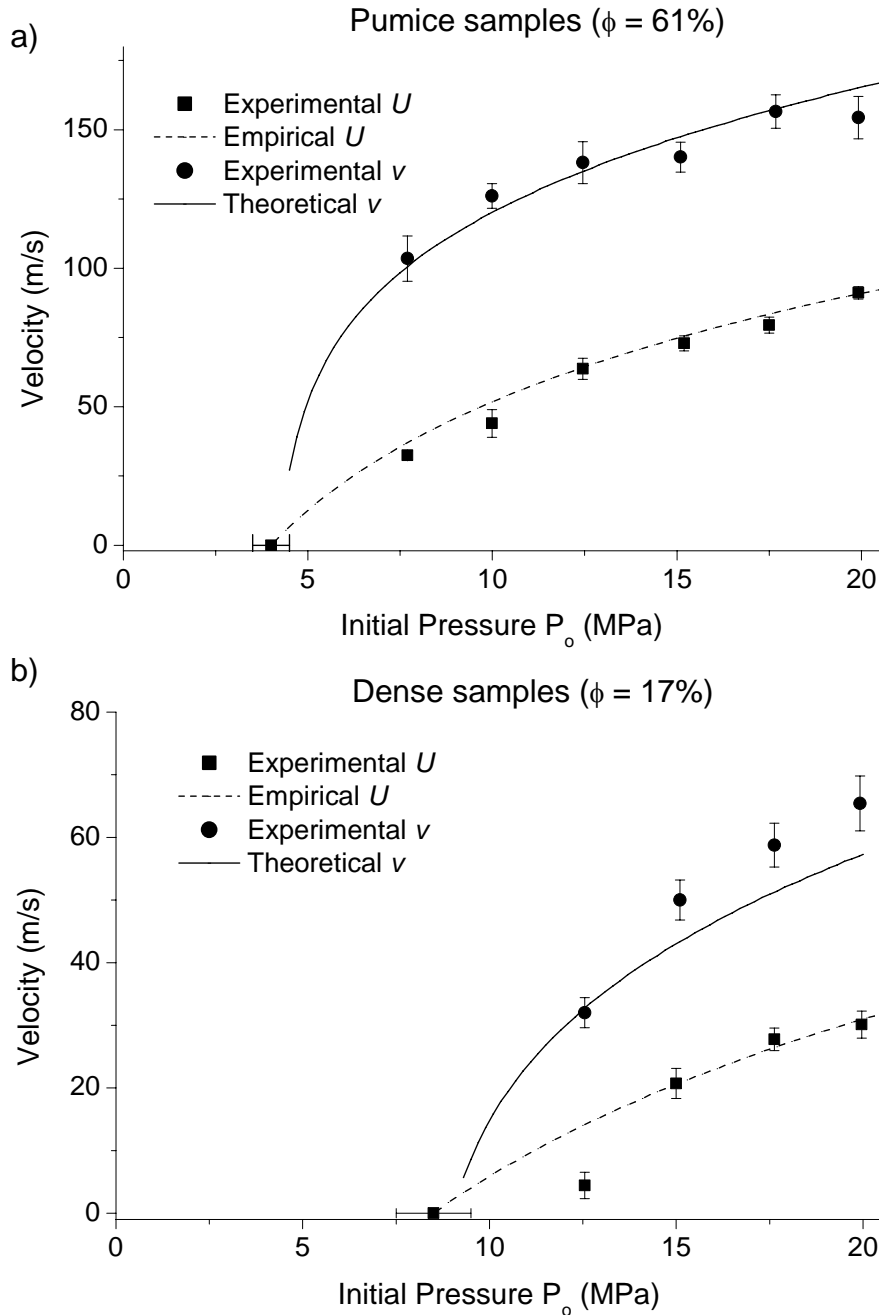


Figure 3.3. Fragmentation speed (U) and ejection velocity (v) of the experiments performed with a) pumice samples, and b) dense samples. The error bars of U indicate the uncertainties in the determination of the fragmentation onset at the pressure drop curves. The experimental v values correspond to the average of the velocities of several particles traveling at the front of the gas-particle mixture and the error bars represent the standard deviations. The velocities at 0 m/s represent the fragmentation threshold of the samples (see text). The dashed lines are the empirical fits for U using Eq. (3.4). The solid lines correspond to the theoretical calculations for v using Eqs. (3.1), (3.2) and (3.4) considering $f = 2\%$ and $f = 5\%$ for the experiments with pumice and dense samples, respectively. Other parameters used in the simulations correspond to the laboratory conditions given in Table 3.1.

In our experiments, the duration of fragmentation and ejection of the gas-particle mixture up to the position observed with the high-speed camera is in the order of 5 ms and 20 ms for the experiments with pumice and dense samples, respectively. Accordingly, the fraction f of particles in thermal equilibrium with the gas was estimated by sieving the particles collected after the experiments and we measured the fraction of particles smaller than ~ 0.09 mm and ~ 0.18 mm. We found that the respective f values are 2 ± 0.5 % and 5 ± 0.5 %.

Finally, we observed a non-linear decay of the velocity of particles (v_p) as a function of time (t), which can be fitted empirically using the following relationship (Alatorre-Ibargüengoitia et al., 2010a):

$$v_p = \frac{v_{\max}}{1 + \frac{v_{\max}}{h} t} \quad (3.5)$$

where $t = 0$ corresponds to the time at which the first particle is observed, v_{\max} is the maximum ejection velocity at the observation position and h corresponds to the distance from the bottom of the original position of the sample to the position observed with the high-speed camera.

3.5. Interpretation

Our experimental results support the theoretical model presented in section 3.2 linking the fragmentation speed and the velocity of the front of the gas-particle mixture, even when the dynamics of each might be different. In fact, U determines the initial conditions for the expansion of the gas-particle mixture as indicated by Eqs. (3.1) and (3.2). This has two important implications:

- A pressure threshold (P_{th}) has to be exceeded for fragmentation and ejection of the particles to take place (Fig. 3.3).
- Since $U < a_o$, the pressure available for the ejection of the gas-particle mixture (P_-) is lower than P_o (Eq. 3.1).

The density, temperature and sound speed of the gas-particle mixture vary accordingly (Eqs. 3A.4, 3A.5 and 3A.9). Further, the energy available to eject the fragmented particles is reduced because of the energy that is required to fragment the sample (Alatorre-Ibargüengoitia et al., 2010a). We emphasize here that the model presented in section 3.2 considers only the

conservation laws across the fragmentation front but not a particular fragmentation criterion (as done e.g. by Koyaguchi et al. (2008)) or the complex dynamics of fracturing during fragmentation (e.g. done by Fowler et al., (2010)).

Figure 3.4 shows how the ejection velocity at the front of the gas-particle mixture is affected by the fraction f of particles in thermal equilibrium with the gas phase. The ejection velocity increases with higher f values because more particles provide additional thermal energy to the expanding gas. In the experiments with pumice samples, the data are well adjusted by the assumed $f=2\%$. In the case of the experiments with dense samples, the data are better adjusted considering a higher value of f than the assumed $f=5\%$ estimated by the simple time-scale analysis presented in section 3.2 and the grain-size analysis of the collected particles. Further work is needed in order to enhance our understanding of the thermal disequilibrium between the particles and gas phase during fragmentation and ejection in our experiments.

In order to model the expansion of the gas-particle mixture we assumed that it behaves as a “pseudo-gas”, whose bulk properties are described as a function of the gas fraction. The experimental results show that this approach is adequate to calculate the average ejection velocity of the front of the flow. In addition, we observed that particles with different sizes (from 0.5 mm to 8 mm) move at approximately the same velocity during the initial stage. This indicates that all the particles within this size range have reached mechanical equilibrium with the gas at this stage, in which the ejection velocity remains almost constant. Moreover, the presence of particles in this size range at different times suggests that the fragmentation efficiency remains approximately constant during the investigated initial stage of the fragmentation process. Nevertheless, we have observed the existence of heterogeneities within the mixture. In particular, we observed layers with different concentrations of particles (Fig. 3.2b) which we associate with the different layers at which the fragmentation process occurs (Alidibirov and Dingwell, 2000; Fowler et al., 2010).

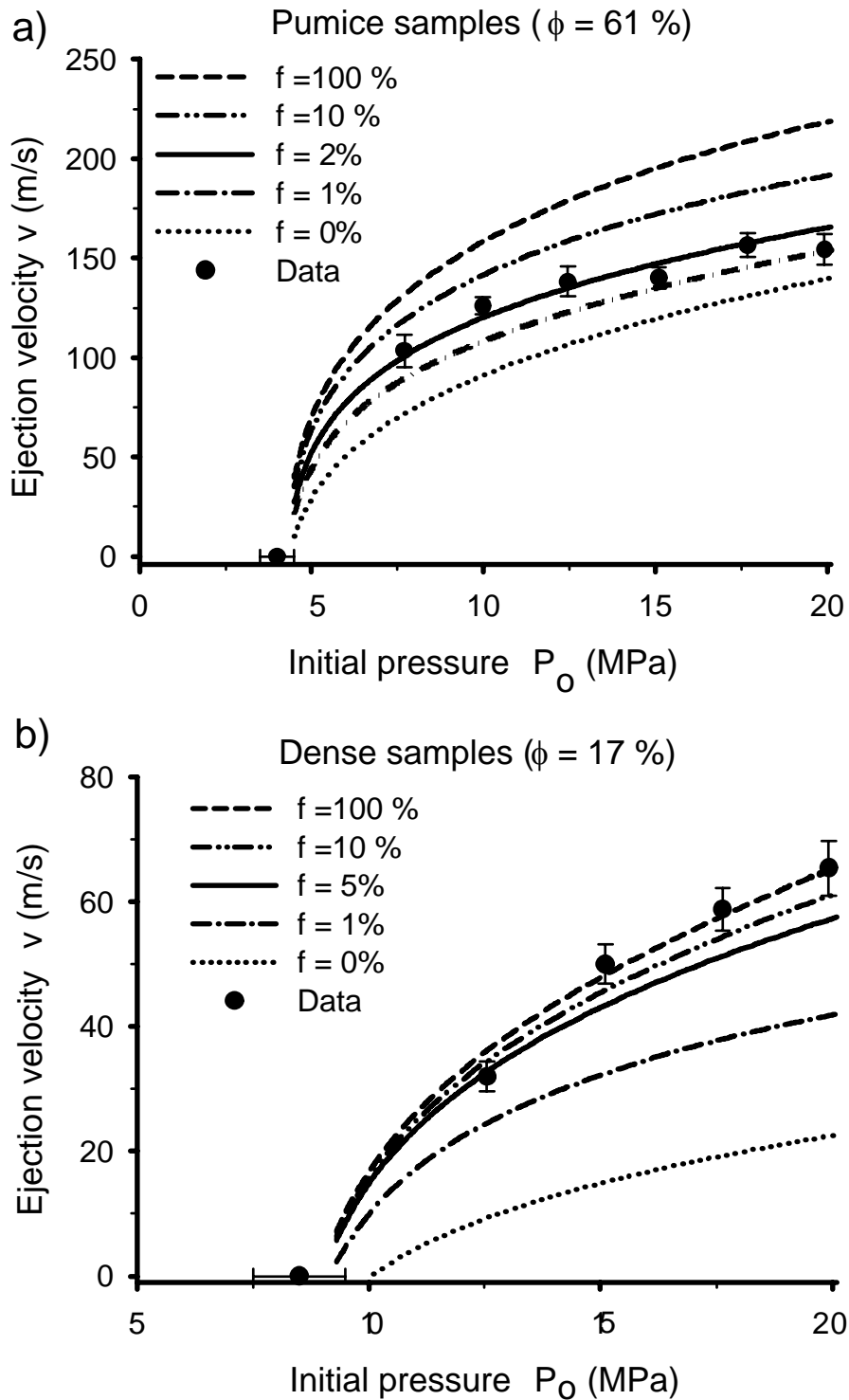


Figure 3.4. Ejection velocity v at the front of the gas-particle mixture in experiments performed with a) pumice samples ($\phi = 61\%$), and b) dense samples ($\phi = 17\%$). The circles indicate experimental results whereas the lines are the theoretical calculations considering different values of the parameter f that represents the fraction of particles in thermal equilibrium with the gas. The solid lines were calculated with the f values estimated from the grain-size distribution of the collected particles and correspond to the curves presented in Fig. 3.3. The values $f = 0\%$ and $f = 100\%$ correspond to adiabatic and isothermal processes, respectively. Other parameters used in the simulations correspond to the laboratory conditions given in Table 3.1.

3.6. Discussion

Our results can be applied to volcanic eruptions as long as the following conditions hold true: 1) brittle fragmentation occurs and 2) the effect of bubble expansion is negligible during decompression so that the gas pressure inside the pore space remains at the initial pressure. Even when magmatic temperatures are much higher than our experiments, high strain rates associated with rapid decompression can maintain the brittle nature of fragmentation (Dingwell, 1996). The applicability of shock-tube experiments to volcanic eruptions has been discussed by Koyaguchi and Mitani (2005). They suggested that the results of shock tube experiments can be applied to natural systems for magmas with viscosities higher than 10^7 Pa·s, in which case bubble expansion is negligible and the features of fragmentation do not depend on system size. We remark that our present results apply solely to magmatic fragmentation, i.e. where fragmentation does not occur as a result of the interaction of magma with external water.

In this section we apply the theoretical model to Vulcanian eruptions. In this case, the values of the parameters differ from the conditions corresponding to the experiments as indicated in Table 3.1 and therefore the calculated ejection velocities are different from the experimental results. The fragmentation speed at magmatic temperatures is not well known. Previous fragmentation experiments performed at 22° C and 850° C reveal that the fragmentation threshold derived by the cold experiments tend to be slightly higher but still comparable to the values gained for similar samples at high temperature (Kueppers et al., 2006 a; Scheu et al., 2006). This indicates that the fragmentation process is similar at low and high temperatures as long as fragmentation remains brittle (Scheu et al., 2006). Effects of the temperature dependence of the sound speed of the mixture on the fragmentation behavior are neglected here, but will be subject to further investigations.

Koyaguchi and Mitani (2005) first noted the importance of the role played by fragmentation speed normalized by the sound speed of the mixture (U/a_o) in the flow parameters and showed that the final pressure (P_{fi}) and the velocities of the shock wave and the gas-particle mixture decrease as the U/a_o ratio diminishes. Additionally, they suggested that when $U/a_o > 0.7$ the flow parameters are almost identical to those of the inviscid case. However, they did not consider the pressure threshold that has to be overcome.

Figure 3.5 shows that the final pressure, ejection velocity, density and mass discharge rate per unit area calculated considering Eqs. (3.1) and (3.2) differ significantly from the results obtained using the classical transient inviscid model in which the influence of the fragmentation process on the dynamics of the gas-particle mixture is not considered (Eq. 3.3). This figure shows that: (1) no particles are ejected at pressures below P_{th} whereas models without considering fragmentation predict very high densities; (2) fragmentation reduces the velocity of the front of the gas-particle mixture, in particular at pressures close to P_{th} , even when the final pressure P_{fi} is lower; (3) at pressures above P_{th} , fragmentation reduces the density of the mixture and the mass discharge rate per unit area at the front of the flow by a factor of 2-4; (4) fragmentation decreases the final pressure P_{fi} and therefore the intensity and velocity of the shock wave propagating into the air are also reduced (see Appendix B; Koyaguchi and Mitani 2005).

Previous inviscid models (e.g. Turcotte et al., 1990; Woods, 1995) predict that all the flow parameters are constrained only by the initial pressure and gas content. In contrast, the results of Figure 3.5 imply that the flow parameters depend on the fragmentation speed because it controls the pressure available for the ejection of the gas-particle mixture (Eq. 3.1). This pressure in turn determines the ejection velocity, density and mass discharge rate, which are key parameters controlling the eruptive dynamics (e.g. Neri and Dobran, 1994; Suzuki et al., 2005; Carazzo et al., 2008; Koyaguchi et al., 2010). These consequences of the fragmentation process illustrate how it can affect the eruption dynamics significantly and therefore should be taken into account in models of explosive eruptions.

Parameter	Experiments	Vulcanian eruptions
Specific gas constant R ($\text{J kg}^{-1}\text{K}^{-1}$)	207.8 (Ar)	461.7 (H_2O)
Gas specific heat capacity C_v ($\text{J kg}^{-1}\text{K}^{-1}$)	312 (Ar)	2000 (H_2O)
Magma specific heat capacity C_s ($\text{J kg}^{-1}\text{K}^{-1}$)	1400	1400
Timescale	5- 20 ms	~ 1-10 s
Temperature T (K)	295	1123
Final pressure P_{fi} (range MPa)	Eq. 3B.1 (0.3 - 1.3)	Eq. 3B.2 (0.1 - 0.3)

Table 3.1. Values of the parameters used for the simulations corresponding to the experiments (Figs. 3.3 and 3.4) and the application to natural cases (Figs. 3.5 and 3.6). The timescale controls the fraction of particles that can remain in thermal equilibrium with the gas phase. In the experiments the final pressure P_{fi} is controlled by the dynamics of the gas that is above the sample in our shock-tube apparatus. In Vulcanian eruptions P_{fi} corresponds to the pressure behind the shock wave propagating into the air (Appendix 3B). The magma specific heat capacity was calculated with CONFLOW software (Mastin and Ghirso, (2000) and references cited therein).

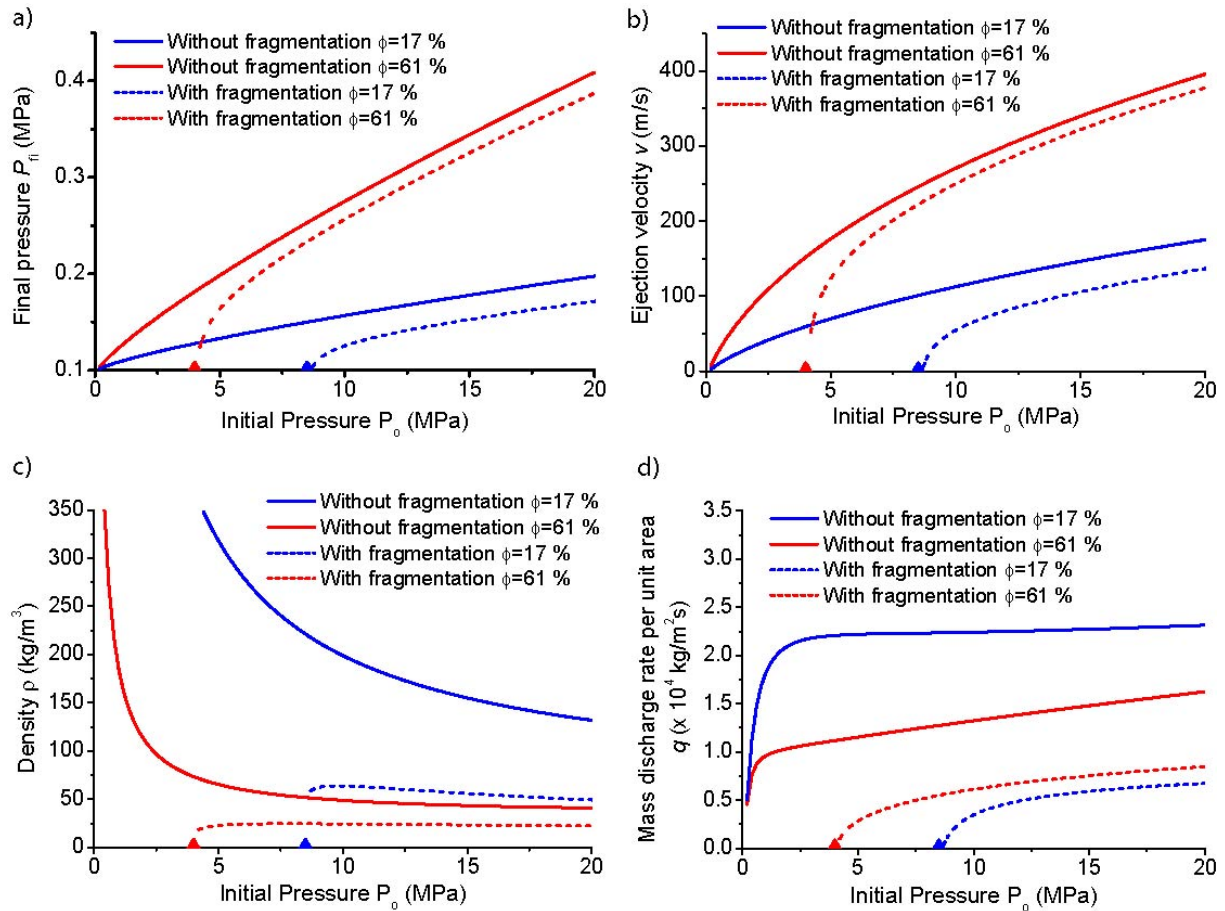


Figure 3.5. (a) Final pressure P_{fi} , (b) ejection velocity v , (c) density of the mixture ρ and (d) mass discharge rate per unit area $q = \rho v$ at the front of the gas-particle mixture as a function of pressure calculated theoretically for two different initial porosities ϕ in transient eruptions. Dashed lines correspond to the model presented in section 3.2 which considers the relationship between fragmentation speed and the initial pressure and velocity of the gas-particle mixture just after fragmentation (Eqs. 3.1 and 3.2). The triangles indicate the position of the respective P_{th} . Solid lines correspond to the classical transient inviscid model in which the influence of the fragmentation process on the dynamics of the gas-particle mixture is not considered (Eq. 3.3). The final pressure corresponds to the pressure behind the shock wave propagating into the air (see Appendix 3B). The density of the mixture decreases with the initial pressure as shown in (c) because, for a fixed porosity and temperature, the mass fraction of the gas phase increases with pressure. For the calculations we used the conditions for Vulcanian eruptions given in Table 3.1.

The influence of the assumed values of the fraction f of solid material in equilibrium with the gas phase on the ejection velocity and the mass discharge rate per unit area (q) in Vulcanian eruptions is presented in Figure 3.6. This figure shows how the velocity at the front of the gas-particle mixture decreases as f diminishes for two different porosities. The ejection velocity obtained with $f = 10\%$ are closer to the values calculated with $f = 100\%$ in the case of the dense magma in comparison with the more porous magma. Since the effective value of γ depends on f and n (Eq. 3A.6), the isothermal condition $\gamma \sim 1$ is reached at lower values of f in

the dense magma with respect to more porous magma. This figure also shows that $q=\rho v$ is almost independent of f because the density at the front of the gas-particle mixture decreases as f increases and counteracts the effect of f on v .

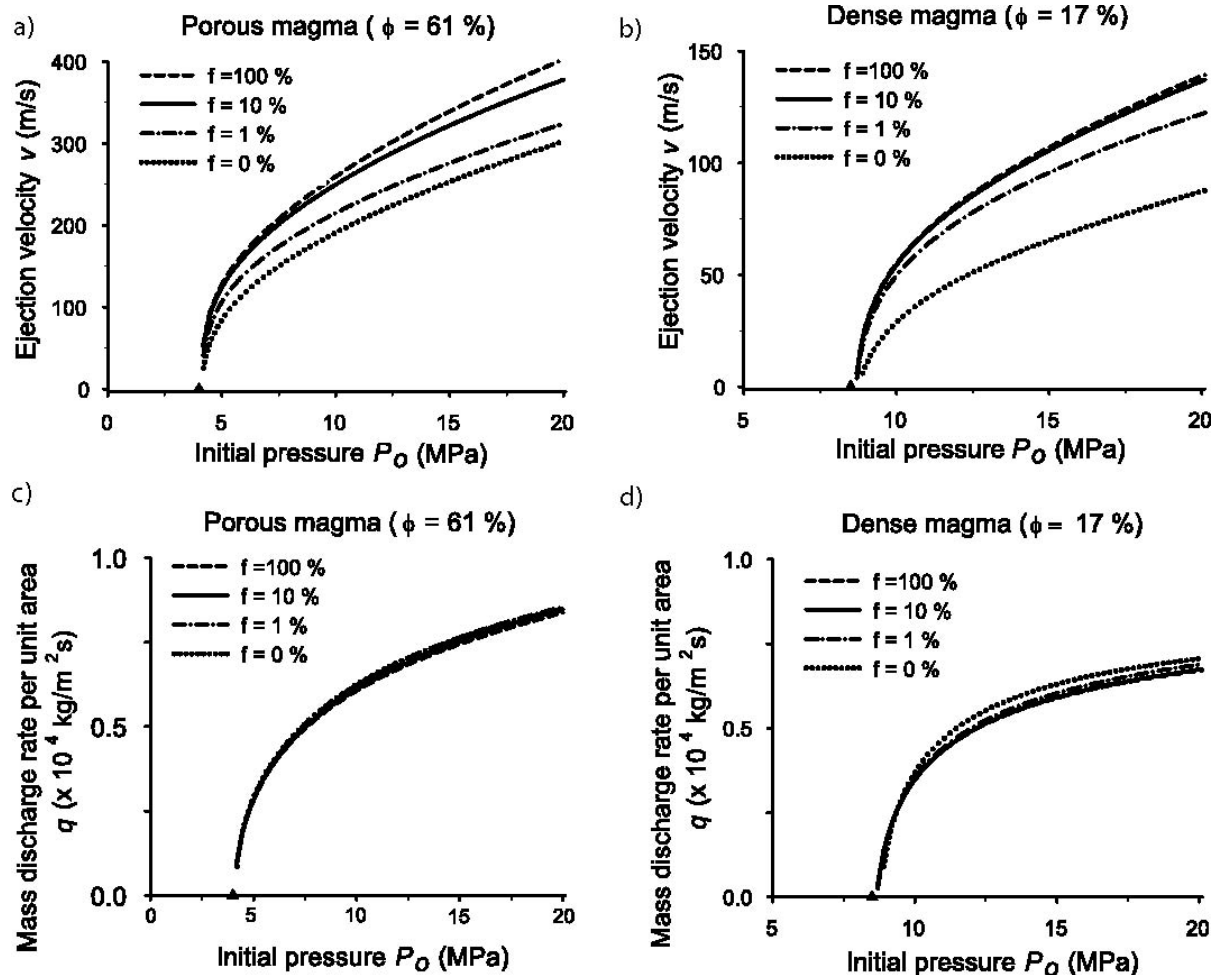


Figure 3.6. (a) and (b) Ejection velocity v and (c) and (d) mass discharge rate per unit area $q=\rho v$ at the front of the gas-particle mixture as a function of the initial pressure P_o considering different values of f and two different initial porosities ϕ . These curves were computed considering the influence of the fragmentation process on the ejection of the gas-particle mixture (Eqs. 3.1 and 3.2). The triangles indicate the position of the respective P_{th} . The values $f = 0\%$ and $f = 100\%$ correspond to adiabatic and isothermal processes, respectively. For the calculations we used the conditions for Vulcanian eruptions given in Table 3.1.

So far, a fundamental theory relating column evolution to vent conditions does not exist for short-lived, highly unsteady momentum- and buoyancy-driven columns. To better understand Vulcanian eruption dynamics, theoretical and numerical models have to be combined with field observations (e.g. Fudali and Melson, 1972; Nairn and Self, 1978; Hoblitt, 1986; Stix et al., 1997; Clarke et al., 2002; Druitt and Young., 2002; Formenti et al., 2003; Johnson et al., 2004) and experimental investigations (e.g. Kennedy et al., 2005; Clarke et al., 2009; Alatorre-

Ibargüengoitia et al. 2010). The model presented here can provide the vent conditions required as input by the pyroclast dispersal models in unsteady eruptions (e.g. Clarke et al., 2002; Neri et al., 2003; Suzuki et al. 2005). Moreover, this model can be used to estimate initial conditions from field observations, for instance, the initial pressure from ejection velocities (e.g. Fagents and Wilson, 1993; Nakada et al., 1999; Cagnoli et al., 2002; Formenti et al., 2003; Taddeucci et al., 2004). Future applications would benefit from an increased coupling of geophysical data (seismic and ground deformation) with Doppler radar measurements during monitoring of Vulcanian eruptions, and from numerical simulations considering unsteady vent conditions.

Finally, we remark that the model presented in section 3.2 is non-steady and therefore it can only be applied to transient explosions such as Vulcanian eruptions. Nevertheless, as suggested by Dellino et al. (2010) the fragmentation process is supposed to also affect the eruptive dynamics in Plinian eruptions. They showed that the fragmentation speed influences the eruptive regime in Plinian eruptions and therefore our results might, to some extent, also apply to initial stages of this kind of eruptions. Further systematic investigation on this topic is still needed.

3.7. Summary

We simultaneously measured the fragmentation speed and ejection velocity of the particles in fragmentation experiments on volcanic rocks. Our results are in good agreement with a 1-D shock-tube model which states that the fragmentation speed determines the initial conditions for the expansion of the gas-particle mixture as indicated by Eqs. (3.1) and (3.2). This implies that a certain pressure threshold has to be exceeded for fragmentation and the ejection of particles to take place and that the pressure available for the ejection of the gas-particle mixture is reduced. These implications of the fragmentation process in turn reduce the velocity, density and the mass discharge rate per unit area of the gas-particle mixture, which can affect the eruption dynamics significantly. The model presented herein may realistically describe the dynamics of brittle fragmentation involved in Vulcanian eruptions and yield more realistic initial pressures at the onset of fragmentation than previous models. Moreover, it can be combined with pyroclast dispersal models in unsteady eruptions to enhance our understanding of Vulcanian eruptions and improve hazard assessment.

Acknowledgments

The authors wish to express their gratitude to Teresa Scolamacchia and Corrado Cimarelli for help while performing the experiments. We also thank Hugo Delgado-Granados, Ulrich Kueppers and Yan Lavallée for field assistance while collecting the samples, and Sandra Karl, Jonathan Hanson and Ulrich Kueppers for their helpful comments. Financial support to the first author was provided by the IDK 31 THESIS program funded by the Elite Network of Bavaria (ENB). Donald B. Dingwell acknowledges the support of a Research Professorship (LMUexcellent) of the Bundesexzellenzinitiative and the EVOKES project of the ERC. This study was partially funded by the FONCICYT program (Mexican Government-European Union), grant 93645 (FIEL-VOLCAN). We are grateful to Takehiro Koyaguchi and Pinaki Chakraborty for their careful review and useful and constructive comments.

Appendix 3A. Derivation of equations (3.1) and (3.2)

At the fragmentation front physical quantities change discontinuously. The mass and momentum conservation laws across this front are given by (Koyaguchi and Mitani, 2005; Koyaguchi et al., 2008):

$$\rho_o U = \rho_-(v_- + U) \quad (3A.1)$$

$$P_o + \rho_o U^2 = P_- + \rho_-(v_- + U)^2 \quad (3A.2)$$

where the densities of the mixture before (ρ_o) and after fragmentation (ρ_-) are given by the following equations of state (Koyaguchi and Mitani, 2005; Koyaguchi et al., 2008):

$$\frac{1}{\rho_o} = \frac{nRT_o}{P_o} + \frac{1-n}{\rho_p} \quad (3A.3)$$

$$\frac{1}{\rho_-} = \frac{nRT_-}{P_-} + \frac{1-n}{\rho_p} \quad (3A.4)$$

where ρ_p is the solid density. Assuming that the gas-particle mixture decompresses adiabatically during fragmentation (neglecting heat transfer to the walls) and considering that only a fixed fraction f of the particles remain in thermal equilibrium with the gas (Woods, 1995), the decrease of the temperature during fragmentation can be calculated from the equation for the conservation of energy:

$$T_- = T_o \left(\frac{P_-}{P_o} \right)^{\frac{\gamma-1}{\gamma}} \quad (3A.5)$$

where the effective heat capacity ratio γ is given by (Woods, 1995):

$$\gamma = 1 + \frac{nR}{C_v n + C_s (1-n) f} \quad (3A.6)$$

where C_v is the specific heat capacity of the gas at constant volume and C_s is the magma specific heat capacity.

In order to describe the dynamics of the gas-particle mixture using the shock-tube theory for inviscid flow, the following relationship must hold true (Koyaguchi and Mitani, 2005; Koyaguchi et al., 2008):

$$v_- = a_- - U \quad (3A.7)$$

Finally, the sound speed of the mixture before (a_o) and after fragmentation (a_-) is given by:

$$a_o = \sqrt{\frac{\gamma}{nRT_o} \frac{P_o}{\rho_o}} = \sqrt{\gamma nRT_o} \left(1 + \frac{(1-n)P_o}{nRT_o \rho_s} \right) \quad (3A.8)$$

$$a_- = \sqrt{\frac{\gamma}{nRT_-} \frac{P_-}{\rho_-}} \quad (3A.9)$$

Eq. (3.1) is derived from Eqs. (3A.1), (3A.5), (3A.7), (3A.8) and (3A.9).

Assuming that the viscosity, wall friction and weight of the mixture can be neglected and that only the fraction f of the particles remains in thermal equilibrium with the gas during the expansion phase (Woods, 1995) but without taking into account fragmentation, the ejection velocity of the gas-particle mixture is given by Eq. (3.3). If the fragmentation process is considered, Eq. (3.3) is transformed into:

$$v = v_- + \frac{2\sqrt{n\gamma RT_-}}{\gamma - 1} \left[1 - \left(\frac{P_{fi}}{P_-} \right)^{\frac{\gamma-1}{2\gamma}} \right] \quad (3A.10)$$

We obtain Eq. (3.2) by substituting Eqs. (3A.5) and (3A.7) into Eq. (3A.10).

Appendix 3B. Determination of P_{fi} in the fragmentation apparatus and volcanic conduits

In our experimental apparatus there is a volume of compressed gas between the diaphragms and the sample (Fig. 3.1), which precedes the ejection of the gas-particle mixture (Fig. 3.2a). The dynamics of this gas after decompression controls the final pressure P_{fi} of the mixture in Eq. (3.2) and can be calculated using the technique for Riemann rarefaction waves in perfect gases (Landau and Lifshitz, 1987). Since the gas velocity is higher than the velocity v of the gas-particle mixture, a region of relative low pressure P_{fi} develops between the expanding gas and the front of the gas-particle mixture (Landau and Lifshitz, 1987; Alatorre-Ibargüengoitia et al., 2010a), which can be estimated from:

$$\frac{2a_g}{\gamma_1 - 1} \left[\left(\frac{P_{fi}}{P_g} \right)^{\frac{\gamma_1 - 1}{2\gamma_1}} - \left(\frac{P_g}{P_o} \right)^{\frac{\gamma_1 - 1}{2\gamma_1}} \right] = v_- + \frac{2\sqrt{n\gamma RT_o}}{\gamma - 1} \left(\frac{P_-}{P_o} \right)^{\frac{\gamma - 1}{2\gamma}} \left[1 - \left(\frac{P_{fi}}{P_-} \right)^{\frac{\gamma - 1}{2\gamma}} \right] \quad (3B.1)$$

where $\gamma_1 = 1.67$ is the heat capacity ratio of Argon, $a_g = \sqrt{347T_o}$ is the sound speed in Argon at temperature T_o ; v_- , P_- and γ are given by Eqs. (3A.7), (3.1) and (3A.6), respectively, and P_g is the pressure at the top of the gas region. Since in all of our experiments P_o is high enough

for the outflow of the gas to be choked, then $P_g = P_o \left[\frac{2}{\gamma_1 + 1} \right]^{\frac{2\gamma_1}{\gamma_1 - 1}} = 0.237P_o$. The remaining

pressure drop occurs in the voluminous tank where the flow is no longer one-dimensional. We observed a roughly linear increment of P_{fi} when increasing P_o : from $P_{fi} = 0.3$ MPa at $P_o = 4.5$ MPa to $P_{fi} = 1.3$ MPa at $P_o = 20$ MPa in the experiments with pumice samples; and from $P_{fi} = 0.6$ MPa at $P_o = 8.5$ MPa to $P_{fi} = 1.3$ MPa at $P_o = 20$ MPa in the experiments with dense samples.

In the case of volcanic eruptions triggered by plug removal within a volcanic conduit, the final pressure P_{fi} of the mixture in Eq. (3.2) corresponds to the pressure behind the shock wave propagating into the air. Using the Rankin-Hugoniot relationship across the shock wave (e.g. Koyaguchi and Mitani, 2005) and the ejection velocity at the front of the gas-particle mixture given by Eq. (3.2) we can calculate P_{fi} from:

$$v_{-+} + \frac{2\sqrt{n\gamma RT_o}}{\gamma - 1} \left(\frac{P_{-}}{P_o}\right)^{\frac{\gamma-1}{2\gamma}} \left[1 - \left(\frac{P_{fi}}{P_{-}}\right)^{\frac{\gamma-1}{2\gamma}}\right] = \frac{a_{air} \left(\frac{P_{fi}}{P_a} - 1\right)}{\sqrt{\frac{\gamma_{air}}{2} \left[(\gamma_{air} - 1) + (\gamma_{air} + 1) \frac{P_{fi}}{P_a}\right]}} \quad (3B.2)$$

where $a_{air} = \sqrt{402T_{air}}$ and $\gamma_{air} = 1.4$ are the heat capacity ratio and the sound speed of air at temperature T_{air} , respectively, and P_a is the atmospheric pressure. The velocity of the shock wave v_s is then given by:

$$v_s = a_{air} \sqrt{\frac{1}{2\gamma_{air}} \left[(\gamma_{air} + 1) \left(\frac{P_{fi}}{P_a}\right) + (\gamma_{air} - 1) \right]} \quad (3B.3)$$

Chapter 4

Hazard Map for Volcanic Ballistic Impacts at Popocatépetl Volcano (Mexico)⁴

Abstract

During volcanic explosions, fragments with ballistic trajectories are frequently ejected. These fragments are called volcanic ballistic projectiles (VBP) and represent a threat to people, infrastructure, vegetation and aircraft due to their high temperatures and impact velocities. In order to protect people adequately, it is necessary to delimit their maximum range within well-defined explosive scenarios likely to occur in a particular volcano. In this study, a general methodology to delimit the hazard zones defined by VBP during volcanic eruptions is applied to Popocatépetl Volcano.

Three explosive scenarios with different intensities have been defined. These are based on the past activity of the volcano and parameterized considering the maximum kinetic energy associated to VBP ejected during previous eruptions. A ballistic model, including a simple estimation of the drag reduction near the vent, is used to reconstruct the initial or “launching” kinetic energy of VBP observed in the field. In the case of Vulcanian eruptions, which represent the most common type of activity at Popocatépetl Volcano, the ballistic model was used in concert with an eruptive model in order to correlate ballistic range with initial gas pressure and gas content, parameters that can be estimated by continuous monitoring techniques. The theoretical results are validated with field data and video observations of different Vulcanian eruptions at Popocatépetl Volcano.

For each explosive scenario, the ballistic model is used to calculate the maximum range of VBP considering the optimum “launching” conditions: ballistic diameter, ejection angle, topography and wind velocity. Our results are presented in the form of a VBP hazard map with topographic profiles that depict the likely maximum ranges of VBP (horizontally and vertically) under explosive scenarios defined specifically for Popocatépetl Volcano. The

⁴ This chapter has been submitted to Bulletin of Volcanology as: Alatorre-Ibargüengoitia, M.A., Delgado-Granados, H., Dingwell, D.B. Hazard Map for Volcanic Ballistic Impacts at Popocatépetl Volcano (Mexico), February 2011.

different-level hazard zones shown on the map allow the responsible authorities to plan the definition, development and mitigation of restricted areas during volcanic crises.

4.1. Introduction

One of the hazards associated with explosive eruptions is the ejection of large rock and magma fragments that follow nearly parabolic trajectories (Alatorre-Ibargüengoitia and Delgado-Granados, 2006). Such fragments are called volcanic ballistic projectiles (VBP) and are defined as particles of any origin that, because of their relative large size ($>10\text{-}15$ cm, depending on the energy), separate rapidly from the eruptive column. Gravity and drag forces mainly determine their trajectories before impacting the earth's surface. Due to their high temperatures and impact energies, the VBP represent an important threat to life, property, vegetation and air navigation (Alatorre-Ibargüengoitia et al., 2006).

Death and serious injury may result directly from ballistic impacts, and even solid shelters can be affected by large projectiles. This is because the impact energy of relative large projectiles (> 15 cm) is enough to penetrate a number of building materials such as wood and concrete (Blong, 1984; Alatorre-Ibargüengoitia et al., 2006). The kinetic energy of VBP during flight can also be enough to produce significant damage to a number of aircraft materials (Blong, 1984; Riddle et al. 1996; Gellert et al. 2000). The temperature of the VBP is also important from the hazard point of view. They can trigger fires because their typical impact temperatures are above the ignition point for vegetation and a variety of man-made objects. Casualties, infrastructure damage and fires produced by VBP have been reported in several volcanoes around the world (Blong, 1984), for instance Sakurajima in Japan (Smithsonian Institution, 1991), Stromboli in Italy (Smithsonian Institution, 2003b), Masaya in Nicaragua (Smithsonian Institution, 2001) as well as Popocatépetl (Delgado-Granados et al., 2001) and Colima (Zobin et al., 2002) in Mexico.

One of the main elements involved in the effective management of a volcanic crisis is the identification of the areas threatened by the products and eruptive processes of a given volcano, together with the definition of the probabilities that specific volcanic phenomena may occur in a given time interval (De la Cruz-Reyna and Tilling, 2008). This study aims to establish a general methodology to delimit hazard zones (both horizontally and vertically) of VBP impact during volcanic explosions. Here, we apply our methodology to VBP ejected by

explosions at Popocatépetl Volcano (Mexico). The results are presented in a VBP-hazard map and topographic profiles where the horizontal and vertical hazard zones are depicted.

4.2. Eruptive activity of Popocatépetl Volcano

Popocatépetl Volcano (19.02° N, 98.62° W, with an altitude of 5452 masl) is located in the Trans-Mexican Volcanic Belt (Fig. 4.1), just 70 km from downtown Mexico City and within a densely populated region ($\sim 500,000$ people living within 10–30 km from the crater, De la Cruz-Reyna and Tilling, 2008). Popocatépetl is one of the most dangerous volcanoes in Mexico due to the highly explosive eruptions that have occurred in the past (Siebe et al., 1996) and one of the 10 most populated active volcanoes in the world (Small and Naumann, 2001).

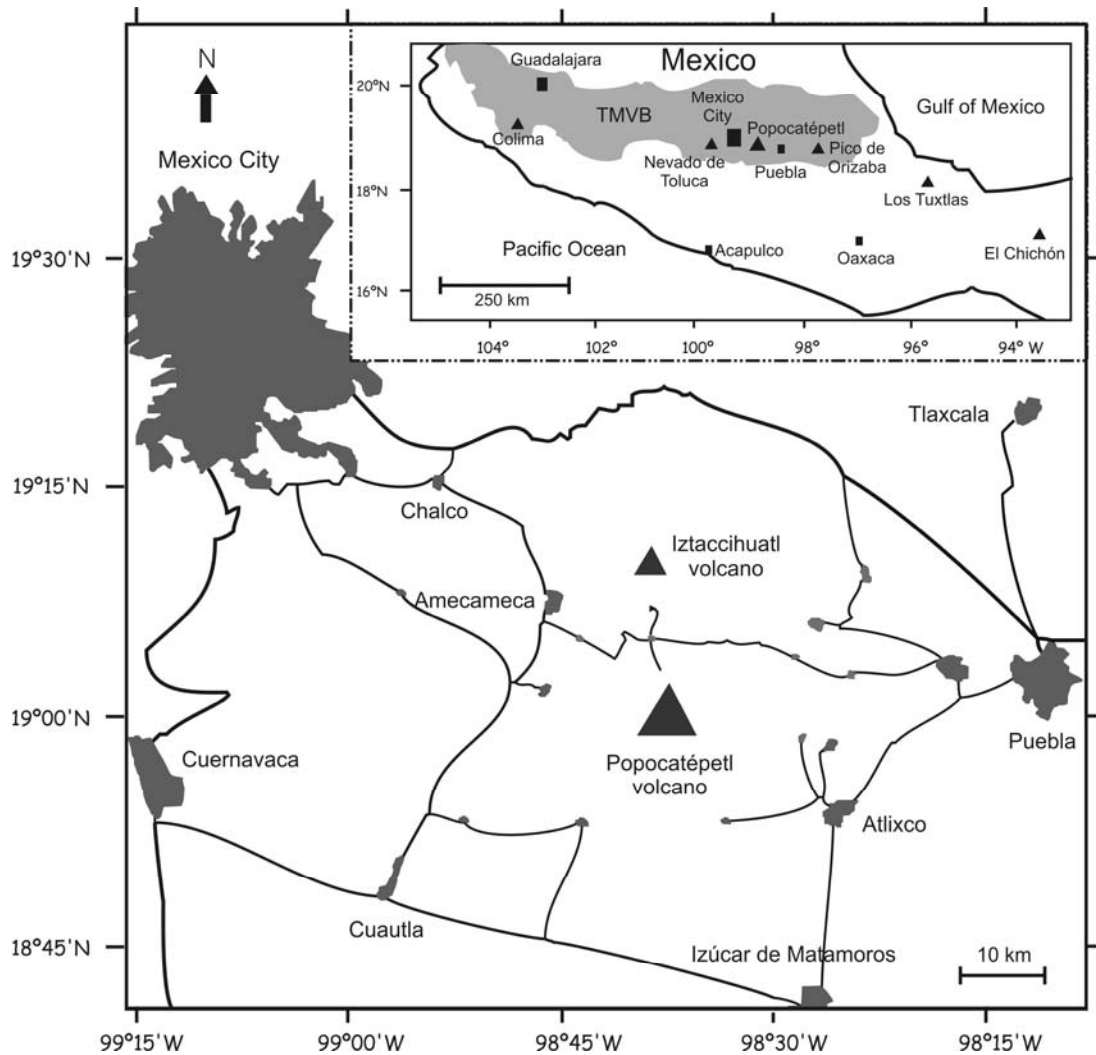


Figure 4.1. Popocatépetl Volcano is located in central Mexico, within the Trans-Mexican Volcanic Belt (TMVB). The cities of Mexico, Puebla, Cuernavaca, Cuautla and others shown in the map sum up a population of 20 million people. Towns, main highways and roads are also shown. Modified after Delgado-Granados et al. (2001).

The modern cone of Popocatépetl Volcano consists of interlayered andesitic to dacitic lava flows and pyroclastic deposits erupted in the last ~ 23,000 years following a cataclysmic Bezymianny type event that destroyed a previously existing cone (Robin and Boudal, 1987; Siebe and Macías, 2004). In that period, Popocatépetl has had at least seven Plinian eruptions that produced extensive deposits (Macías and Siebe, 2005). One of Popocatepetl's most powerful Plinian eruptions occurred at ~ 14,000 yr B.P. which generated the "Tutti-Frutti" fall deposit that mantled a large area including the region currently occupied by Mexico City (Siebe and Macías, 2004). The more recent Plinian eruptions occurred ca. 5000, 2100 and 1100 years BP, which devastated large areas on the northeast flank of Popocatépetl and destroyed several human settlements (Siebe et al. 1996, Macías and Siebe, 2005).

Historical records contain no mention of large-scale eruptions in the last 600 years but they do report 12 eruptive periods between 1500 and 1990 (De la Cruz-Reyna et al., 1995; De la Cruz-Reyna and Tilling, 2008). These eruptions have been relatively mild, characterized by the repeated formation of small domes inside the summit crater and Vulcanian events associated with the destruction of these domes, generating 1-10-km-high ash plumes that did not produce identifiable deposits around the volcano (Siebe and Macías, 2004). In each episode, such activity lasted for a few years and no major damage or casualties were reported (De la Cruz-Reyna et al., 1995).

On the 21st of December, 1994, Popocatépetl Volcano started to erupt after ~70 years of dormancy with Vulcanian explosions clearing out the main conduit system and putting out ash columns as high as 7 km above sea level (Delgado-Granados et al. 2001). As a consequence of these explosions more than 25,000 people were temporarily evacuated from the closest towns (De la Cruz-Reyna and Tilling, 2008). The explosions became intermittent during January-March 1995 and in August the explosive activity stopped completely. On March 5th, 1996, the explosive activity resumed, and a few days later a new lava dome was observed. Since then, the eruptive activity of Popocatépetl has been characterized by dome emplacement and subsequent destruction by explosive events (Delgado-Granados et al. 2001). This activity has been intermittent and fluctuating. Between March 1996 and July 2005, at least 26 dome growth-destruction cycles were reported (De la Cruz-Reyna and Tilling, 2008). It is believed that the chemical composition of the magma has not changed significantly since 1996 (Wright et al., 2002; Macías and Siebe, 2005). Nevertheless, the domes have exhibited significant

differences in dimensions, eruption rates and morphology, reflecting differences in viscosity that have been attributed to variations in eruption temperature (Wright et al., 2002). According to the daily activity reports of the National Center for Disaster Prevention (CENAPRED), in this period at least 250 explosions have produced ash columns > 1 km high.

Here, the most important explosive events are briefly described. On the 30th of April, 1996, an eruption ejected ballistics several hundreds of meters from the crater killing five climbers that ignored official warnings (the only reported victims directly related to the Popocatépetl eruptive activity). On the 30th of June, 1997, one of the strongest eruptions occurred, generating an eruptive column that reached nearly 15 km in height. The ash fall related to this event resulted in the closure of the international airport of Mexico City for several hours. Pyroclastic flows were observed reaching the timberline ~ 4 km from the crater (Delgado-Granados et al. 2001). On the 17th of December, 1998, a relatively strong explosion ejected incandescent VBP into a terrain covered by bushes at the north flank of the volcano, igniting several vegetation fires (Alatorre-Ibargüengoitia and Delgado-Granados, 2006). These VBP travelled 3.7 km from the crater, which is the maximum range that has been reported during the current activity at Popocatépetl Volcano (1994-2010).

On the 12th of December, 2000, activity increased significantly and, within a few days, set records in terms of tremor, dome extrusion rates, SO₂ emission rates and tilt, liberating in a few hours more seismic energy than in any 12 months period during the 1994-2009 activity. The succession of tremor episodes resembled a load-and-discharge process that was actually used to forecast the onset of the 18 December eruption (De la Cruz-Reyna and Tilling, 2008). An evacuation was ordered. During the following days, the dome was partially destroyed by successive explosions with plumes rising to 8 km above the crater. Ballistics were ejected to a distance estimated of 3.5 km from the vent (Smithsonian Institution, 2000). On the 22nd of January, 2001, a relatively strong eruption generated a pyroclastic flow which traveled ~ 4.5 km from the crater and reached the timberline, triggering forest fires (Macías and Siebe, 2005). This pyroclastic flow melted the remnants of the glacier and produced a lahar that reached the outer limits of the village of Xalitiztla (Capra et al., 2003; Julio Miranda et al. 2005; Julio Miranda et al. 2008).

4.3. Ballistic projectiles from Popocatépetl Volcano

Ballistic projectiles ejected during different explosive events have been investigated and sampled in different field campaigns that were carried out in November-December 1999, February-March 2006, February 2009 and April 2010. Considering the location of the ballistics, and after a detailed review of the daily activity reports of CENAPRED and videos of the explosions, we believe that the investigated VBP were ejected by the explosive events that occurred in November-December 1998 (Smithsonian Institution, 1998a, b), February 2003 (Smithsonian Institution, 2003a) and March 8, 2008 (CENAPRED). In order to ensure that they were emplaced ballistically, only fragments found within impact craters were investigated. The degree of preservation of these craters was also used to constrain the age of the ejected VBP.

Of the 122 studied impact craters, the corresponding fragments were able to be measured in 67. In the other cases, they were completely shattered or could not be found even after digging around the impact crater. We focused mainly on the VBP that reached the maximum distance since they are the most relevant for hazard assessment. Each crater was localized using GPS and described. When possible, the dimensions of the VBP fragments were also measured. In the last campaign, the fragments were weighed in the field to have a more precise value of their size and mass. The dimensions of the impact craters increase with the size of the fragments but a lot of scatter is observed due to differences in the field. In average, the mean diameter of the impact craters is 4-5 times the equivalent diameter of the corresponding fragments. Most of the ballistics are angular and dense although some fragments exhibit a poorly vesicular exterior and a more vesicular interior.

In each campaign, several VBP were sampled and analyzed in the laboratory. Their bulk density, open and closed porosity was measured by Helium pycnometry and the bulk compositions of representative fragments were determined. We observed no significant differences in the physical properties of VBP ejected in different events and our chemical analyses yielded results similar to the measurements reported for tephra produced in different explosive events (Straub and Martin-Del Pozzo, 2001; Martin-Del Pozzo et al., 2003; Witter et al., 2005). Table 4.1 presents the characteristics of the investigated ballistics.

Several ballistic projectiles 30-40 cm in diameter were also found in the deposits of the “Tutti-Frutti” Plinian eruption (~ 14,000 y. B.P.) at a maximum distance of 11.2 km from the

crater on the northwest flank of the volcano. These altered fragments exhibited impact sagging indicating their ballistic emplacement.

Parameter	Observed
Average diameter (m)	0.20 – 0.60
Bulk density (kg/m ³)	2100 – 2600
Matrix density (kg/m ³)	2600 – 2680
Interconnected Porosity (%)	3-23
Total Porosity (%)	5- 25
Composition (SiO ₂ %)*	Andesitic (61) – Dacitic (65)
Crystallinity (vol. % vesicle-free basis)	30 – 50 (Plagioclase, pyroxene, amphibole, Fe-Ti oxides and olivine in the andesitic fragments)

Table 4.1. Characteristics of the investigated ballistics ejected during different eruptive events of Popocatépetl Volcano. * The chemical composition was only measured for representative samples collected in the field campaign of 2006.

4.4. Models

4.4.1 Ballistic model

Several models have been developed to correlate the ejection velocity of the gas-pyroclast mixture at the vent to the range reached by the VBP during explosive eruptions (Sherwood 1967; Fudali and Melson 1972; Wilson 1972; Self et al. 1980; Steinberg and Lorenz 1983; Fagents and Wilson 1993; Waitt et al. 1995; Bower and Woods 1996; Mastin, 2001; Alatorre-Ibargüengoitia and Delgado-Granados, 2006; de' Michieli Vitturi et al., 2010). These models have been used to estimate the initial velocity of the VBP reaching the maximum range in a particular event, or to estimate the distance that the VBP can travel at given ejection conditions.

During flight, VBP are subjected to gravity and drag forces. The ballistic equation describing the trajectory of VBP results from these forces and can be expressed in a rectangular coordinate system as follows (Wilson, 1972; Waitt et al., 1995, Alatorre-Ibargüengoitia and Delgado-Granados, 2006):

$$\frac{dv_x}{dt} = -\frac{AC_d \rho_a(z)(v_x - u_x)|\mathbf{v} - \mathbf{u}|}{2m} \quad (4.1a)$$

$$\frac{dv_z}{dt} = -\frac{AC_d \rho_a(z)v_z|\mathbf{v} - \mathbf{u}|}{2m} - g \quad (4.1b)$$

where x and z are the horizontal and vertical position coordinates respectively, $\mathbf{v} = (v_x, v_z)$ is the velocity vector of the projectile, t is time, A and m are the cross-sectional area and mass of the VBP, respectively, C_d is the drag coefficient, $\rho_a(z)$ is air density as a function of altitude, $\mathbf{u} = (u_x, 0)$ is wind velocity (considering only tailwind velocity u_x), $|\mathbf{v} - \mathbf{u}| = \sqrt{(v_x - u_x)^2 + v_z^2}$ and g is gravitational acceleration. For ellipsoidal VBP the ratio $A/m = 3/(2\rho_b D)$, where ρ_b is the ballistic density and D is the geometric mean of three perpendicular diameters. Air density decreases with the altitude and can be described as a quadratic function fitting published altitude-density data (Waite et al., 1995). Equations 4.1a and 4.1b can be integrated numerically throughout the trajectory using a fourth-order Runge-Kutta method as described by Wilson (1972). The calculations stop when the vertical position (z) of the VBP reaches a specified landing elevation (z_f).

The drag coefficient plays a key role in the trajectory of the VBP. It depends on the shape, orientation and roughness of the VBP and on the Reynolds and Mach numbers, which indicate the flow regime. Alatorre-Ibargüengoitia and Delgado-Granados (2006) report C_d values measured in a subsonic wind tunnel for different pyroclastic particles expelled by Popocatépetl Volcano. Measured C_d ranges from 0.6 for semi-rounded porous samples to 1.0 for highly irregular ones. These values are only slightly affected by the Reynolds number if it is above a critical value ($\sim 2 \times 10^4$) corresponding to the change from laminar to turbulent regime at the boundary layer. These authors also extrapolated their results to compressible flows and obtained C_d as a function of Mach number that can be used to calculate the trajectories of VBP ejected at velocities around the speed of sound in air.

Most of the above mentioned ballistic models assume that VBP are ejected into still air from the moment they leave the vent and therefore their trajectories can be described as “purely” ballistic. However, visual observations and more recent models indicate that the VBP are ejected into an expanding gas cloud, which significantly reduces the drag force near the vent (Fagents and Wilson 1993; Bower and Woods 1996; de’ Michieli Vitturi et al., 2010). Moreover, in certain cases, such as that of the 30-cm-diameter fragments that produced clear impact sagging found 11.2 km from the crater at Popocatépetl, cannot be explained considering a purely ballistic model. If VBP are assumed to be ejected into a stationary atmosphere, the initial velocity of the clasts is very high and leads to an overestimation of the drag force.

In order to cope with this effect, Fagents and Wilson (1993) postulated that the ejected material accelerates to a maximum velocity (v_o) at some distance (R_o) and time (t_o) from its initial position, and then decelerates at the rate:

$$v = v_o \left(\frac{R_o}{R} \right)^2 \exp(-t / \tau) \quad (4.2)$$

where the time constant τ is related to the ratio of initial gas pressure (P_g) to atmospheric pressure (P_a):

$$\tau = \frac{P_g}{P_a} t_o \quad (4.3)$$

Similarly, Mastin (2001) incorporated an arbitrary distance from the vent over which the drag coefficient is reduced. In these approaches it is assumed that the VBP are launched into the surrounding atmosphere from a fixed position and with a chosen velocity and angle. More recently, de' Michieli Vitturi et al. (2010) presented a Lagrangian particle model for the ejection of volcanic clasts coupled with a multiphase model of the carrier flow, including the acceleration phase. They applied this model to Vulcanian explosions which occurred in August 1997 at Soufriere Hills Volcano (Montserrat) and showed that the dynamics of the carrier flow play a fundamental role even for meter-sized particles.

4.4.2 Caprock model

Ballistic models provide a relationship between the initial velocities and the distance that the VBP can reach in explosive eruptions. Complementary eruptive models are necessary to correlate initial velocities with gas content and pressure, which are parameters that can be estimated by continuous monitoring techniques. The explosive activity at Popocatépetl Volcano has been dominated by Vulcanian eruptions, and therefore an appropriate model for this kind of eruption is required. Vulcanian eruptions are often considered to occur when a caprock plugging the vent is disrupted (Morrisey and Mastin, 2000). Video observations of the Vulcanian eruptions at Popocatépetl Volcano show that the VBP are ejected at the beginning of the explosion, indicating that these dense and angular clasts are fragments of the caprock that are accelerated by the expansion of the underlying gas-particle mixture.

Alatorre-Ibargüengoitia et al. (2010a) presented a 1-D model for Vulcanian eruptions that considers the acceleration of the caprock and takes into account the energy that is consumed during fragmentation. According to this model, when the caprock is disrupted the underlying pressurized porous magma fragments by rapid decompression and the resulting gas-particle mixture expands propelling the caprock fragments. It is assumed that during the first few seconds of the acceleration phase these fragments behave as a coherent plug retaining its original cross-sectional area with no escape of the expanding gas. Since fragmentation consumes a significant amount of energy, these authors assumed that the effective pressure (P_{ef}) available for particle ejection is given by:

$$P_{ef} = P_o - P_{th} \quad (4.4)$$

where P_o is the initial gas pressure and P_{th} is the fragmentation threshold of the magma, defined as the minimum pressure differential that leads to complete fragmentation of the pressurized porous magma (Spieler et al., 2004a). The ejection velocity of the particles thereby depends on the surplus kinetic energy available after fragmentation.

The equation of motion of the caprock propelled by the expansion of the gas-particle mixture is (Alatorre-Ibargüengoitia et al., 2010a):

$$\frac{dV_c}{dt} = \frac{A_c}{m_c} \left\{ P_{ef} \left[1 - \frac{1}{2}(\gamma - 1) \frac{V}{\sqrt{n\gamma R_g T_o}} \right]^{\frac{2\gamma}{\gamma-1}} - P_{ext} \right\} - g \quad (4.5)$$

where V_c , m_c and A_c represent the velocity, mass and cross-sectional area of the caprock, respectively, γ is the specific heat capacity ratio of the mixture considering only the fraction of particles in thermal equilibrium with gas, n is the mass fraction of gas, R_g is the gas constant, T_o is the initial temperature, and P_{ext} is the pressure above the caprock. This equation can be solved numerically to obtain the caprock velocity as a function of time provided the flow remains one-dimensional. Alatorre-Ibargüengoitia et al. (2010a) validated this model via decompression experiments of natural samples from Popocatépetl at high temperature (850°C) and pressures (5-20 MPa) using a shock-tube apparatus. The model is consistent with the experimental results and can be applied to Vulcanian eruptions of Popocatépetl Volcano.

4.4.3 Coupling of caprock and ballistic models

The caprock model of Alatorre-Ibargüengoitia et al. (2010a) can be used together with the ballistic model to estimate the range of the VBP from the initial magma conditions in Vulcanian eruptions: the former model is used to estimate the ejection velocity of the caprock which is then used as the launching velocity of the VBP. This method also helps to account for the drag reduction near the vent using the simple approach proposed by Fagents and Wilson (1993) given by Eqs. (4.2) and (4.3). However, these equations must be used with caution. R_o and t_o are the distance and time required for the caprock to reach its maximum velocity which, in principle, occurs when the mixture reaches the atmospheric pressure. According to the 1-D caprock model, this takes place at distances of few km and several seconds (>10). At this point the 1-D model is no longer valid because the gas and pyroclasts can escape at the sides.

Video analysis of different Vulcanian eruptions at Popocatépetl Volcano suggest that the caprock behaves as a coherent plug until it reaches a distance of ~ 600 - 700 m above the original position, which occurs within 3-6 seconds. In this region, the caprock model can be used. Theoretical calculations indicate that at this point the acceleration of the caprock is less than $\sim 8\%$ of the initial acceleration. Accordingly, we assume that the ejection of the VBP occurs when the acceleration of the caprock is 8% of the initial acceleration and that R_o and t_o in Eqs. (4.2) and (4.3) are the corresponding distance and time. For the region of reduced drag after the acceleration phase we considered a radial geometry (Fagents and Wilson, 1993) considering the restrictions imposed by the crater walls. It is very likely that the initial position of the particles and the near-vent geometry of the conduit exert a strong control on the ejection of individual VBP, but this requires more sophisticated models (e.g. de' Michieli Vitturi et al., 2010) that are beyond the scope of the present paper.

The caprock model involves several parameters (Eq. 4.5) but the most important ones are initial pressure and gas content. The variation of any other parameter within a reasonable range changes the ejection velocity and ballistic range by less than 10%. Figure 4.2 shows the variation of the ejection velocity and the VBP range with initial gas pressure for different porosities. This figure illustrates how the coupled caprock-ballistic model can be used to estimate the maximum range of the VBP from given initial conditions, or estimate the initial conditions that were required to eject a certain ballistic to the observed distance.

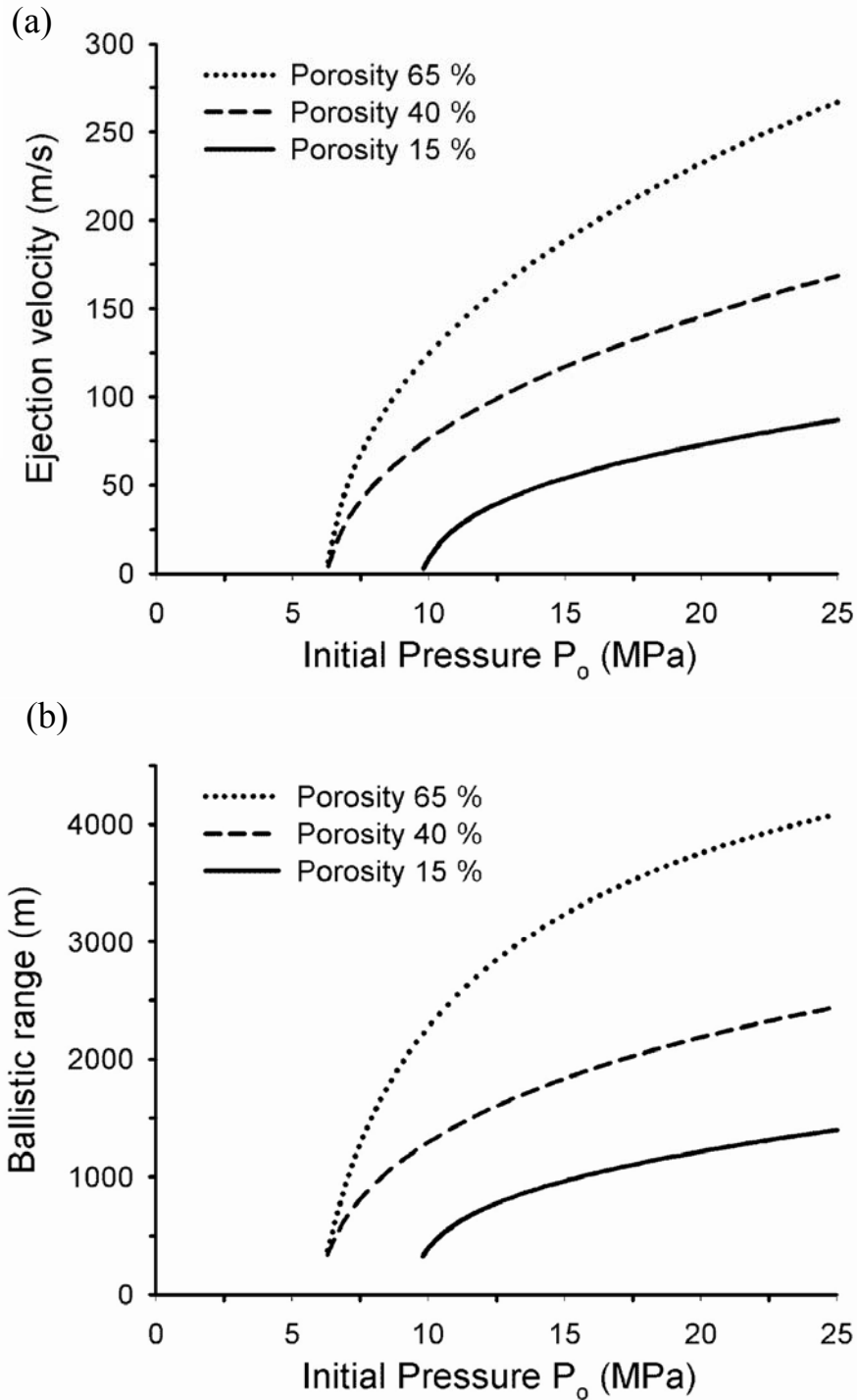


Figure 4.2. (a) Ejection velocity of the VBP as a function of the initial gas pressure for different magma porosities according to the caprock model. A pressure threshold has to be exceeded for fragmentation and ejection of the caprock to take place. Here, we assumed the threshold values measured experimentally for natural samples of Popocatépetl Volcano by Alatorre-Ibargüengoitia et al. (2010a). We computed the ratio $m_c/A_c = \rho_c \cdot T_c$ where ρ_c and T_c are the density and thickness of the caprock, respectively. For the calculations we considered water as the gas phase, $T_o = 850$ °C, $\rho_c = 2300$ kg/m³, $T_c = 25$ m and we assumed that 10% of the magma remains in thermal equilibrium with the gas phase to estimate the effective value of γ (Alatorre-Ibargüengoitia et al., 2010a). Magma porosity is used to calculate n in Eq. (5). The ejection velocity corresponds to the position where the acceleration of the caprock is 8 % of the initial acceleration (see section 4.3). (b) Range for a ballistic with $D = 0.35$ m ejected at the same conditions as in (a) assuming an ejection angle of 42° (optimum angle).

4.4.4 Comparison with videos of Vulcanian eruptions from Popocatépetl Volcano

In order to validate our coupled model, we compared the theoretical results with the observations from videos of different Vulcanian explosions of Popocatépetl Volcano recorded at CENAPRED. The video camera (which sends images continuously to CENAPRED) is located at Alzomoni station, ~ 11 km north of Popocatépetl, at an altitude of 4000 m above sea level (asl). The videos analyzed were from three Vulcanian events that occurred at night, allowing a more thorough observation of the VBP: 17 December 1998, 4 and 14 February 2003. We also analyzed the video of one event which occurred during the day on the 8th of March, 2008, which was recorded with a video camera situated in Cerro Tlamacas ~ 5 km north of the crater. The VBP ejected by these explosions were investigated in the field campaigns.

Three phases of the eruptions were analyzed (Fig. 4.3): (1) the expansion phase from the beginning of the explosions until the caprock ceases to behave as coherent plug, which occurs at a distance of ~ 600 -700 m above the vent; (2) the moment at which the VBP reach their maximum altitude; (3) the phase in which the VBP start to impact the ground. Even when it is not possible to discern in the videos the trajectory of individual ballistics, the mean values of the following parameters can be determined: the times corresponding to each phase, the ejection velocity of the ballistics at the end of the expansion phase and the maximum altitude of the VBP which travelled the maximum distance. The ejection velocity and altitude were corrected for oblique viewing effects following the method of Formenti et al. (2003). The maximum distance from the impact point to the vent was measured during the field campaigns. Table 4.2 shows the comparison of the observed parameters with the values obtained theoretically with the coupled model. For each event, we calculated the initial pressure required to eject the VBP at the maximum observed range considering their size and density measured in the field. This table shows that the couple model reproduces adequately the mean values of the observed parameters and can be used to calculate the maximum range of VBP in Vulcanian eruptions.

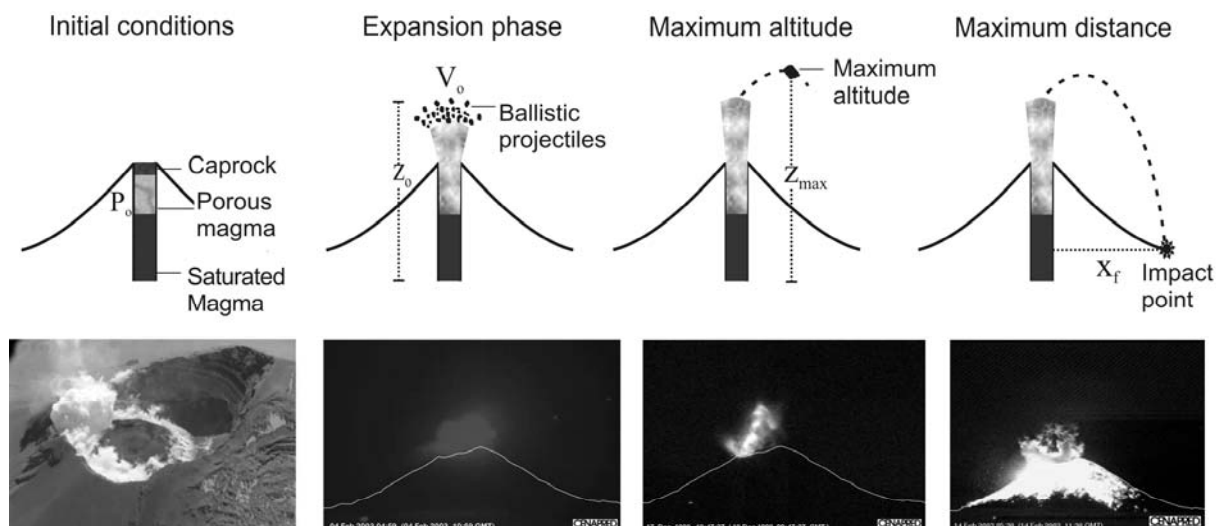


Figure 4.3. Above: Schematic illustration of the Vulcanian eruptions: initially, a dense caprock plugs the conduit and keeps the underlying porous magma at high pressure. When the caprock is disrupted, the porous magma fragments and expands propelling the caprock fragments (expansion phase). At certain point, these fragments separate from the eruptive column and follow ballistic trajectories reaching a maximum altitude before moving downward until they impact the ground. Below from left to right: photograph of a dome (caprock) taken on 16 December 2000, and video stills of Vulcanian events at Popocatépetl Volcano that occurred on 4 February 2003, 17 December 1998 and 14 February 2003. These images correspond to the different phases. Bright returns are incandescent fragments. Source is CENAPRED Web site:

(<http://www.cenapred.unam.mx/es/Instrumentacion/InstVolcanica/MVolcan/>)

Date		Initial Pressure (MPa)	Expansion phase		Maximum altitude		Maximum distance	
			Time (s)	Velocity (m/s)	Time (s)	Altitude (km asl)	Time (s)	Distance (km)
17.12.98	Observed	-	3 - 4	180- 230	12- 14	6.3 - 6.5	31 - 42	3.7
	Theory	18- 22	4	210- 250	12- 14	6.3 - 6.6	38 - 43	3.7
2.02.03	Observed	-	4 - 6	110- 150	11- 12	5.8 - 6.0	27 - 30	2.3
	Theory	9- 11	6 - 7	110- 145	10- 13	5.9 - 6.0	28 - 33	2.3
14.02.03	Observed	-	-	120- 160	7- 10	5.7 - 6.0	24 - 32	2.6
	Theory	10- 12	6 - 7	120- 160	7- 10	6.0 - 6.2	27 - 33	2.6
08.03.08	Observed	-	-	-	-	-	28 - 40	3.2
	Theory	12- 15	5 - 6	150- 190	10- 12	6.3 - 6.5	32 - 37	3.2

Table 4.2. Comparison between the mean observed values and theoretical calculations for different parameters corresponding to three eruptive phases for four Vulcanian events. The pressure was calculated considering the maximum distance reached by the VBP and their size and density measured in the field.

4.5. Explosive scenarios definition

Volcanic hazard is defined as the probability that an area can be affected by potentially destructive volcanic phenomena in a given time interval (Tilling, 1989). In order to delimit hazard zones by VBP impact during volcanic explosions in a realistic way, it is necessary to

establish different explosive scenarios together with their associated probability of occurrence based on statistical evidence. These scenarios can be defined in terms of the maximum kinetic energy associated with the VBP (Alatorre-Ibargüengoitia et al., 2006). This parameterization does not depend on the eruptive processes and therefore yields general scenarios. Analysis of the videos of volcanic explosions from Popocatépetl Volcano shows that not all VBP are ejected with the same kinetic energy. For this reason, the maximum launching kinetic energy alone is used as the parameter that defines the explosive scenarios.

We define high-, intermediate- and low-hazard scenarios depending on the probability of the occurrence of each event according to the past eruptive activity of Popocatépetl Volcano. The high-hazard scenario, the most likely to occur, was defined considering the maximum kinetic energy associated with the VBP with an average diameter of 35 cm that were launched to a maximum distance of 3.7 km from the crater on December 17, 1998. This is the maximum distance that the VBP have reached during the current activity at Popocatépetl Volcano (1994-2010). For the low-hazard scenario, the one with largest intensity but least likely to occur, we used the kinetic energy associated with the ejection of the 35-cm-diameter ballistic found 11.2 km from the crater related to the ~ 14,000 B. P. Plinian eruption at Popocatépetl Volcano. Finally, the intermediate-hazard scenario was defined by using the geometrical average of the kinetic energies of high-hazard and low-hazard scenarios. Table 4.3 presents the kinetic energy for the three scenarios defined for Popocatépetl Volcano.

In order to calculate the maximum kinetic energy for each of these VBP, we used the ballistic model and considered the drag reduction near the vent according to the method of Fagents and Wilson (1993) given by Eqs. (4.2) and (4.3). We considered $R_o = 600$ m for the high-hazard scenario (according to the observations of the videos of Vulcanian eruptions), $R_o = 1600$ m for the low-hazard scenario and an average value of $R_o = 1100$ m for the intermediate-hazard scenario. We also found that the selection of τ in Eq. 4.2 has only a minor influence in the theoretical calculations if $\tau > 600$, which is the case for the three scenarios. Here we note that the selection of these two parameters has a small influence on the calculations of the maximum range if the same values are used to estimate the kinetic energy corresponding to a certain scenario and then to determine the maximum distance in this scenario.

Once the explosive scenarios have been defined, it is necessary to estimate the probability associated with the occurrence of each scenario in a given time interval. De la Cruz-Reyna

(1991) suggested that there is a logarithmic relationship between the rates of occurrence and the Volcanic Explosivity Index (VEI) that can be expressed as follows:

$$\log \lambda_i = aVEI_i + c \quad (4.6)$$

where λ_i is the rate of occurrence of eruptions per year in the magnitude class VEI_i , and a and c are constants. For Popocatépetl Volcano, $a = -0.530$ and $c = -0.524$ (De la Cruz-Reyna and Tilling, 2008). The high-hazard scenario defined here corresponds to the typical Vulcanian eruptions that have occurred during the current activity at Popocatépetl Volcano and during the historical period, with $VEI = 2-3$. The low-hazard scenario corresponds to a Plinian eruption with $VEI = 5$ and the intermediate hazard scenario represents an eruption with $VEI = 4$. Assuming that the eruptive sequence of Popocatépetl Volcano can be described by a stationary Bernoulli process, an approximate estimate of the probability of occurrence of future eruptions can be obtained from the mean occurrence rates using simple probability computations (De la Cruz-Reyna and Tilling, 2008). Table 4.3 shows the probability of at least one eruption occurring for each explosive scenario in any 20-year interval at Popocatépetl according to this method. The probabilities estimated considering different statistical methods are explored elsewhere (Mendoza-Rosas and De la Cruz-Reyna 2008, 2009).

In the case of the high-hazard scenario corresponding to Vulcanian eruptions, the coupled caprock-ballistic model described in section 4.4 can be used to correlate the range of the VBP and their maximum kinetic energy with the initial pressure and gas content, which are parameters that can be estimated from continuous monitoring techniques. With this approach, the probability that certain areas can be affected by VBP can be linked with data from volcano monitoring providing the basis for short term hazard assessment.

Hazard Scenario (VEI)	Kinetic energy (J)	Mean occurrence rate (events/year)	Probability (20 years)	Maximum range (km)	Maximum altitude (km asl)
High (2-3)	1.3×10^6	16/500	0.478	5.1	9.1
Intermediate (4)	1.0×10^7	2/1000	0.039	8.3	12.2
Low (5)	8.0×10^7	10/15,000	0.013	13.1	18.3

Table 4.3. Kinetic energies associated with ballistic projectiles and corresponding maximum ranges and altitudes for the three explosive scenarios defined for Popocatépetl Volcano. The probability that at least one eruption corresponding to each explosive scenario occurs in any 20-year interval was calculated assuming that the eruptive sequence of Popocatépetl can be described by a stationary Bernoulli process. The mean occurrence rate for each scenario corresponds to the data presented by De la Cruz-Reyna and Tilling (2008) for each VEI category.

4.6. Maximum range calculation

In order to calculate the maximum range of the VBP for each explosive scenario it is necessary to determine the optimum launching conditions. The parameters that control the maximum distance of the VBP with a given kinetic energy are: ballistic diameter, launching angle, volcano altitude, topography and wind velocity.

Figure 4.4 shows the range of the VBP as a function of their diameter for three different launching kinetic energies. The movement of the particles smaller than 10-15 cm (depending on the energy) is dominated by the carrier flow field and cannot be adequately described by a ballistic model. For this reason, our results can be applied exclusively to fragments >10-15 cm in diameter. Considering only these fragments, there is an optimum diameter, which depends on the energy, that allows them to reach larger distances than VBP with other sizes (smaller and larger) ejected at same kinetic energy (Fig. 4.4). The initial velocity of larger particles is smaller and therefore their range decreases with size. On the other hand, the velocity of smaller particles is higher, but also the drag force (which is proportional to square velocity) acting on them is much more important, so their range is also reduced. The optimum ballistic diameter is a balance of both situations and depends on the kinetic energy. It is worth noting that in the field campaigns we observed that the diameters of the VBP that reached maximum distance were 20 - 40 cm, which is within the diameter range that yields more than 80 % of the calculated maximum distance.

There is also an optimum angle that allows the VBP to reach the maximum distance at given initial conditions. This angle depends on the altitude difference between the ejection and the landing points, the kinetic energy and ballistic diameter. In our calculations the optimum angle was between 40° and 50° and was calculated for each scenario.

Volcano altitude is also an important factor in the maximum VBP range calculation. The drag force is proportional to the air density, which decreases as a quadratic function of the altitude (Waite et al., 1995). This fact is important in the particular case of Popocatépetl Volcano whose crater altitude is more than 5000 m asl, and therefore the VBP launched by this volcano will reach larger distances than ballistics ejected by volcanoes with lower altitude. Topography is also important because the altitude difference between the crater and the landing spot allows the VBP to travel for longer times and reach larger distances. Finally,

tailwind velocity in the same direction as the VBP could increase the maximum range. For example, a tailwind velocity of 20 m/s in the same direction of a ballistic can increase the maximum range up to 15%.

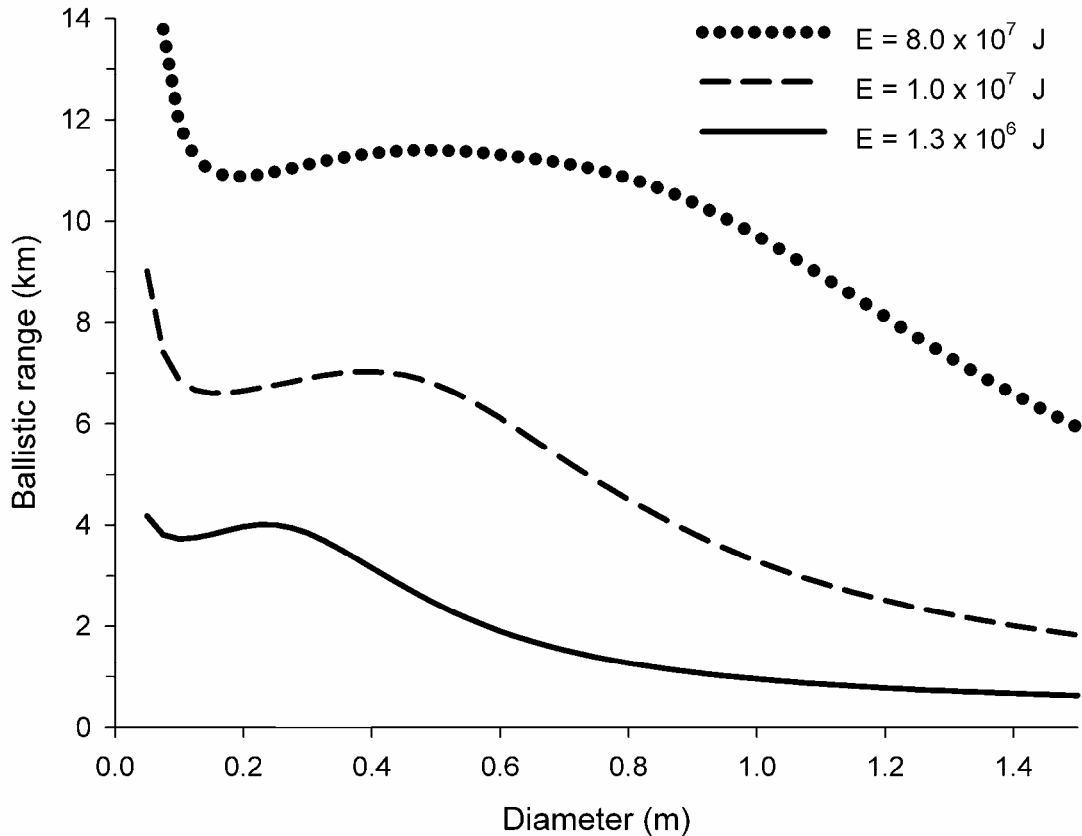


Figure 4.4. Ballistic range as a function of average ballistic diameter for three different launching kinetic energies (E) corresponding to the explosive scenarios defined for Popocatépetl Volcano.

4.7 Volcanic ballistic projectile-hazard map construction for Popocatépetl Volcano

The volcanic ballistic hazard map for Popocatépetl Volcano (Fig. 4.5) graphically depicts the maximum expected distance that the VBP can achieve under the different explosive scenarios defined in section 4.5 according to the past eruptive activity of the volcano. The map was prepared using altimetric digital models (GEMA) with a resolution of 10 m from the Instituto Nacional de Estadística, Geografía e Informática (INEGI), processed with Surfer[®]. The areas that can be potentially affected by VBP were represented in the map using the following convention: high hazard level (the most likely) in red; intermediate hazard level in orange; and low hazard (the least likely to occur) level in yellow.

The VBP maximum range depends on the direction they are launched in because of the topography of the volcano. For this reason, calculations for 16 different directions around the volcano's edifice were made considering the altitude of the expected landing spot. Maximum ranges were calculated using optimum conditions (angle and diameter) corresponding to each case. Considering that our purpose is to estimate the maximum possible distances, a positive tailwind of 20 m/s was used in all the calculations as a reasonable upper value.

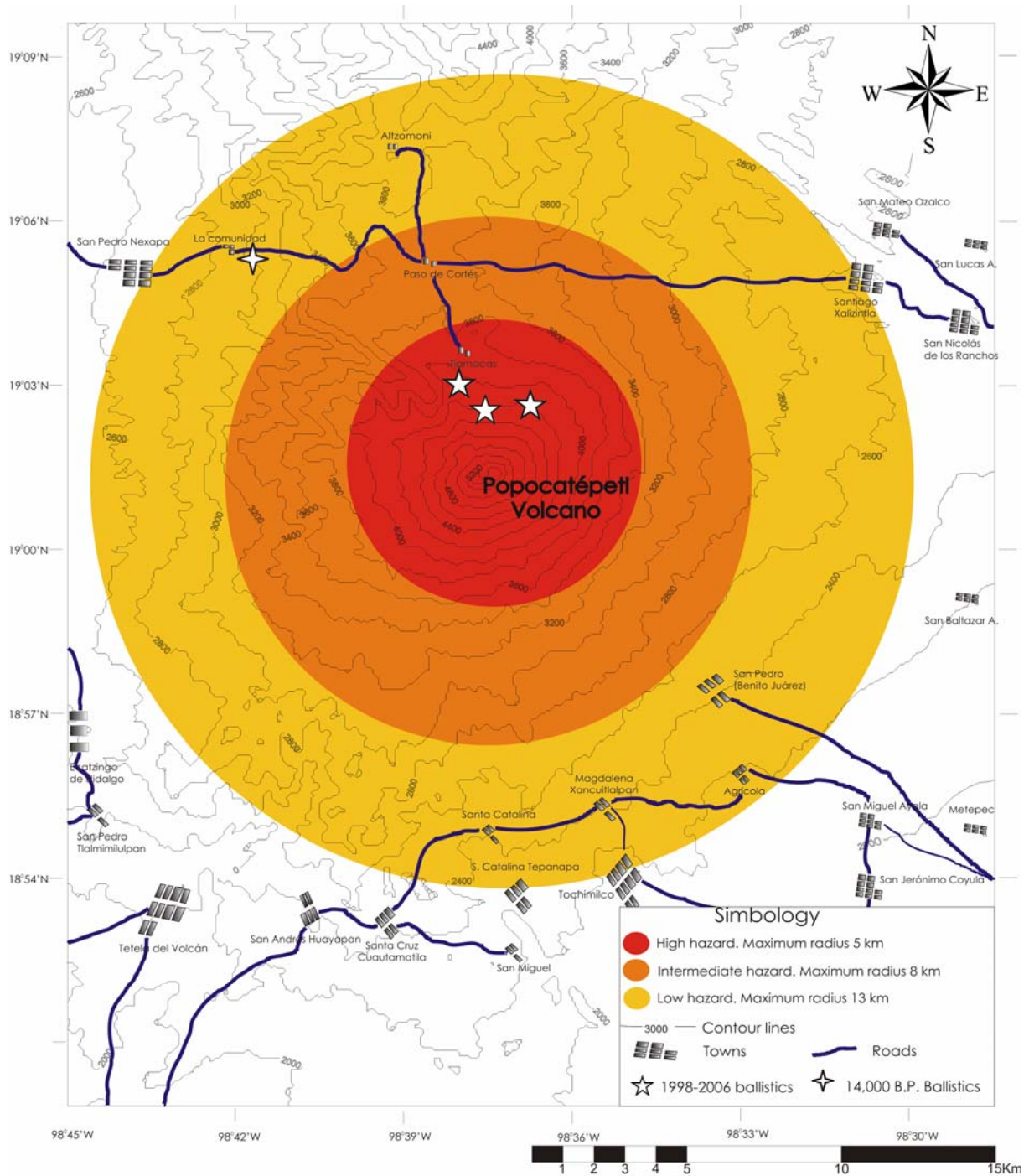


Figure 4.5. Volcanic ballistic projectile hazard map for Popocatépetl Volcano.

VBP also represent a threat for aircrafts in the vicinity of the volcano. For this reason, it is also important to delimit vertical-hazard-zones. In order to define these zones for each scenario, it is necessary to calculate the trajectories of VBP launched with different angles and consider the highest altitude at a given distance, using the diameter that allows the VBP to achieve the maximum altitude in each case. This must be done iteratively for different distances from the crater up to the maximum range that can be reached by the VBP. Table 4.3 shows the maximum ranges and altitudes calculated for each scenario defined in section 4.5.

The aerial hazard zones by VBP can be depicted graphically using vertical and topographic profiles where the maximum distances and highest altitudes attainable are shown for each of the three explosive scenarios using the same color-code conventions as in the map. Figure 4.6 shows two profiles of Popocatépetl Volcano (west-east and south-north) where vertical-hazard-zones represent the areas where impact or encounter with VBP is likely according to our calculations. The maximum altitude of the VBP just above the crater is expected to be controlled by the eruption dynamics, which is reduced in our model to Eqs. (4.2) and (4.3). For this reason, the depicted areas above the crater should be regarded only as first-order estimations.

The different-level hazard zones shown on the VBP hazard map together with the vertical profiles depict the three-dimensional hazard zonation for each scenario, allowing the responsible authorities to make mitigation plans and define horizontal and vertical restriction areas in the case of volcanic crises.

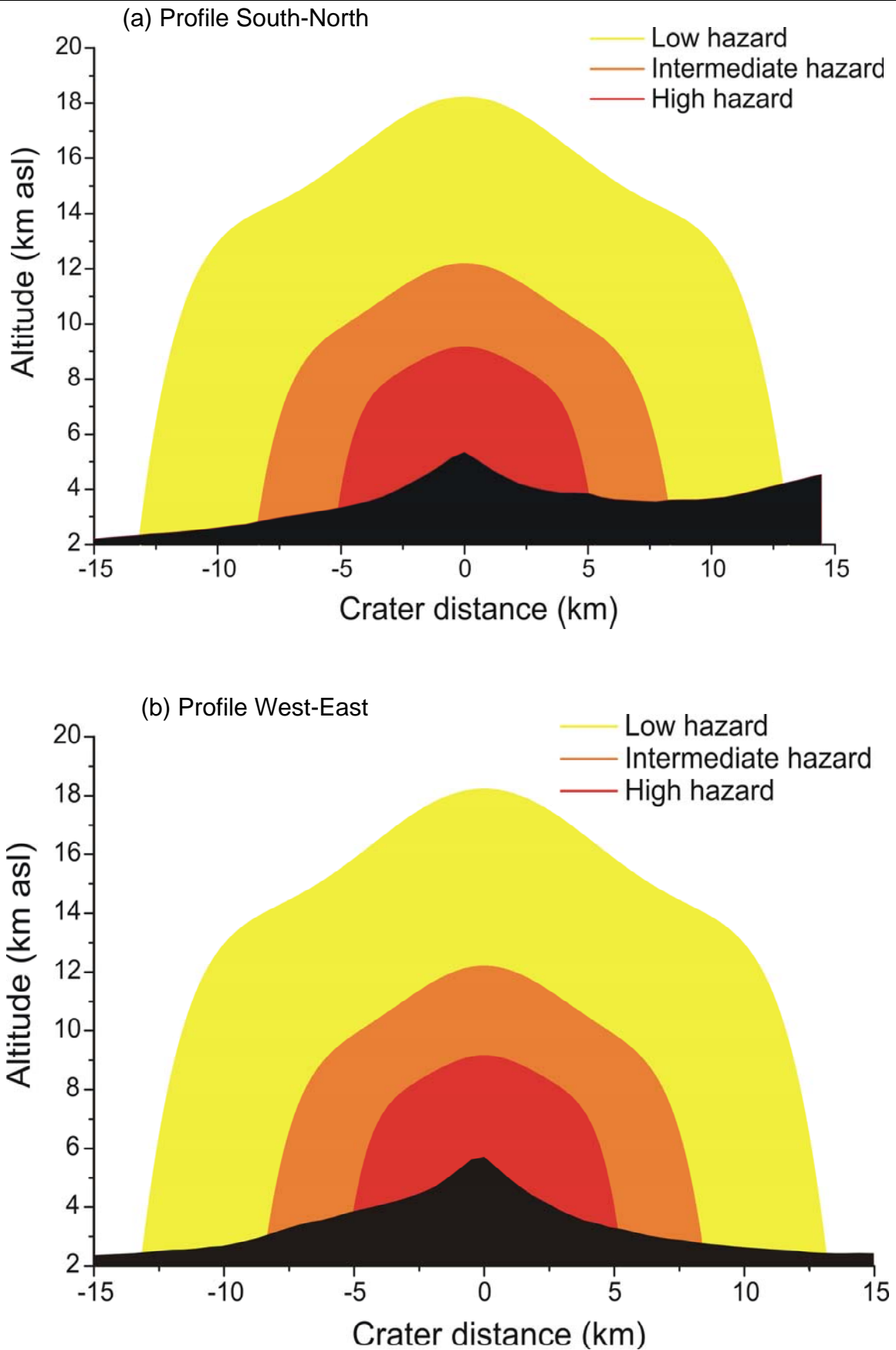


Figure 4.6. Aerial hazard zones for ballistic projectile impact from Popocatépetl Volcano shown with topographic profiles South-North (a) and West-East (b). The color-code conventions corresponding to the three explosive scenarios are the same as in the hazard map (Fig. 4.5).

4.8. Summary

Volcanic ballistic projectiles represent an important hazard to people's lives, infrastructure and air navigation during volcanic eruptions. We present a general methodology to delimit the zones that can be affected by VBP with an application to Popocatépetl Volcano. Three explosive scenarios were defined according to the geological and historical records of the eruptive activity of the volcano in the past. These scenarios were parameterized using the maximum kinetic energy associated to VBP from the relevant eruptions. The probability of at least one eruption occurring in a 20-years interval corresponding to each scenario was estimated with the assumption that the eruptive sequence of Popocatépetl Volcano can be described by a stationary Bernoulli process.

The launching kinetic energy associated with the VBP observed in the field was estimated using a ballistic model using the drag coefficient values for volcanic fragments measured experimentally. The drag reduction near the vent was taken into account using the simple empirical equations suggested by Fagents and Wilson (1993). In the case of Vulcanian eruptions, the most common type of eruptions at Popocatépetl Volcano, the ballistic model was used in concert with the caprock model proposed by Alatorre-Ibargüengoitia et al. (2010a). The coupled model correlates ballistic range with gas content and initial gas pressure, which are parameters that can be estimated by continuous monitoring techniques. The theoretical results are in good agreement with observations from videos of different Vulcanian explosions of Popocatépetl Volcano, which indicates that the coupled model can be used to calculate the maximum range of VBP in this kind of eruptions. With this approach, the probability that certain areas can be affected by VBP can be linked with data from volcano monitoring providing the basis for short term hazard assessment.

The maximum distance reached by VBP in each scenario was calculated considering optimal ballistic diameter, launching angle, altitude, topography and positive tailwind velocity. The horizontal and vertical zones that can be affected by VBP were calculated for the three explosive scenarios defined for Popocatépetl Volcano and are shown on a VBP hazard map with two topographic profiles (west-east and south-north). This graphical representation allows the responsible authorities to make development and mitigation plans, and to define restricted areas in the horizontal and vertical senses during volcanic crises.

Making accessible this kind of maps to the authorities and the general public is an important issue for the planning and mitigation countermeasures (Alatorre-Ibargüengoitia et al. 2001).

Acknowledgments

The authors wish to express their gratitude to (in alphabetic order): Jerónimo Alatorre, Miguel Alatorre-Mendieta, Corrado Cimarelli, Isaac Farraz-Montes, Carlos Fernández, Alberto González-Huesca, Patricia Jácome-Paz, Patricia Julio-Miranda, Ulrich Kueppers, Yan Lavallée, Beatriz Oropeza-Villalobos, Eric Téllez and Esther Romero-Terán for field assistance and Jonathan Hanson for his helpful comments. We also thank Ing. Roberto Quaas for allowing us the access to the video collection of CENAPRED and Lucio Cárdenas (CENAPRED) for the observation and careful selection of explosive events at Popocatépetl Volcano. Financial support to the first author was provided by the Instituto de Geofísica (UNAM) and later by the IDK 31 THESIS program funded by the Elite Network of Bavaria (ENB). Donald B. Dingwell acknowledges the support of a Research Professorship (LMUexcellent) of the Bundesexzellenzinitiative and the EVOKES project of the ERC. This study was partially funded by the FONCICYT program (Mexican Government-European Union), grant 93645 (FIEL-VOLCAN).

Chapter 5

Conclusions and Outlook

5.1 Conclusions

We present a general eruptive model for Vulcanian eruptions based on the 1-D shock-tube theory, including magma fragmentation, via two different approaches. First, we consider the ejection of the caprock that was plugging the vent propelled by the expansion of the underlying gas-particle mixture. To account for the energy consumed by fragmentation we simply assumed that the effective pressure available to eject the particles after fragmentation corresponds to the difference between the initial gas pressure and the fragmentation threshold, (i.e, the minimum pressure required to fragment the magma). This model was validated via decompression experiments in a shock-tube apparatus at 850°C, where we measured the ejection velocity of a caprock placed loosely on top of a volcanic natural sample. In the second approach, we did not account for the ejection of the caprock but instead we considered the dynamics of the fragmentation process assuming the conservation laws across the fragmentation front. To validate this model, we simultaneously measured the fragmentation speed and ejection velocity of the gas-particle mixture in decompression experiments using volcanic rocks at room temperature. The results obtained in the two types of experiments are in good agreement with the corresponding modality of the theoretical model.

In conclusion, the dynamics of magma fragmentation exert a strong influence on the explosive behavior of volcanic eruptions. Fragmentation consumes a significant amount of energy and the fragmentation speed controls the pressure available for the ejection of the gas-particle mixture. The energy consumed by fragmentation and the fragmentation speed depend on magma porosity, initial pressure and the minimum pressure required to completely fragment the samples (fragmentation threshold), which in turn also depends on magma porosity. Our results imply that a certain pressure threshold has to be exceeded for fragmentation and the ejection of particles to take place and that the pressure available for the ejection of the gas-particle mixture is diminished, which in turn reduces the velocity, density and the mass discharge rate of the gas-particle mixture, all factors which can affect eruption dynamics significantly.

Important characteristics of the gas-particle dynamics were observed in the performed experiments. We observed in all experiments that the velocity and concentration of particles in the flow is higher at the initial stage of the flow, implying that most of the kinetic energy is released at this stage. Throughout the experiment, we measured a non-linear decay of the velocity of particles as a function of time. During the initial stage of the flow, we did not notice a systematic difference in the ejection velocities of particles with different sizes (ranging between 0.5 and 8 mm) and we did not discern a change in the fragmentation efficiency with time. Our experiments show that the grain-size distribution produced during fragmentation controls the mechanical and thermal coupling between the gas phase and the particles. Analysis of the experimentally generated pyroclasts reveals that the efficiency of fragmentation increases with the applied pressure and sample porosity (Kueppers et al., 2006 a, b; Alatorre-Ibargüengoitia et al., 2010b). Furthermore, we observed heterogeneities in the concentration of particles that might be related to the layer-by-layer fragmentation process. These heterogeneities may also occur in volcanic explosions and might be one reason for the shift from a stable plume regime to an unstable one with partial plume collapse in which pyroclastic flows are simultaneously along generated with eruptive clouds.

The model, with the two modalities presented herein, may describe the dynamics of brittle fragmentation in Vulcanian eruptions and yield more realistic initial pressures at the onset of fragmentation than previous models. This is important because calibrating more realistic gas pressures allows interpreting adequately the data obtained by monitoring techniques. Moreover, our model can be combined with pyroclasts dispersal model in unsteady eruptions to enhance our understanding of Vulcanian events. We applied the caprock model to recent Vulcanian eruptions of Popocatepetl and Colima volcanoes and estimated the initial gas pressure required to disrupt the caprock, fragment the underlying magma and eject ballistic projectiles at the observed distance.

One of the most common hazards associated with Vulcanian eruptions are ballistic projectiles. We present a general methodology to delimit the zones that can be affected by these projectiles with an application to Popocatepetl Volcano. Three explosive scenarios were defined according to the past activity of the volcano and parameterized using the maximum kinetic energy associated to these projectiles calculated using a ballistic model. The probability of occurrence of at least one eruption in a given time interval was estimated. In the case of Vulcanian eruptions, the most frequently observed type of activity at Popocatepetl, the

ballistic model was used in concert with the caprock model to relate initial pressure and gas content to ballistic range. The coupled model was calibrated and validated with field and video observations of ballistics ejected during different Vulcanian eruptions at Popocatepetl Volcano. This coupled model relates the zones that could be affected by the impact of ballistic projectiles with the initial pressure that can be estimated from seismic and geophysical monitoring, providing valuable information for more refined short-term hazard assessment at active explosive volcanoes. The maximum ranges expected for the ballistics in the three different explosive scenarios defined for Popocatepetl Volcano are presented in a ballistic hazard map with two topographic profiles (west-east and south-north). This graphical representation allows the people and concerned authorities to make development and mitigation plans, and to define restricted areas, in the horizontal and vertical senses, during volcanic crises.

5.2 Outlook

The study presented herein opens the possibility of several new lines of scientific research, some of which are briefly introduced here. As mentioned above, our results show that the fragmentation speed determines the initial condition for the expansion of the gas-particle mixture. To date, fragmentation speed at magmatic temperatures is not well known. However, the model presented in Chapter 3 provides the basis to estimate the fragmentation speed at high temperature from the ejection velocity of the gas-particle mixture if the rest of the parameters are controlled. An experimental study to investigate the influence of temperature on the fragmentation speed is in progress. Further experiments will be designed to monitor with a high-speed camera the complete process, including fragmentation and particle ejection, to investigate the origin of the heterogeneities observed in the two-phase flow and explore possible implications for volcanic eruptions.

Rapid decompression experiments, such as the ones presented herein, are very useful to calibrate and interpret the data obtained from monitoring techniques of volcanic eruptions. Fragmentation experiments performed in the field under well controlled conditions have been thoroughly monitored with: 1) Doppler Radar, 2) high-speed and high-definition cameras, 3) acoustic and infrasound sensors, and 4) pressure transducers. These experiments have been aimed to check for common results achieved by the different approaches and, if so, calibrate

state-of-the-art monitoring tools (Kueppers et al., 2010). Some encouraging results have been obtained, but more experiments are required and will be performed in future campaigns.

Moreover, our experiments successfully reproduce the main characteristics of the jets produced by the impulsive release of pressurized gas-particle mixtures in explosions at Stromboli volcano (Italy) that have been monitored with a high-speed camera. In particular, the velocity of the particles within individual jets decay with time following the same pattern as observed in our experiments (Fig. 2.6). The experiments and theoretical model presented herein significantly helps to interpret the observations and provide the basis to quantify -for the first time- the number, frequency, timing, pressure, volume, and depth of the individual gas release events produced during a single explosion (Tadeucci et al., 2011).

Finally, micro-seismic evaluation of our well-controlled fragmentation experiments offers the hope of a better understanding of source mechanisms in natural volcanic seismicity. It is possible to investigate the relationships between pressure and decompression time versus maximum amplitudes, source duration, decay of seismic waves and force. From these relationships, the pre-eruption conduit state can be estimated in volcanic systems, and thus the ejection velocity can be estimated in order to evaluate the implications for hazard analysis. This experimental approach is very useful to obtain a direct measure of the source parameters of the physical mechanism and evaluate the viability of the theoretical single force model to quantify natural volcanic eruptions (Arciniega et al., 2010).

All these topics are currently under investigation and eventually will lead to still more questions to be addressed in our permanent pursuit of a better understanding of volcanic systems.

References

- Alatorre-Ibargüengoitia M.A., Delgado-Granados H., Farraz-Montes I., 2001. Mapa de Peligros por Caída de Productos balísticos del Volcán Popocatepetl (in Spanish) <http://www.geofisica.unam.mx/divulgacion/mapas/balisticos.zip>.
- Alatorre-Ibargüengoitia, M.A. and Delgado-Granados, H., 2006. Experimental determination of drag coefficient for volcanic materials: Calibration and application of a model to Popocatepetl volcano (Mexico) ballistic projectiles. *Geophys. Res. Lett.* 33, L11302. doi:10.1029/2006GL026195.
- Alatorre-Ibargüengoitia, M.A., Delgado-Granados, H. and Farraz-Montes, I.A., 2006. Hazard zoning for ballistic impact during volcanic explosions at Volcán de Fuego de Colima (Mexico). *Geol. Soc. Am. Special Paper* 402, 26-39.
- Alatorre-Ibargüengoitia, M.A., Scheu, B., Dingwell, D.B., Delgado-Granados, H., and Taddeucci, J., 2010a. Energy consumption by magmatic fragmentation and pyroclast ejection during Vulcanian eruptions. *Earth Planet. Sci. Lett.* 291, 60-69. doi:10.1016/j.epsl.2009.12.051
- Alatorre-Ibargüengoitia, M., Capuccini, F., Kueppers, U., Perugini, D., Dingwell, D.B., 2010b. Determination of volcanic eruption explosivity from fractal analysis of experimentally generated pyroclasts. *Geophys. Res. Abstr.*, 12, EGU2010-9379-1.
- Alatorre-Ibargüengoitia, M.A., Scheu, B., Dingwell, D.B., 2011. Influence of the fragmentation process on the dynamics of Vulcanian eruptions: An experimental approach, *Earth Planet. Sci. Lett.*, 302, 51-59. doi:10.1016/j.epsl.2010.11.045
- Alidibirov, M., 1994. A model for viscous magma fragmentation during volcanic blast. *Bull. Volcanol.* 56, 459-465.
- Alidibirov, M. and Dingwell, D.B., 1996a. Magma fragmentation by rapid decompression. *Nature* 380, 146-148.
- Alidibirov, M. and Dingwell, D.B., 1996b. An experimental facility for the investigation of magma fragmentation by rapid decompression. *Bull. Volcanol.* 58, 411-416.
- Alidibirov, M., and Dingwell, D.B., 2000. Three fragmentation mechanism for highly viscous magma under rapid decompression. *J. Volcanol. Geotherm. Res.* 100, 413-421.
- Arciniega-Ceballos A., Alatorre-Ibargüengoitia M., Scheu B., Dingwell D.B. and Delgado-Granados H., 2010. Analysis of micro-seismic signals and source parameters of eruptions generated by rapid decompression of volcanic rocks. Abstract V33C-2401 presented at 2010 Fall Meeting, AGU, San Francisco, Calif., 13-17 Dec.

-
- Blong R.J., 1984. Volcanic hazards: A Sourcebook on the Effects of Eruptions. Orlando, Academic Press.
- Bower S.M. and Woods A.W., 1996. On the dispersal of clasts from volcanic craters during small explosive eruptions. *J. Volcanol. Geotherm. Res.* 73,19-32.
- Cagnoli, B., Barmin, A., Melnik, O. and Sparks, R.S.J., 2002. Depressurization of fine powders in a shock tube and dynamics of fragmented magma in volcanic conduits. *Earth Planet. Sci. Lett.* 204, 101-113.
- Capra L., Poblete M.A., Alvarado R., 2004. The 1997 and 2001 lahars of Popocatépetl volcano (Central Mexico), textural and sedimentological constraints on their origin and hazards. *J. Volcanol. Geotherm. Res.* 131, 351-369.
- Carazzo, G., Kaminski, E. and Tait, S., 2008. On the dynamics of volcanic columns: A comparison of field data with a new model of negatively buoyant jets. *J. Volcanol. Geotherm. Res.* 178, 94-103.
- Cashman, K.V., Sturtevant, B., Papale, P. and Navon, O., 2000. Magmatic fragmentation, in Sigurdsson H. (Editor), *Encyclopedia of Volcanoes*, Academic Press, San Diego, USA, pp. 421-430.
- Chojnicki, K., Clarke, A.B. and Phillips, J.C., 2006. A shock-tube investigation of the dynamics of gas-particle mixtures: Implications for explosive volcanic eruptions. *Geophys. Res. Lett.* 33, L15309.
- Clarke, A.B., Voight, B., Neri, A., and Macedonio, G., 2002. Transient dynamics of vulcanian explosions and column collapse. *Nature*, 415, 897– 901.
- Clarke, A.B., Phillips, J.C. and Chojnicki, K.N., 2009. An investigation of Vulcanian eruption dynamics using analogue experiments and scaling analysis, in Thordarson, T., Self, S., Larsen, G., Rowland, S.K. and Hoskuldsson, A. (Eds.), *Studies in Volcanology: The Legacy of George Walker*.
- De la Cruz-Reyna S., 1991. Poisson-distributed patterns of explosive eruptive activity. *Bull. Volcanol.* 54, 57–67.
- De la Cruz-Reyna S. and Tilling R., 2008. Scientific and public responses to the ongoing volcanic crisis at Popocatépetl Volcano, México: importance of an effective hazards warning system. *J. Volcanol. Geotherm. Res.* 170, 121–134.
- De la Cruz-Reyna S., Quezada J.L., Peña C., Zepeda O., Sanchez T., 1995. Historia de la actividad reciente del Volcán Popocatépetl. *Volcán Popocatépetl Estudios Realizados durante la Crisis de 1994–1995*. SINAPROC-CENEPRED-UNAM, Mexico City, pp 3–22 (in Spanish).

-
- De la Cruz-Reyna, S., Meli, R.P. and Quaas, R.W., 2000. Volcanic crises management, in: Sigurdsson H. (Editor), *Encyclopedia of Volcanoes*, Academic Press, San Diego, USA, pp. 1199–1214.
- Delgado-Granados H., Cárdenas González L. and Piedad Sánchez N., 2001. Sulfur dioxide emissions from Popocatepetl volcano (Mexico), case study of a high-emission rate, passively degassing erupting volcano. *J. Volcanol. Geotherm. Res.* 108, 107-120.
- Dellino P., Dioguardi F., Zimanowski B., Büttner R., Mele D., La Volpe L., Sulpizio R., Doronzo D. M., Sonder I., Bonasia R., Calvari S. and Marotta E., 2010. Conduit flow experiments help constraining the regime of explosive eruptions. *J. Geophys. Res.*, 115, B04204, doi:10.1029/2009JB006781.
- de' Michieli Vitturi M., Neri A., Esposti Ongaro T., Lo Savio S., Boschi E., 2010. Lagrangian modeling of large volcanic particles: Applications to Vulcanian explosions. *J. Geophys. Res.* 115, B08206, doi:10.1029/2009JB007111.
- Dingwell, D.B., 1996. Volcanic dilemma: flow or blow? *Science*, 273, 1054-1055.
- Dingwell, D.B. and Webb, S.L., 1989. Structural relaxation in silicate melts and non-Newtonian melt rheology in geological processes. *Phys. Chem. Miner.* 16, 508-516.
- Druitt, T.H. and Young, S.R. 2002. Episodes of cyclic Vulcanian explosive activity with fountain collapse at Soufrière Hills volcano, Montserrat. in: Druitt T.H. and Kokelaar, B.P. (Eds.) *The Eruption of Soufrière Hills Volcano, Montserrat, from 1995 to 1999*. Geological Society, London, *Memoirs*, 21, 281–306.
- Fagents, S.A. and Wilson, L., 1993. Explosive volcanic eruptions- VII. The ranges of pyroclasts ejected in transient volcanic explosions. *Geophys. J. Int.* 113, 359-370.
- Formenti, Y., Druitt, T.H., and Kelfoun, K., 2003. Characterisation of the 1997 Vulcanian explosions of Soufrière Hills Volcano, Montserrat, by video analysis. *Bull. Volcanol.* 65, 587-605.
- Fowler, A.C., Scheu B., Lee W.T. and McGuinness, M.J., 2010. A theoretical model of the explosive fragmentation of vesicular magma. *Proc. R. Soc. A.*, 466 (2115) 731-752. doi:10.1098/rspa.2009.0382.
- Fudali, R.F., and Melson, W.G., 1972, Ejecta velocities, magma chamber pressure and kinetic energy associated with the 1968 eruption of Arenal volcano. *Bull. Volcanol.* 35, 383–401.
- Gellert E.P. Cimpoeru S.J. and Woodward R.L., 2000. A study of the effect of target thickness on the ballistic perforation of glass-fibre-reinforced plastic composites. *Int. J. Impact Eng.* 24, 445-456.

-
- Hoblitt, R. 1986. Observations of the Eruptions of July 22 and August 7, 1980, at Mount St. Helens, Washington. U.S. Geol. Surv. Professional Papers, 1335.
- Johnson, J. B., Harris, A. J. L., Sahetapy-Engel, S. T. M., Wolf, R. and Rose W. I., 2004. Explosion dynamics of pyroclastic eruptions at Santiaguito Volcano, *Geophys. Res. Lett.*, 31, L06610, doi:10.1029/2003GL019079.
- Julio-Miranda P., González-Huesca A.E., Delgado Granados H. and Kääh A., 2005. Glacier melting formation during January 22, 2001, eruption, Popocatepetl volcano (Mexico), *Zeitschrift für Geomorphologie* 140, 95-102.
- Julio-Miranda P., Delgado Granados H., Huggel C. and Kääh A., 2008. Impact of the eruptive activity on glacier evolution at Popocatepetl volcano (Mexico) during 1994-2001, *J. Volcanol. Geotherm. Res.* 170, 86-98. doi:10.1016/j.jvolgeores.2007.09.011.
- Kennedy, B., Spieler O., Scheu B., Kueppers U., Taddeucci J. and Dingwell, D.B., 2005. Conduit implosion during Vulcanian eruptions. *Geology* 33 (7), 581–584.
- Koyaguchi, T. and Mitani, N. K., 2005. A theoretical model for fragmentation of viscous bubbly magmas in shock tubes. *J. Geophys. Res.* 110, B10202, doi:10.1029/2004JB003513.
- Koyaguchi, T., Scheu, B., Mitani, N. and Melnik, O., 2008. A fragmentation criterion for highly viscous bubbly magmas estimated from shock tube experiments. *J. Volcanol. Geotherm. Res.* 178, 58-71.
- Koyaguchi, T., Suzuki, Y. J. and Kozono, T., 2010. Effects of the crater on eruption column dynamics. *J. Geophys. Res.*, 115, B07205, doi:10.1029/2009JB007146.
- Kremers, S., Scheu, B., Cordonnier, B., Spieler, O. and Dingwell, D.B., 2010. Influence of decompression rate on fragmentation processes: An experimental study. *J. Volcanol. Geotherm. Res.* 193, 182-188.
- Kueppers, U., Scheu, B., Spieler, O. and Dingwell, D.B., 2006a. Fragmentation efficiency of explosive volcanic eruptions: A study of experimentally generated pyroclasts. *J. Volcanol. Geotherm. Res.* 153, 125-135.
- Kueppers, U., Perugini, D. and Dingwell, D.B., 2006b. “Explosive Energy” during volcanic eruptions from fractal analysis of pyroclasts. *Earth Planet. Sci. Lett.* 248, 800–807.
- Kueppers, U., Alatorre-Ibargüengoitia, M., Hort, M., Kremers, S., Meier, K., Scharff, L., Scheu, B., Taddeucci, J. and Dingwell, D.B., 2010. Volcanic monitoring techniques applied to controlled fragmentation experiments. Abstract V21E-2366 presented at 2010 Fall Meeting, AGU, San Francisco, Calif., 13-17 Dec.

-
- Landau, L.D. and Lifshitz, E.M., 1987. Fluid Mechanics. Pergamon Press, Great Britain, 551 pp.
- Lavallée, Y., Varley, N., Alatorre-Ibargüengoitia, M.A., Hess, K.U., Kueppers, U., Mueller, S., Richard, D., Scheu, B., Spieler, O. and Dingwell, D.B. Magmatic architecture of dome-building eruptions at Volcán de Colima, Mexico. Submitted to Bull. Volcanol.
- Macías J.L. and Siebe C., 2005. Popocatepetl's crater filled to the brim: significance for hazard evaluation. *J. Volcanol. Geotherm. Res.* 141,327–330.
- Mader, H.M., Manga, M. and Koyaguchi, T., 2004. The role of laboratory experiments in vulcanology. *J. Volcanol. Geotherm. Res.*, 129, 1-5.
- Martín del Pozzo, A.L., Cifuentes, G., Cabral-Cano, E., Bonifaz, R., Correa, F. and Mendiola, I.F., 2003. Timing magma ascent at Popocatepetl Volcano, Mexico, 2000-2001. *J. Volcanol. Geotherm. Res.* 125, 107-120.
- Mastin L.G., 2001. A Simple Calculator of Ballistic Trajectories for Blocks Ejected During Volcanic Eruptions. Open-file Report 01-45, U.S. U.S. Geol. Surv., Vancouver, Washington, USA.
- Mastin, L.G., and Ghiorso, M.S., 2000. A numerical program for steady-state flow of magma-gas mixtures through vertical eruptive conduits. U.S. Geol. Surv. Open-file Report, 00-209.
- McBirney, A.R. and Murase, T., 1970. Factors governing the formation of pyroclastic rocks. *Bull. Volcanol.* 34, 372-384.
- Mendoza-Rosas A.T. and De la Cruz-Reyna S., 2008. A statistical method linking geological and historical eruption time series for volcanic hazard estimations: Applications to active polygenetic volcanoes. *J. Volcanol. Geotherm. Res.* 176, 277–290.
- Mendoza-Rosas A.T. and De la Cruz-Reyna S., 2009. A mixture of exponentials distribution for a simple and precise assessment of the volcanic hazard. *Nat. Hazards Earth. Syst. Sci.* 9, 425–431.
- Morrisey, M., and Mastin, L., 2000. Vulcanian Eruptions, in: Sigurdson H. (Editor), *Encyclopedia of Volcanoes*. Academic Press, San Diego, USA, pp. 463-475.
- Mueller, S., Melnik, O., Spieler, O., Scheu, B. and Dingwell, D.B., 2005. Permeability and degassing of dome lavas undergoing rapid decompression: an experimental determination. *Bull. Volcanol.* 67, 526-538.
- Mueller, S., Scheu, B., Spieler, O. and Dingwell, D., 2008. Permeability control on magma fragmentation. *Geology* 36 (5), 399–402.

-
- Nairn, I. A. and Sef, S. 1978. Explosive eruptions and pyroclastic avalanches from Ngauruhoe in February 1975. *J. Volcanol. Geotherm. Res.* 3, 39–60.
- Nakada, S., Shimizu, H. and Ohta, K., 1999. Overview of the 1990-1995 eruption at Unzen Volcano. *J. Volcanol. Geotherm. Res.* 89, 1-22.
- Neri, A., and Dobran F., 1994. Influence of eruption parameters on the thermofluid dynamics of collapsing volcanic columns, *J. Geophys. Res.*, 99 (B6), 11,833–11,857.
- Neri, A., Esposti Ongaro, T., Macedonio, G. and Gidaspow, D., 2003. Multiparticle simulation of collapsing volcanic columns and pyroclastic flow. *J. Geophys. Res.* 108 (B4), 2202, doi:10.1029/2001JB000508.
- Papale, P., 1999. Strain-induced magma fragmentation in explosive eruptions. *Nature* 397, 425-428.
- Ramos, J.I., 1995. One-dimensional, time-dependent, homogeneous, two-phase flow in volcanic conduits. *Int. J. Num. Methods in Fluids* 21, 253-278.
- Riddle R., Lesuer D., Syn C., Gogolewski R. and Cunningham B., 1996. Application of metal laminates to aircraft structures: Prediction of penetration performance. *Finite Elem. Anal. Des.* 23, 173-192.
- Robin C. and Boudal, C., 1987. A gigantic Bezymianny-type event at the beginning of modern Popocatepetl. *J. Volcanol. Geotherm. Res.* 31, 115–130.
- Sahagian, D., 2005. Volcanic eruption mechanisms: Insights from intercomparison of models of conduit processes. *J. Volcanol. Geotherm. Res.* 143, 1-15.
- Scheu, B., Spieler, O. and Dingwell, D.B., 2006. Dynamics of explosive volcanism at Unzen volcano: an experimental contribution. *Bull. Volcanol.* 69, 175-187.
- Scheu, B., Kueppers, U., Mueller, S., Spieler, O. and Dingwell, D., 2008. Experimental volcanology on eruptive products of Unzen volcano. *J. Volcanol. Geotherm. Res.* 175, 110-119.
- Self, S., Wilson, L. and Nairn, I., 1979. Vulcanian eruption mechanisms. *Nature* 277, 440-443.
- Self S., Kienle J. and Huot J., 1980. Ukinrek Maars, Alaska, II. Deposits and Formation of the 1977 Craters. *J. Volcanol. Geotherm. Res.* 7, 39-65.
- Sherwood A.E., 1967. Effect of Air Drag on Particles Ejected during Explosive Cratering. *J. Geophys. Res.* 72 (6), 1783-1791.
- Siebe, C., and Macías, J.L., 2004, Volcanic hazards in the Mexico City metropolitan area from eruptions at Popocatepetl, Nevado de Toluca, and Jocotitlán stratovolcanoes and monogenetic scoria cones in the Sierra Chichinautzin Volcanic Field: Field Guide, Penrose Conference. Boulder, Colorado, Geological Society of America, 77 p., doi: 10.1130/2004.

-
- Siebe C., Abrams M., Macías J.L., Obenholzner J., 1996. Repeated volcanic disasters in Prehispanic time at Popocatepetl, Central Mexico: past key to the future? *Geology* 24, 399–402.
- Sigurdsson, H., 2000. Introduction, in: Sigurdsson, H. (Editor), *Encyclopedia of Volcanoes*. Academic Press, San Diego, CA, USA, pp. 1–13.
- Simkin, T., Seibert, L. and Blong, R., 2001. Volcano fatalities—lessons from the historical record. *Science* 291, 255.
- Small C. and Naumann T., 2001. The global distribution of human population and recent volcanism. *Environ. Hazards* 3, 93–109.
- Smithsonian Institution, 1991. Sakurajima, Explosions remain frequent; tephra from one explosion damages houses and cars. *Bull. Glob. Volcanism Netw.* 16 (6).
- Smithsonian Institution, 1998a. Popocatepetl. Growing lava body in crater leads to larger explosions. *Bull. Glob. Volcanism Netw.* 23 (11).
- Smithsonian Institution, 1998b. Popocatepetl. Ash emissions, fires following energetic explosions in December. *Bull. Glob. Volcanism Netw.* 23 (12).
- Smithsonian Institution, 1999. Colima. Lava lobes continue to advance, explosion on 10 February ejects ash and ballistic blocks. *Bull. Glob. Volcanism Netw.* 24 (1).
- Smithsonian Institution, 2000, Popocatepetl. December set records in tremor, dome extrusion rates, SO₂ flux, and tilt. *Bull. Glob. Volcanism Netw.* 25 (12).
- Smithsonian Institution, 2001. Masaya. Tourists experience a brief, bomb-charged 23 April 2001 explosion: no fatalities. *Bull. Glob. Volcanism Netw.* 26 (4).
- Smithsonian Institution, 2003a, Popocatepetl. Cycles of dome growth and destruction; continuing activity. *Bull. Glob. Volcanism Netw.* 28 (2).
- Smithsonian Institution, 2003b. Stromboli. Strong explosion on 5 April covers much of the summit in pyroclastic deposits. *Bull. Glob. Volcanism Netw.* 28 (4).
- Spieler, O., Kennedy, B., Kueppers, U., Dingwell, D.B., Scheu, B. and Taddeucci, J., 2004a. The fragmentation threshold of pyroclastic rocks. *Earth Planet. Sci. Lett.* 226, 139-148.
- Spieler, O., Dingwell, D.B. and Alidibirov, M., 2004b. Magma fragmentation speed: an experimental determination. *J. Volcanol. Geotherm. Res.*, 129, 109-123.
- Steinberg G.S. and Lorenz V., 1983. External Ballistic of Volcanic Explosions. *Bull. Volcanol.* 46 (4), 333-348.

-
- Stix, J., Torres, R. C., Narvaez, L., Cortes S. P., Raigosa, J., Gomez, D.M. and Castonguay, R., 1997. A model of Vulcanian eruptions at Galeras volcano, Colombia. *J. Volcanol. Geotherm. Res.* 77, 285–303.
- Straub S.M. and Martin-Del Pozzo A.L. 2001. The significance of phenocryst diversity in tephra from recent eruptions at Popocatepetl volcano (central Mexico). *Contrib. Mineral. Petrol.* 140, 487-510.
- Suzuki, Y. J., Koyaguchi, T., Ogawa, M. and Hachisu, I., 2005. A numerical study of turbulent mixing in eruption clouds using a three-dimensional fluid dynamics model, *J. Geophys. Res.* 110, B08201, doi:10.1029/2004JB003460.
- Taddeucci, J., Spieler, O., Kennedy, B., Pompilio, M., Dingwell, D.B. and Scarlato, P., 2004. Experimental and analytical modeling of basaltic ash explosions at Mount Etna, Italy, 2001. *J. Geophys. Res.* 109, B08203, doi :10.1029/2003JB002952.
- Taddeucci J., Scarlato P., Alatorre-Ibargüengoitia M., and the GVS, 2011. How much? How deep? How often? Parameterizing explosive gas release during Strombolian activity. *Geophys. Res. Abstr.*, 13, Vol. 13, EGU2011-6225. Will be presented at 2011 EGU General Assembly, Vienna, Austria, 3-8 April.
- Tilling R.I., 1989. Introductions and overview, in: Tilling R.I. (Editor), *Volcanic hazards: Short course presented at the 28th International Geological Congress*. AGU, Washington DC, USA, pp. 1–8.
- Turcotte, D.L., Ockendon, H., Ockendon, J.R. and Cowley, S.J., 1990. A mathematical model of vulcanian eruptions. *Geophys. J. Int.* 103, 211-217.
- Waitt R.B., Mastin L.G. and Miller T.P., 1995. Ballistic Showers During Crater Peak Eruptions of Mount Spurr Volcano, Summer 1992. *U.S.G.S. Bulletin* 2139, 89-106.
- Wilson L., 1972. Explosive Volcanic Eruptions II. The Atmospheric Trajectories of Pyroclasts. *Geophys. J. R. Astron. Soc.* 30, 381-392.
- Wilson, L., 1980. Relationships between pressure, volatile content and ejecta velocity in three types of volcanic explosion. *J. Volcanol. Geotherm. Res.* 8, 297-313.
- Witter, J.B., Kress, V.C. and Newhall, C.G., 2005. Volcán Popocatepetl, Mexico. Petrology, Magma Mixing, and Immediate Sources of Volatiles for the 1994-Present Eruption. *Jour. Petrol.* 46 (11), 2337-2366.
- Wright R., De la Cruz-Reyna S., Harris A., Flynn L., Gómez-Palacios J.J., 2002. Infrared satellite monitoring at Popocatepetl: Explosions, exhalations, and cycles of dome growth. *J. Geophys. Res.* 107 (B8). doi:10.1029/2000JB000125.
- Woods, A.W., 1995. A model for Vulcanian explosions. *Nucl. Eng. Design.*, 155, 345-357.

-
- Zhang, Y., 1999. A criterion for the fragmentation of bubbly magma based on brittle failure theory. *Nature* 402, 648-650.
- Zobin V.M., Luhr J.F., Taran Y.A., Bretón M., Cortés A., De La Cruz-Reyna S., Domínguez T., Galindo I., Gavilanes J.C., Muñíz J.J., Navarro C., Ramírez J.J., Reyes G.A., Ursúa M., Velasco J., Alatorre E., Santiago H., 2002. Overview of the 1997-2000 activity of Volcán de Colima, México: *J. Volcanol. Geotherm. Res.* 117, 1-19.

Curriculum Vitae

Personal data

Miguel Ángel Alatorre Ibarguengoitia, Born on 8 September 1979 in Mexico D.F., Mexico

Education

- 2007 – 2011 **Doctor rerum naturalium in Volcanology through the Elite Network of Bavaria-** Ludwig-Maximilians University, Munich, Germany.
- 2005 – 2007 **Master of Earth Science in Volcanology**
National Autonomous University of Mexico (UNAM), Mexico D.F. Mexico.
Grade 9.88 (Max.10). Medal “Alfonso Caso”, UNAM, 2007.
- 1998 – 2003 **Bachelor in Physics**
National Autonomous University of Mexico (UNAM), México D.F. Mexico.
Grade: 9.75 (Max 10). Graduated with honors, Diploma of 2nd highest grade.

Professional experience

- Since 2007 Department of Earth and Environmental Sciences, Ludwig Maximilians University, Munich, Germany.
- Spring 2006 Department of Earth and Environmental Sciences, Ludwig Maximilians University, Munich, Germany.
- 1999 – 2006 Associated student at the Department of Volcanology and Seismology at the Institute of Geophysics, UNAM, Mexico.

Teaching experiences

- 2007 Undergraduate courses on Geophysical Fluid Mechanics in the Faculty of Sciences, UNAM, Mexico.
- 2004 – 2006 Teaching assistant B of undergraduate courses in Thermodynamics and Fluid Mechanics in the Faculty of Sciences, UNAM, Mexico.
- 2002 – 2007 High School Teacher of Mathematics and Physics at the Panamerican University, Mexico D.F., Mexico.

Publications

Papers published in peer-reviewed journals: 6 (4 as first author).
Papers submitted to peer-reviewed journals: 1 (1 as first author).
Volcanic Hazards maps: 4 (1 as first author).

Languages: Spanish (native speaker), English (fluent), Italian and German (basic).